NASA CR-72549

DEVELOPMENT OF A THERMAL BARRIER COATING FOR USE ON A WATER-COOLED NOZZLE OF A SOLID PROPELLANT ROCKET MOTOR

by

V. R. Stubbs

AEROJET-GENERAL CORPORATION

Prepared for

NATIONAL AERONAUTICS AND SPACE ADMINISTRATION

Technical Management
NASA-Lewis Research Center
Contract NAS 3-10302
James J. Pelouch, Jr., Project Manager

NOTICE

This report was prepared as an account of Government-sponsored work. Neither the United States, nor the National Aeronautics and Space Administration (NASA), nor any person acting on behalf of NASA:

A.) Makes any warranty or representation, expressed or implied, with respect to the accuracy, completeness, or usefulness of the information contained in this report, or that the use of any information, apparatus, method, or process disclosed in this report may not infringe privately-owned rights; or

B.) Assumes any liabilities with respect to the use of, or for damages resulting from the use of, any information, apparatus, method or process disclosed in this report.

As used above, "person acting on behalf of NASA" includes any employee or contractor of NASA, or employee of such contractor, to the extent that such employee or contractor of NASA or employee of such contractor prepares, disseminates, or provides access to any information pursuant to his employment or contract with NASA, or his employment with such contractor.

Requests for copies of this report should be referred to

National Aeronautics and Space Administration
Scientific and Technical Information Facility
P.O. Box 33
College Park, Md. 20740

NASA CR-72549

FINAL REPORT

DEVELOPMENT OF A THERMAL BARRIER COATING FOR USE ON A WATER-COOLED NOZZLE OF A SOLID PROPELLANT ROCKET MOTOR

By

V. R. Stubbs

Aerojet-General Corporation
P.O. Box 15847, Sacramento, California

Prepared for

National Aeronautics and Space Administration

3 May 1969

Contract NAS 3-10302

Technical Management
NASA-Lewis Research Center
Cleveland, Ohio
Chemical and Nuclear Rocket Procurement Section

James J. Pelouch, Jr.

PREFACE

This report was prepared by V. R. Stubbs for NASA-LeRC under Contract NAS 3-10302 for Mr. James J. Pelouch, the NASA LeRC Project Manager. The author wishes to acknowledge the contributions of A. Kobayashi for the heat transfer analysis and G. Fuller for the plasma-arc-coating and plasma-arc-testing.

The test firing was performed at the Air Force Rocket Propulsion Laboratory, Edwards Air Force Base, Edwards, California. The author wishes to thank the Solid Test Area personnel at AFRPL and, in particular, Lt. D. R. Zorich, A. A. Bassoni and William J. Sando for their expeditious handling of the test firings.

This report was reviewed and approved by R. E. Anderson, Manager, Powder Metallurgy Section, and A. V. Levy, Manager, Materials Technology Department.

ABSTRACT

An analytical study and laboratory evaluation of plasma-arc-sprayed coatings was conducted. At the conclusion of this effort, three coating systems were recommended for testing with subscale nozzles. For subscale testing, three Titan II second-stage combustion chambers were modified and installed on surface Wing I Minuteman solid propellant motors. The first test firing was with an uncoated nozzle and resulted in a typical heat transfer type burnout. The second and third tests were with coated nozzles and were successful. On the third firing, the water flow rate was reduced by 58% after start-up.

TABLE OF CONTENTS

LIST OF TABLES

LIST OF FIGURES

FIGURE LIST (Continued)

Figure No.

I. SUMMARY

This report covers the investigative, laboratory evaluation and static test evaluation phases of a program performed with the objective of developing a thermal barrier coating to be used with a water-cooled nozzle of a large solid propellant rocket motor.

A thermochemical analysis of candidate plasma-arc-sprayed thermal barrier materials was performed. The promising materials were then evaluated by laboratory testing. Plasma-arc-sprayed disc specimens were used in screening tests designed to provide thermal conductivity data and preliminary assessment of resistance to oxidation and thermal shock. Selection of candidate coatings for evaluation with subscale nozzle test firing was made on the basis of 5-tube specimen oxidation and thermal shock tests. In these tests, the specimens were cycled in and out of a plasma flame providing a heat flux of 6 Btu/in.^{2}-sec-°F and a nominal surface temperature of 3200°F. The cooling systems recommended for further evaluation by subscale testing were Al_2O_3/Mo, Al_2O_3/Ni and Ni-coated Al_2O_3.

Concurrent with the analytical and laboratory evaluation of coatings, three subscale nozzles were designed and fabricated. In the interest of cost saving, Titan II Second-Stage combustion chambers were modified for use as water-cooled nozzles on surplus Minuteman Wing I motors. An adapter to provide a manifold and water outlet and an aft closure to replace the existing four-nozzle Minuteman aft closure were designed and fabricated.

A heat transfer analysis was performed to determine the thermal barrier thermal resistance requirements and the water flow requirements. Design

parameters were to obtain a coating temperature of 3000 to 3200°F while holding the coating side tube wall temperature to 1700°F or less and a burnout heat flux ratio of 0.7 or less. The burnout heat flux ratio is defined or the ratio of the actual heat flux to the theoretical burnout heat flux.

Test facilities were constructed at AFRPL, Edwards, California where three test firings were performed during the course of the program.

TEST HISTORY-WATER-COOLED NOZZLES

Test No.	Nozzle	Thermal Barrier	Water Flow Rate, lb/sec Max	Min	Results
1	01	None	164*	117	Heat transfer burnout.
2	02	(Figure 12)	171	165	Successful - coating intact. No regression.
3	03	(Figure 12)	200	84	Successful - coating intact. No regression, water flow reduced by 58%.

* Before burnout

Four test firings were planned, one uncoated and three coated; however, unanticipated post-test analysis costs and schedule delays necessitated the decision to delete the fourth test.

The first test firing was with an uncoated nozzle and resulted in a tube burnout. Post-test analysis indicated that the burned out tubes were in a pattern directly related to the propellant grain pattern. Heat transfer analysis supported the conclusion that at startup localized heat fluxes due to the grain pattern were equal to double the average value predicted.

Nozzle SN 02 was coated with one of the candidate systems studied in Task I and was test fired in September 1968. This test was successful. Based on the metallurgical post-test analysis and on analysis of the test data, the following major conclusions were made:

1. The coating remained intact.
2. The alumina in the propellant exhaust gas plated out in a uniform manner over the nozzle with thickness up to 3/8 inch in the exit area and on cooling cracked and fell off in the divergent section.
3. The bulk temperature rise was considerably less than predicted indicating that the propellant plated alumina was very effective in reducing heat flux for times greater than a few seconds after ignition.

To further test the theory that the thermal barrier coating is possibly needed only on startup and that the propellant alumina provides an excellent thermal barrier once the high local heat fluxes during startup are survived, it was proposed that for the third test, the water flow rate can be reduced in steps after 10 seconds to one-half that required during the start transient.

The third nozzle was test fired in February 1969. The water flow rate was reduced as planned and the nozzle survived with no apparent leaks or abnormalities.

II. INTRODUCTION

Solid propellant rocket nozzles and liquid propellant rocket combustion chambers perform the same function and are subject to the same limitation, that existing materials do not retain their strength and integrity at the extreme temperatures developed. There are four basic methods for withstanding the high temperature: one, removing the heat from the nozzle and chamber wall and piping it elsewhere (regenerative cooling); two, cooling the wall by spraying a coolant on or through the wall (film and transpiration cooling); three, cooling the surface by chemical reaction of the material (ablation); and, four, cooling the surface by conduction to a large heat sink. Regenerative cooling is the most efficient system, if the quantity and quality of coolant available is sufficient to cool the wall material to an acceptable level. However, the balance has become increasingly difficult to obtain. High energy propellants are often not effective coolants and with these propellants heat fluxes up to 50 $Btu/in.^2 sec$, coupled with poor coolant has made necessary either thermal barriers, film or transpiration cooling or a combination of these to make regenerative cooling practical.

Past attempts to use thermal barrier coatings have not been particularly successful. In part, this is because the coatings were not specifically designed for the environment within which they were required to function. Considerable analysis and study has been done since early attempts and an increasing number of successful applications have shown that a properly designed and applied coating can be relied upon to reduce the heat flux to the coolant and therefore extend engine life and improve engine performance.

The concept of employing a water-cooled nozzle with a solid propellant rocket motor is a technological extension of the proven regenerative-cooling systems employed in liquid engines. However, since the coolant is not used as a fuel and serves no other purpose, it is evident that the coating system employed must be one of maximum efficiency in order to result in minimum coolant and additional motor weight.

The objective of the investigation described herein was to develop a reliable Al_2O_3 thermal barrier coating that could be applied to a large water-cooled nozzle and provide a substantial reduction of heat flux to the coolant.

Plasma-arc-spraying was selected as the method for applying the thermal barrier because it is the most practical method that can be employed with large nozzles where accurate dimensional control of thickness is required.

The approach followed was to design and select candidate coating systems compatible with the environment, screen and evaluate these by laboratory testing, and select and test the best coatings in a subscale nozzle.

III. SELECTION OF COATING SYSTEM

A. MATERIAL SCREENING

A list of candidate materials was compiled from applicable literature and recent Aerojet programs. These materials were subjected to thermochemical analysis for the purpose of eliminating those whose corrosion resistance would be poor because of reaction with the gas species or with Al_2O_3.

1. Compatibility of Candidate Coating Materials with Al_2O_3

The systems studied were based on Al_2O_3 with Mo, W, Ni and Cr additions as reinforcing agents. The possibility of reaction between Al_2O_3 and the reinforcing materials was examined by evaluation of the free energies of possible reactions. These were calculated as follows:

	F, K cal	
	2240°F	3140°F
$Mo + Al_2O_3 \rightleftharpoons MoO_3 + 2Al$	+190	+159
$2Cr + Al_2O_3 \rightleftharpoons Cr_2O_3 + 2Al$	+107	+ 99
$W + Al_2O_3 \rightleftharpoons WO_3 + 2Al$	+174	+163
$3Ni + Al_2O_3 \rightleftharpoons 3NiO + 2Al$	+208	+202

The free energies are all positive and, therefore, the reaction to the right in the above equations is unfavorable. The candidate materials may be considered compatible with Al_2O_3. Since the metal phase will be distributed throughout the alumina, and the alumina will be maintained at a temperature of 3000°F or less, higher temperatures of reaction in the above cases were not considered. Thermochemical data for the above oxides and other candidate oxides are shown in Table I.

2. Thermochemical Compatibility-Thermal Barrier Materials with Exhaust Gas Species

The principal chemical species present in the exhaust gas of the most oxidizing of the two solid propellants under consideration for use in the program, ANB 3105, are shown below with the volume percentage of each specie in the total gas species present at a chamber pressure of 500 psi.

Specie	% Vol.
HCl	13.1
N_2	8.4
H_2O	16.9
H_2	27.0
H	3.9
CO	24.8
CO_2	1.9
Al_2O_3 (liquid)	25.5 (Wt % of propellant)

The remaining species, including many of the oxidants such as O_2, P, OH, and NO, are present in amounts of less than 1% by volume and their effect on the total reaction with the thermal barrier, therefore, is minimal.

Thermochemical analysis of the possible reactions involving the exhaust gas species and the prime thermal barrier candidate materials, Al_2O_3, W, Mo and Ni are shown in Table II.

The only reactions which are favorable to proceed to the right have a negative free energy. The species in the exhaust gases which are present in the largest amounts are compatible at the temperatures shown since they exhibit positive free energy of reaction. References used for the literature search and the compatibility studies presented above are listed in the Bibliography at the end of the report.

3. Thermal Conductivity

The literature search performed during the initial stage of the material screening task failed to provide adequate thermal conductivity data for a good heat transfer analysis. There was no data for mixtures of materials and data given was for solid materials rather than plasma-sprayed materials. Thus, it was evident early in the program that conductivity measurements of the materials in the as-sprayed condition were necessary.

The method developed at Aerojet-General for oxidation and thermal shock testing of thermal barriers permits derivation of a rough measure of thermal conductivity. The test is performed by mounting a coated disc specimen in a water-cooled fixture and exposing the specimen to a plasma flame. The gas-side temperature is measured with an optical pyrometer and the heat flux is measured with a water-cooled calorimeter. Coating thermal resistance $(\frac{t}{K})$ is calculated as follows:

$$Q/A \text{ (heat flux)} = \frac{T_g \text{ (gas side temp)} - T_2 \text{ (water side temp)}}{\frac{t}{K} \text{ (stainless)} + \frac{t}{K} \text{ coating}}$$

Since the thermal conductivity of the stainless-steel disc is known, $\frac{t}{K}$ of the coating can be calculated. The thermal conductivity of the coating is derived by dividing the thickness by the thermal resistance.

To provide a starting point for the initial tests, thermal conductivity of mixtures of Al_2O_3 and candidate metals were calculated using the Lichtenecker formula given below, which is applicable to mechanical mixtures of two materials between which no solubility or chemical reaction occurs:

$$Km = K_1^{P_1} \cdot K_2^{(1-P_1)}$$

or $$\text{Log } Km = P_1 \log K_1 + (1-P_1) \log K_2$$

where

Km = thermal conductivity of mixture

K_1 & K_2 = thermal conductivity of components and one and two, respectively

P_1 = volume fraction of component one

The conductivity of the mixture is, as noted above, dependent on the volume fraction of the components involved, but to determine the proper proportion of mixture in spraying, the weight fraction of the components in the mixture must be known. The relation between volume fraction and weight fraction is given by the following formula:

$$W_1 = \frac{V_1 D_1}{D_2(1-V_1)+V_1 D_1}$$

where

W_1 = weight fraction of component one

D_1 & D_2 = densities of components one and two, respectively

V_1 = volume fraction of component one

The thermal conductivity of alumina used was that presented in vendor's data (both Norton and Metco), 1.58 Btu/ft-hr-°F over the range of temperature between 1000 and 2000°F, and two values of the conductivity of chromium and nichrome alloy were used, 2/3 and 1/3, respectively, of the average values given in tables for these metals between room temperature and 1000°F. Two values of thermal conductivity for both molybdenum and tungsten were also used; 2/3 of the average value between 1000 and 3000°F, and the experimentally determined values obtained for the sprayed metals in previous Aerojet programs.

After calculating the thermal conductivity of the various volume mixtures of each of the metals with alumina, the thickness of coating required for each of the volume mixtures was calculated to provide the desired thermal resistance of 250 ($in.^2$-sec-°F/Btu). The thermal resistance is the coating thickness of a given coating divided by the thermal conductivity of the coating. The required thicknesses were plotted on semi-logarithmic graph paper with thickness of coating in mils as the ordinate and percent volume of metal addition as the abscissa - the corresponding percent weight of metal addition to alumina is also shown on the abscissa. Figure 1 is shown for illustration. K was calculated for all the coatings tested.

Results of the thermal conductivity, oxidation and thermal shock tests are shown in Table II. Calculations made from the temperature and heat flux data indicated that the K values used were generally too high. Revised values were used for the second series of tests. As can be seen in Table III, the surface temperature obtained on most specimens exceeded the 3000°F desired indicating that the revised K values were again too high. Thermal conductivity was calculated for this series of tests as shown in the last column of Table IV. To more accurately determine K values for use in 5-tube specimen testing, special specimens were prepared for measurement of thermal diffusivity. The thermal diffusivity was measured by the method described by Parker (1). Thermal conductivity is derived from the thermal diffusivity measurement as follows:

$$K = \alpha \cdot P \cdot C_p \; 0.0056$$

where

K = thermal conductivity Btu in./sec/in.^{2}/°F

α = thermal diffusivity cm^2/sec

P = Density grams/cm^3

C_p = specific heat per unit mass

The results of thermal diffusivity measurements converted to K are shown in Table V. These data were used in calculating coating thickness for the test nozzles. The measurements were taken at 1400°F, the upper temperature limit of the equipment, while the average temperature of the coating at the test nozzle throat is calculated to be around 2300°F. However, it appeared reasonable to extrapolate based on known behavior of solid materials from 1400°F to 2300°F. The thermal conductivity of Al_2O_3 and Mo both decrease slightly from 1400°F to 2400°F. The K values determined by these tests agree reasonably well with those calculated from the disc coupon tests shown in Table IV. This comparison is shown in Figure 2.

B. MATERIAL SELECTION

1. Coating Adherence

A test plan was prepared for determining coating adherence as related to substrate preparation and precoating material. The test apparatus constructed to perform bond shear tests was patterned after that used by Grisaffe (2). The load required to shear the coating from the substrate is indicated in psi in Table VI. The primers evaluated were Nichrome, Mo, Nickel Aluminide wire and Nickel Aluminide powder. Tests 1 through 4 were made with no surface preparations of the substrate. The value indicated for specimens 8 and 14 are probably not comparable in that it proved impossible to spray inside the 0.625 in. dia x 0.25-in.-dia hole of the test fixture with the oxy-acetylene wire gun and hold the coating thickness desired. The throat

size of the test nozzle used precluded the use of the wire gun as an application method. Based on these tests, Nickel Aluminide powder applied by plasma-arc was selected as the primer and grit blast with silicon-carbide grit to obtain maximum (250 microinches) roughness was selected as the surface preparation. The use of SiC, 24-28 mesh grit, was established as optimum at the time of a previous substrate preparation evaluation program at Aerojet (Ref 3) and confirms findings by Grisaffe (2).

2. Oxidation and Thermal Shock Testing

The heat transfer study conducted under the nozzle design task of the program concurrently with the material screening and material selection task predicted that a thermal resistance of 250 $in.^2$-sec-°F/Btu in the nozzle throat would be required to obtain a gas side temperature of the coating of 3000°F. This was the targeted maximum gas side temperature for Al_2O_3. Calculations were made to determine the coating thickness required and the initial series of disc specimens were used as a screening test for oxidation and thermal shock testing as well as to provide the previously discussed data for calculating thermal conductivity.

The test consisted of exposing the specimen to a plasma-arc-flame for a period of time sufficient to obtain the surface temperature reading with an optical pyrometer than cycling 10 cycles of 10 sec of heating and 5 sec cooling. The tests were performed at 7 Btu/$in.^2$-sec-°F. Table II contains the results of the testing. The surface temperatures were too high because of the previously discussed use of K values that were too high and considerable melting and spalling were observed. However, the tests were useful in establishing more accurate values for subsequent specimens.

The results of the second series of tests are shown in Table IV. The thickness of the coatings was reduced proportionally to provide the desired thermal resistance of 250 $in.^2$-sec-°F/Btu. The test again consisted of 10 cycles of 10 sec exposure and 5 sec cooldown at 7 $in.^2$-sec-°F/Btu and a nominal surface temperature of 3000°F. The gas-side surface temperatures were somewhat higher than desired and some melting occurred. No cracking was observed. Erosion was quite evident especially on coatings formulated with a high percentage of chromium. The results of thermal conductivity calculations in the two series of tests described suggests that there is a relation between thermal conductivity and coating thickness. Thermal conductivity increases with an increase in thickness. This should be investigated in future work. It is evident that more accurate measurement of thermal conductivity of plasma-sprayed coatings is needed.

Based on the results of the second disc specimen test series, 6 coating systems were selected for application and testing with 5-tube specimens. Five-tube specimens W-1 through -6 were constructed equivalent to disc specimens 19, 22, 24, 25, 26 and 29. See Table VII. These specimens were subjected to thermal shock and thermal resistance tests at 6 Btu/$in.^2$-sec-°F and at a nominal 3000°F surface temperature. In addition, the oxidizing effect of the 260-in. motor exhaust gas was simulated by the addition of oxygen and acetylene to the plasma gas. The results of these tests confirmed the results obtained with the disc specimens.

The superior corrosion resistance of the pure alumina was demonstrated and there was evidence that brittleness and susceptibility to cracking of an unreinforced oxide was avoided by the thinness of the coating.

To determine the as-sprayed effect of Ni-coated alumina powders, a comparison was made of the microstructure before and after plasma spraying, and further with the as-sprayed condition of the 80 Al_2O_3/20 Ni mix powder. Photomicrographs of the powder particles (Figure 3) show that the particles are in fact coated, however, examination after plasma-arc spraying does not indicate that the coating continues to exist in the as-sprayed material to a great extent. Specimen W6 has several large grains (Figure 4) in the intermediate coat with a suggestion in the large grain at the right that the nickel still surrounds the particle. However, this evidence of nickel is not apparent in the large particles in the center of the picture. The coating on specimen X18 (Figure 5) was an 80 Al_2O_3/20 Ni mix. The horizontal stringer or platelet effect experienced with most metal ceramic mixes is evident. Referring to Table V will show that the thermal conductivity of Ni-coated Al_2O_3 is more than twice that of the Ni/Al_2O_3/20 mix, and nearly double that of pure Al_2O_3. Although the value for the 80 Al_2O_3/20 Ni mix is unexplainably low (probably due to measurement error or excess porosity) the comparisons indicate that a continuous metal matrix probably exists throughout the Ni-coated Al_2O_3 structure, thus creating a heat flow path and accounting for the high conductivity.

A final test series was made in which the 4 remaining coating system candidates were compared on the basis of coating regression. Three identical 5-tube specimens were prepared with each coating system and one specimen was coated with pure alumina. One end of the specimen was tested in the plasma flame for 150 sec continuous exposure, and the other end was tested 250 sec 25 cycles of 10 sec on and 5 sec off. To simulate rocket combustion gases, oxygen 100 SCF/hr and methane at 50 SCF/hr were introduced into the plasma flame for 5-tube specimen tests. These gases were not used for the disc specimen tests. The coating composition and the test results are shown in Table VIII.

After testing, measurements were made to determine regression. Considerable spread was noted. However, it is evident that the surface of specimens with a pure alumina topcoat over an alumina-nickel second coat, regress less than that with the alumina-moly and the alumina-moly with a pure alumina topcoat in both the steady exposure and cycling tests. Some spalling of the topcoat occurred in the cycling tests of specimens X13, X14, and X15 which are a 70 Al_2O_3/30Mo second coat with a pure Al_2O_3 topcoat.

The three specimens (X10, X11, and X12), coated with a 0.006-in. of 70 Al_2O_3/30 Mo powder, had the same regression rate as the pure alumina coating for the continuous 150 sec firing, but had a much higher regression rate for the 25 cycle firing consisting of 10 sec on, 5 sec off, for each cycle. This probably indicates the effects of thermal stresses. It is also possible that some oxidation of the molybdenum is occurring during the off cycle; the off cycle time is not included in calculating the regression rate. The appearance of the specimens suggests some spalling occurred. The thermochemical analysis made at the beginning of the program indicated that reaction of molybdenum with H_2O, CO_2 and O_2 was favorable.

The next three specimens, X13, X14, and X15 consisted of a two-layer coating, 3 mils of $70Al_2O_3/30$ Mo overlayed with 2 mils of Al_2O_3 (X14), 3 mils of Al_2O_3 (X13), and 4 mils of Al_2O_3(X15). All these specimens had lower regression rates in the 150 sec continuous firing than either the pure Al_2O_3 coating (X19) or the straight $70Al_2O_3/30$Mo (X10, X11, and X12). This may have been due to oxidation protection of the molybdenum by the Al_2O_3 overlay. During the intermittent cycled firings, higher regression rates were observed and it appeared likely that the difference in the thermal expansion characteristics caused some loss of material by spalling. The appearance of the specimens suggests spalling in some areas. The dioxide, MoO_2, melts at about the same temperature (4730°F) as the metal. The dioxide, however, can be readily oxidized by oxygen to the volatile trioxide MoO_3 which sublimes at about 2100°F. The free energies for the reactions of carbon dioxide and water vapor with molybdenum dioxide, are positive; however, this indicates that these gases will not readily oxidize the MoO_2 to MoO_3. A comparison of the vapor pressure of MoO_3 and NiO at 2240°F points up the differences in the volatility of these two oxides. NiO has a vapor pressure of 1.43×10^{-8} atmospheres at 2240°F while MoO_3 has a vapor pressure at 2240°F of 0.6 atmosphere. Therefore MoO_3 is much more likely to vaporize than NiO.

Specimens X7, X8, and X9, were coated with three mils of nickel-coated alumina powder overlayed with three mils of alumina. Specimens X16, X17, and X18 consisted of three mils of $80Al_2O_3/20$Ni overlayed with three mils of alumina. These, in general, performed better than the coatings containing Mo. The oxidation of nickel by H_2O and CO_2 is shown below on a free energy basis (ΔF) at 2000 and 3000°F.

	ΔF, Kcal	
	2000°F	3000°F
$2Ni + 2CO_2 \rightarrow 2NiO + 2CO$	-7	+25
$Ni + H_2O \rightarrow Ni\ O + H_2$	-16	+18
$2Ni + O_2 \rightarrow 2NiO$	-50	-30

This would indicate that the reaction is favorable in the case of CO_2 at 2000°F and unfavorable in the case of H_2O. Any excess oxygen would also favor oxidation in a reaction with nickel at these temperatures. At 3000°F, both H_2O and CO_2 in the above reactions with nickel have positive free energies and are therefore unfavorable.

It should be noted that nickel oxide melts at 3610°F while nickel melts at 2650°F. Thus, oxidation of nickel promotes the formation of a more refractory and stable product (NiO) than the metal itself.

The free energies of CH_4, CO, and H_2O with Al_2O_3 are positive at both 2000 and 3000°F as indicated below, and, therefore, regression due to oxidation is not predicted. However, measurement of specimens before and after testing indicate a reduction in thickness had occurred.

		ΔF, Kcal	
		2000°F	3000°F
$CH_4 + 2Al_2O_3$	$4AlOH + CO_2$	+459	+312
$CO + Al_2O_3$	$Al_2O_3 + CO_2$	+164	+142
$H_2O + Al_2O_3$	$2Al_2O\ H + O_2$	+248	+217

The regression rates of specimens with a nickel-coated alumina second coat are compared in Table IX with specimens employing a 80 Al_2O_3/20 Ni mixture. The average regression rate in mils per second are as follows:

	Ni-Coated Alumina	Ni=Alumina Mix
Continuous	0.0022	0.0055
Cycling	0.0019	0.0120

These above comparisons indicate that superior results were obtained with nickel-coated alumina. However, examination of the regression rates of individual specimens shows that specimen X17 has a regression rate of 0.0133 for the 150 continuous exposure test, but only 0.0020 for the cycling tests (250 sec). This difference suggests a measuring error. If specimen X17 is omitted from the calculation, the average regression rate for continuous exposure for nickel alumina mix specimens becomes 0.0017 (slightly less than the rate of nickel-coated alumina) an insignificant difference.

The following comparison can be made of cycling test results of 5-tube specimens and disc specimens considered separately:

	Ni-Coated Alumina	Ni=Alumina Mix
	5-Tube Specimens	
Continuous	0.0022	0.0017
Cycling	0.0007	0.0033
	Disc Specimens	
Continuous	-	0
Cycling	0.0058	0.0250

It can be seen from Table IX that the regression rates of disc specimens 34 and 35 (0.02 and 0.03, respectively) have the greatest influence on the combined averages. Th· fact that these specimens were tested with a nitrogen plasma and an argon shield gas without the addition of oxidizers 0_2 and CH_4 suggests that the reduction in coating thickness may be due to a mechanism such as sintering rather than oxidation. The introduction of 0_2 and CH_4 into the flame in the 5-tube specimen tests spreads the flame over a larger area and thus results in less measured reduction of coating thickness than with the disc specimens where the flame is concentrated on the center of the disc. The concentrated heat in that area may result in a localized shrink due to sintering.

Evidence of sintering of Alumina coatings can be found in the temperature trace during the 150 sec exposure test. The temperature readings obtained appear to be peculiar for each coating system but all start high and drop rapidly, then continue to decrease at a very much slower rate throughout the test. A range of 300° has been noted.

Specimen X18 (Table VIII) was sectioned and examined for comparison of microstructure as sprayed to after 150 sec exposure. The before and after photomicrographs are shown in Figure 5. Note the refinement of the microstructure along the top surface of the exposed area.

To further postulate concerning the apparent lower regression rate of nickel-coated powders in the plasma-arc-tests, the finer particles of the Ni-alumina mix would be expected to compact or shrink more on partial sintering than the coarse particles that make up the nickel-coated alumina powder. This occurs because finer powders have a greater number of points of contact and a greater free energy associated with their surface area and therefore they will densify at a lower temperature than coarse powders.

At this point in the investigation, it was recommended that the nickel-alumina mix be used on the nozzle for the first hot firing test because of its lower cost and lower thermal conductivity and that the nickel-coated alumina system be used for the second test firing with the third coating system to be selected after the planned uncoated test and the two coated tests.

As will be brought out in Section IV, C of this report, it was necessary to reconsider the coating system recommendations made at the conclusion of the Material Screening and Material Selection Task in the light of the results of the uncoated nozzle test firing. Also due to unanticipated post-test analysis costs and schedule delays a decision was made to delete the third coated test. The uncoated nozzle was fired under water flow conditions predicted as safe, however, due to unanticipated local high heat flux area related to the solid propellant grain, the nozzle suffered a burnout.

3. Wire Reinforced Coatings

As part of the Material Selection Task, the feasibility of reinforcing the basic alumina coating with molybdenum wires was investigated. This use of wire or screen in reinforcing a plasma-arc-sprayed coating is not new, but generally it is accomplished by wrapping wire over a mandrel simultaneously with application of the coating. Most efforts have been pointed toward obtaining a free standing body after removing the mandrel. A different approach is needed where the desire is to produce a wire-reinforced coating on the ID of a regenerative tube bundle. In several schemes of disbursing chopped wire up to 1/4 in. length over the surface of disc specimens, it was found that the wires tended to bunch and uniform distribution was not obtained. Experiments with available powder feeders indicated the possibility of feeding small wires with

one power feeder and directing them into the plasma stream which includes the alumina. Since this would require the design and fabrication of a special powder (wire) feeder, a separate program was undertaken to accomplish the development of the wire feeder and the testing of wire reinforced coatings. The criteria set forth for maximum effectiveness of wire reinforcement was as follows:

1. Random uniform distribution throughout the coating and over the substrate.
2. Wires to be entirely surrounded by the coating.
3. Orientation of wires such that the surface is not appreciably rougher than can be obtained with conventional coatings.
4. Criteria 1 through 3 above to be obtained with minimum melting of the wires.

The cost of wires in the initial size selected,0.002 in. dia x 0.050 in. length, was very high. Bids received ranged from $1500 per pound to $698.50 per pound. Two pounds were purchased from General Electric Company at a $1,397 lot price. Discussion with the suppliers indicate that the cost is primarily that of cutting the wires to length. The demand for chopped wires has not been sufficient to encourage any supplier to install high production equipment. Such equipment while it must be high speed and capable of precision adjustment for size and length is considered to be easily within the capability of most machine tool producers.

a. Development of Wire Feeder

An apparatus for feeding wire was successfully developed using a Syntron Vibrator to feed the wire into a specially designed aspirater which could be directed at any desired angle into the plasma stream. Experiments conducted to optimize the gas flow setting, the vibrator setting the

torch setting and the wire feed to substrate distance, seemed encouraging and it was decided to proceed with disc specimen preparation and testing. The original supply of 2 lb of wire had been exhausted at this point and a new supply was ordered. To assess the effect of slightly larger wires, the second lot was specified to be 0.005 in. dia x 0.060 in. length. It was found that the feeder and aspirator handled this size very well; however, the deposition rate was judged to be lower than with the smaller wires. The smaller wires tended to melt slightly and stay in the plasma stream, whereas the larger wires did not melt and tended to bounce off the substrate giving poor results. However, the feeding mechanism fed the wires into the plasma at a uniform and adequate rate.

b. Testing of Wire-Reinforced Coatings

To compare a molybdenum wire-reinforced alumina coating to the nickel-reinforced alumina coatings for resistance to thermal shock, it is necessary to subject the coatings to severe enough thermal shock that cracking can be induced. The tests performed in the first stages of the program did not produce cracks in any of the specimens. Experience at Aerojet on this and other programs points to the relative thinness of the coating as the reason no cracks occurred. Cracks have been induced with the same test conditions where thick coatings are being tested. Therefore, several specimens of each of the previously developed nickel-alumina coatings as well as the anticipated molybdenum wire-alumina coating were prepared in thicknesses of over 30 mils.

The first series of tests were with disc specimens tested as delineated in Table X with the objective of determining the effect of varying percentages of Mo wire content. Deposition was poor at all the settings used. It was not possible in tests of the specimens to differentiate between high and low wire content. The regression rates were very low, but some cracks were observed indicating the spraying process may have been compromised by introduction of the wires.

The second series of tests, Table XI, were with 5-tube specimens and included thick coatings of the compositions previously tested as thin coatings in the early part of the program. The Mo wire coatings appeared rougher and contained voids in some cases around the wires. The results insofar as wire deposition and dispersement are concerned were disappointing. Deposition rate was observed to be poor during plasma spraying. This was confirmed by examination at 40X magnification.

The heat flux during testing was established at 6.9 Btu/in.^{2}-sec-°F. The specimens were moved in and out of the plasma jet 25 times with 10 seconds exposure and 5 seconds cooldown. The surface temperatures were recorded and corrected to give true temperatures. It is evident that temperatures were generally higher than planned. Regression was very slight in all cases but greater where temperatures higher than 3200°F are recorded. There is no significant difference in regression rate or amount of cracking between thick control coatings and thick Mo wire coatings. The test

results do not favor the further use of wires in coatings at least in the size used and in the manner of deposit used. Test results do confirm, however, that thin coatings are considerably less susceptible to cracking than thick coatings.

Figure 6 upper is a photomacrograph of a disc coupon and shows poor wire deposition and dispersion as is also evident in the 5-tube specimen in the lower photo. Figure 7 shows a 5-tube specimen after testing. The wires and partially melted wires on the surface have oxidized.

c. Wire Production Cost Study

When it was discovered early in the wire-reinforced coating investigation that the cost of small wires in small quantities was around $700.00/lb it was decided to investigate the reasons for the high cost and make a search to determine if a supplier exists who can produce wires at a reasonable cost. The planned approach was to survey all known wire producers and fabricators for the required wire cutting capability and if an existing facility was not found to prepare specifications for the design and fabrication of a wire cutting machine. Previous discussion with suppliers had indicated that the cost is primarily that of cutting wires to length, the cost of cold drawn wire being approximately $90.00/lb.

Quotation requests were sent to ten suppliers for cost of 0.002 in.-dia x 0.050 in. length molybdenum wires in lots of 25, 50 and 100 lb. Bids received were as high as $2,723.00/lb with the lowest bid being $301.00/lb for 25 lb, 255.00/lb for 50 lb and $214.00/lb for 100 lb. This

supplier stipulated, however, that his quotations were based on a $750.00 best effort evaluation order. To determine if high-speed cutting equipment existed, the specification appearing below was prepared and sent to 17 machinery design and fabrication companies. Only one reply was received, this was for design and fabrication to the specification at a cost of $52,250.00.

SPECIFICATION

Name:	Wire Cutoff Machine
Wire Size:	Molybdenum and Tungsten Cold Drawn Wires in Range of 0.002 to 0.005 in. dia
Wire Data:	Wire is furnished in spools containing approximately 7,000 meters (22,967 ft)
Production Capacity:	40,000 pcs/minute (minimum)
Cutoff Length:	0.050 $\pm$ 0.005 in. to 0.125 $\pm$ 0.010

This is a high production machine and should be capable of running 8 hours without stop for resharpening or other maintenance; however, the total life operation time expectancy is relatively short -- approximately 1,000 hours.

The wire to be used has been cleaned. The feeding and gathering system must be free from oil and other foreign matter that would contaminate the material.

The gathering hopper should feed into a small funnel to fill approximately quart size powder cans.

Two separate cutting mechanisms each providing half the required production capacity would be acceptable. Modified existing equipment is likewise acceptable.

To properly evaluate proposals from outside suppliers, a preliminary design of a wire cutter was made at Aerojet and an estimated cost of the equipment and production from the equipment was made.

The design presented in Figure 8 consists of a constant speed revolving 2-bladed cutter which is fed by a powered wire feeder. The wire must be rewound on the storage spools which are mounted above the shearing mechanism. Wire is positioned through a starter tube and into a roller assembly which feeds it into the cutoff die. The speed of the roller feeder and the cutting blade are independently controllable. The relative settings, therefore, control the length of the wire.

For example:

With the 2-blade cutter traveling at 1000 rpm (2000 cuts/min) to obtain a wire length of 0.050 in., the wire feed roller would have to feed wire at the rate of 100 in./min (0.050 x 2000). A 0.320-in.-dia feed roller would, therefore, bet set at $\frac{100}{\pi\ 0.320}$ = 100 RPM

The output of 0.002 in. dia x 0.050 in. length Mo wires at the feed and speed of the example above would be 25 x 2000 x 60 = 3×10^6 pcs/hr. Since there are 18.2×10^6 pcs/lb, one days production figuring 7 hours run time would be $\frac{7 \times 3 \times 10^6}{18.2 \times 10^6}$ = 1.15 lb/day. If a labor and overhead rate of $15.00/hr is used, the cost per lb is:

Material	1.15/lb	@	$90.00	= 103.50
Labor	8 hr	@	15.00	120.00
			TOTAL	$223.50

$$\frac{\$223.50}{1.15\ \text{lb}} = \$194.35/\text{lb}$$

The practical top production rate of the design shown is likely dependent on the success of the spool overspeed control system. A simple preloaded formed washer spring design is used here, however, higher speeds may require a more sensitive and sophisticated mechanism to maintain a uniform drag through an 8 hour run time.

The cost of completing the design, fabrication and tool proofing the machine is estimated to be $22,000.00.

The conclusions to be drawn from the results of the wire cutting cost study are:

1. Prices quoted by present suppliers for small lots are not unreasonable.

2. The quotation of $213.00/lb for a 100 lb lot falls well within the price range estimated for production from a high-speed special machine. If a requirement of 100 lb is ever anticipated, this source should be investigated further to determine if the $750.00 trial run is a good investment.

3. The present supplier (General Electric Company) quoted $457.00/lb in 100 lb lots. This is a proven source. Based on this cost, design and fabrication of a machine should be considered for any production requirements of 100 lb or more.

IV. FABRICATION AND TESTING

A. NOZZLE DESIGN ANALYSIS

1. Nozzle Design

The basic program requirement was to test a water-cooled nozzle with a Wing I Minuteman motor. It was determined in discussion with NASA that this could be a non-submerged nozzle, and secondly that in the interest of cost saving, a Titan II second-stage combustion chamber could be modified for use. An adapter to provide a water outlet from the tube that normally would feed into the injector was designed. In addition, a new aft closure to mate the Minuteman motor to the adapter was required. The method chosen to effect the transition into the nozzle from the motor was to provide the nozzle with an ablative liner of carbon phenolic and blend from the aft closure with V61 trowellable rubber. Figure 9 shows the completed design.

The completed design was reviewed by the stress section and determined to be acceptable. No effort was made to minimize weight as this is not a consideration for static testing.

2. Heat Transfer Analysis

A heat transfer study was made to optimize the water flow requirements and to determine the basic thermal barrier resistance to be used in coating design and development.

Predicted gas side, coolant side and bulk coolant temperature for an uncoated nozzle are shown in Figure 10. On the basis of these data, the initial estimate of water supply system minimum requirements were confirmed at 130 lb/sec flow and 750 psi inlet pressure.

From the gas side temperature profile shown, a plan was formulated for applying braze patches along the contour of the uncoated chamber. This technique has been used successfully many times at Aerojet in confirming predicted gas side temperatures. Accuracy in interpretation within 100°F can be expected.

The maximum safe gas side temperature for the alumina base thermal barrier system was set at 3000°F. The thermal resistance calculated to reach that temperature in the throat was 250 $in.^2$-sec-°F/Btu. These data were used in preparing and testing the laboratory specimens described in the first sections of this report. Figure 11 shows the predicted coating and tube wall temperatures for a t/K of 250 $in.^2$-sec-°F/Btu.

The first test firing with an uncoated nozzle SN 01 resulted in a burnout. The failure analysis performed on the fired nozzle and study of the test data indicate that the failure was marginal and permitted certain assumptions to be made as the basis for a revised heat transfer study. For continuity of events and to show the relation between test results and design revisions, further design and heat transfer analysis is included in sequence of testing and post-test analysis under the heading Static Tests and Post-Test Analysis appearing later in this report.

B. NOZZLE FABRICATION

Three nozzles were fabricated to the design shown in the Nozzle Design Section above (see Figure 9). Three adapter assemblies and two aft closures were fabricated. The first nozzle was for the uncoated firing test and included the braze patches on the tube crowns. The nozzle was leak checked at 750 psig before shipping to AFRPL for test firing. Changes in the nozzle

as a result of the post-test analysis of the test firing were incorporated in the second nozzle SN 02. These changes were the rework of the ablative liner to a tapered configuration and the thinning of the tube wall in the throat area from 0.020-in. thick to 0.015 in.

On the basis of experiments with a hand-operated grit blast nozzle on some 5-tube specimens, a grit blast program was prepared for the purpose of reducing the tube wall from 0.020 in. to 0.015-in. at the nozzle throat. Post-test analysis determined that the wall had in fact been reduced to 0.013 in. Tukon hardness tests on specimens indicated that the grit blasted side of the tube was R/C 35 compared to R/C 27.5 on the side not grit blasted. This represents roughly an increase in tensile strength to 150K due to work hardening. This increase in strength is not useful inasmuchas the stresses would be relieved at 900°F in less than 15 seconds.

The second nozzle SN 02 was plasma-arc-sprayed with the selected coating system (see Figure 12), assembled, leak checked at 1000 psig, and shipped to AFRPL for testing.

The third nozzle SN 03 was fabricated and coated with the same coating system as SN 02 except that additional bands of plasma-arc-sprayed high-temperature materials were added in the exit end as delineated below.

Station No.	Coating
0-7	Base
7-9	Base - grit blasted
9-11	Hafnia
11-1 13.0	Strontium Zirconate
13-1 14-9	Zirconia
10-11	Tungsten (Topcoat)
12-12.9	Tungsten (Topcoat)
14-14.8	Tungsten (Topcoat)

C. STATIC TESTS AND POST-TEST ANALYSES

1. Facility

The water flow facility for test firing the Titan II combustion chamber with the Minuteman motors was designed and constructed by AFRPL, Edwards Air Force Base, California. A description of the system and the calibration and checkout procedures is contained in Reference (4). AFRPL personnel also assembled the nozzle with the aft closure and V61 insulation and installed this assembly on the Minuteman Wing I motor (see Figure 9).

The water system capability is as follows:

Tank pressure	- 250 to 1200 psi
Flow rate	- 500 to 1266 gpm
Maximum nozzle inlet pressure	- 825 psi at 1200 gpm flow

Instrumentation was supplied in accordance with the specifications furnished by Aerojet and is shown in Table XII. Thermocouples TCN_1, TCN_2, TCN_3, and TCN_4 were located on down tubes opposite the propellant grain valleys with TCN_5, TCN_6, TCN_7, and TCN_8 located 45° counter clockwise opposite the propellant grain peaks.

In addition to the digital recorder, quick look data was provided for tank pressure, inlet pressure, outlet pressure, and flow rate.

2. Static Test Serial No. 01

The first static test firing of nozzle Serial No. 01 was made on 5 June 1968. Before firing, five cold flow test runs of 5 to 10 seconds duration were made to establish the downstream valve setting in relation to inlet pressure and water flow requirements. The fifth cold flow test was made with the downstream valve 23% open, inlet pressure 775 psig, outlet pressure 560 psig and flow rate 880 gpm. This was considered to be as near to the

desired rates as possible in that the downstream valve is not calibrated finely and is difficult to adjust.

The test firing was made at approximately 1:00 p.m. and continued for 62.08 seconds. It was noted on the visual gauges that water flow increased within one second after start from 850 gpm to approximately 1100 gpm. Also, inlet pressure decreased from 788 psig to approximately 690 psig while outlet pressure decreased from 570 to 468 psig. Later inspection of the data indicated that the water flow conditions changed at 0.21 seconds. P_c appeared normal throughout the firing and there was no visual evidence of malfunction of equipment, however, it was discovered later that the water inlet valve closed at 60.2 seconds due to a failure of electricity on the pad. This loss of water flow permitted excessive soak back of heat through the chamber and caused the backside of the nozzle wall to overheat. In addition, the programmed N_2 purge was delayed several minutes permitting stored heat in the chamber to soak into the nozzle.

Inspection of the nozzle several minutes after firing confirmed that a burnout had occurred in the throat area. There were also several small leaks in the aft manifold joint between the tubes.

3. Post-Test Analyses, SN 01

a. Discussion

The nozzle was removed from the stand at AFRPL, disassembled and shipped to Aerojet. Preliminary inspection confirmed a typical burnout appearance, complicated by the fact that there were two areas of burnout. The first and most obvious was the throat region which was not covered with aluminum oxide buildup. In this region, almost all the burned out tubes were up tubes implying an R_{Bo} type failure where the heat exceeded

the cooling capacity of the coolant, or film boiling. The burned-out sections were in a definite pattern, i.e., four locations reflecting the star pattern of the propellant grain. There was a buildup of slag in the area between the throat and the nozzle insulation. In this region, both the up and down coolant tubes were burned out. It is postulated that these burnouts could be related to gas flow disturbance or boundary layer tripping caused by the rather abrupt ending of the insulation. This junction represents a sudden change in gas flow due to discontinuity in the wall.

The area around the leaks in the tubes at the aft manifold closing weld had the appearance of being ground by a grinder or wire brush. In approximately 180° of area, the weld bead was entirely missing and the patent metal was thinned to the extent that holes appeared in the area between the tube end fittings and the manifold. All the valleys between the tubes had what appear to be grind or wire brush marks; however, the marks appeared in such a symmetrical pattern that erosion was a more likely cause than unauthorized grinding.

A complete failure analysis was performed on the fired nozzle. The metallographic examination revealed no other possible cause of failure other than inadequate cooling resulting in burnout. Figure 13 is presented to illustrate the appearance of the typical burned through tube.

Conclusions based on visual observation, metallurgical examination and analysis of test data are as follows:

(1) Tube ruptures in the throat regions were heat transfer burnout in nature.

(2) The tubes upstream of the throat adjacent to the ablative insulation failed by melting either due to boundary layer tripping occurring at the end of the insulation or by soak back of heat from the thick

layer of Al_2O_3. The latter case is a more likely explanation in that water was shut off before tail off and the nitrogen purge was delayed several minutes.

(3) The small leaks in the tube valleys at the junction of the aft manifold are due to stream erosion and Al_2O_3 particle impingement at the discontinuity formed by the round to rectangular tube adapters and the closing weld bead at the aft manifold. Failure occurred by rupture from internal pressure when the scrubbed area became too thin to withstand the internal pressure.

b. Heat Transfer Analysis SN 01

A count of burned-out tubes was made and oriented to the propellant grain pattern. Fifty-one tubes were burned through. Of these, 10 were downtubes or 1st pass and 41 were uptubes or return pass. Twenty tubes showed slight surface melting and the balance (77) were intact. The majority of the burned-out tubes were opposite the peak of the propellant grain pattern. Based on these data, the assumption was made that the downtubes had burned out at a burnout heat flux ratio of 1.0. To determine what gas-side heat transfer coefficient was necessary to satisfy this assumption a post-test heat transfer analysis was made with the actual test conditions, coolant water flow rate (117 lb/sec) inlet pressure ($\sim$ 750 psia) and temperature of coolant (71°F). The results shown in Figure 14 indicate that a heat transfer coefficient that is 2.4 times the original design value would satisfy the downtube burnout assumption. It is felt that the heat transfer coefficient used in the original study may have been correct, however, it is evident from the burnout pattern that the local heat fluxes due to mass flow effects were considerably higher than average.

Using this higher coefficient, a parametric study of cooling requirements for the uncoated chamber was made. The results are shown in Figure 15. Water flow was varied from 140 to 200 lb/sec at inlet pressure of 650, 750, and 850 psia. Both 70 and 90°F water inlet temperatures were

investigated. This figure (Figure 15) plainly shows the high tube wall temperatures (2200°F) experienced by the chamber regardless of the water flow. For example, with 170 lb/sec of water at 650 psia inlet pressure and 70°F inlet temperature, the wall temperature is approximately 2239°F. The latest water flow data from AFRPL indicate a maximum flow of approximately 170 lb/sec. It is evident from this study that an uncoated chamber probably would not survive.

A coated chamber study was then made to determine the coating thermal resistance required for safe operation of the chamber. Coating thermal resistance is defined as the ratio of coating thickness (t_c) to the coating thermal conductivity (k_c). This resistance was varied from 60 to 120 $in.^2$-sec-°F/Btu at coolant flows of 100, 140, and 170 lb/sec. The results of the parametric study are shown in Figure 16. At a thermal resistance of 100 $in.^2$-sec-°F/Btu and water flow of 140 lb/sec, the maximum R_{BO} is 0.62, while the coating and tube wall temperatures are 3310 and 1860°F, respectively. The tube wall temperature (1860°F) at the coating tube interface is much higher than the desired design limit of approximately 1600°F; therefore, a study was made to investigate methods of lowering this temperature.

One way of lowering the tube wall temperature is to thin the tube wall thickness by controlled grit blasting prior to the coating application. The effects of such thinning is shown in Figure 17 for coating thermal resistances (t/k) of 100 and 110 $in.^2$-sec-°F/Btu; the latter t/k is included to show that an increased coating thickness can be used with thinner tube wall. This figure indicates for t/k of 100 a reduction in tube wall temperature from 1860 to 1600°F and coating temperature from 3310°F to 3160°F, as the tube wall is thinned from 0.020 to 0.015 in. The tube thinning does slightly increase the coolant-side tube wall temperature (less than 10°F for a 0.015-in. wall).

Calculations were made that indicated that a thermal resistance (t/k) of 600 $in.^2$-sec-°F/Btu instead of 100 $in.^2$-sec-°F/Btu at the exit would reduce the heat flux approximately 16 percent and the coating temperature in this area would increase from 990 to 1690°F. This would provide an increased margin and a better chance for nozzle survival in the event that some of the coating failed during the test.

c. Selection of Design, Coating System and Test Plan for Second Test

A joint conference was held with Aerojet and NASA personnel for the purpose of adopting a course of action for the second nozzle test. Based on the failure analysis and the data provided by the post-test heat transfer analysis, the following items were agreed upon.

(1) Thin the tube wall in the throat area to 0.015 in. by grit blasting.

(2) Coat the throat and forward sections with a 70 $Mo/30Al_2O_3$ mixture to give a (t/K) of 100 $in.^2$-sec-°F/Btu.

(3) Coat the exit end of the nozzle with the nickel-coated alumina-alumina topcoat system to obtain a t/K of 100 5.0 in. aft of the throat to 600 $in.^2$-sec-°F/Btu at the exit end. See Figure 12.

(4) Eliminate the discontinuity below the upstream insulation and the nozzle by machining a taper on the ID of the lower insert.

(5) Flow water at maximum system capacity.

The selection of a 70 Mo/30 Al_2O_3 mixture for coating the throat area rather than the 20 Ni/80 Al_2O_3 mix recommended as first choice at the end of the material selection phase, was based on the necessity to provide a thicker coating to facilitate dimensional control of thickness. The 20 Ni/80 Al_2O_3 coating has a thermal conductivity of approximately

1.6 Btu-in./sec/in.^{2}/°F x 10^{-5}. With a t/K of 100 in.^{2}-sec-°F/Btu, the coating thickness required over the 0.002 in. nickel aluminide primer was determined to be 0.00137 in.

		t/K	K x 10^{-5}
Primer N Al_3	0.002	14.3	35.0*
20/Ni/80 Al_2O_3	0.00137	85.7	1.6
		100.0	

*Subsequent thermal diffusivity testing established the thermal conductivity of Nickel Aluminide at 11.2 x 10^{-5}

The obvious difficulty of obtaining a coating of slightly over a mil in thickness indicated that a coating of higher conductivity should be used. Also, because of the local high heat flux regions apparent from analysis of the first test and the uncertainty of the predictions in these regions, it was decided that a higher melting temperature metal should be used in place of nickel which melts at 2631°F. Molybdenum melts at 4730°F. It was expected that Mo would perform better in a nozzle than in the disc and 5-tube specimen tests insofar as regression due to oxidation. The laboratory tests are made in the open and entrain undetermined amounts of air into the plasma stream. The oxygen content expected in the gas species is actually less than expected with laboratory tests. The coating thickness required for several different weight percent mixtures of Mo and Al_2O_3 were calculated. A 70 Mo/ 30 Al_2O_3 mixture was determined to give a coating thickness of 0.0039 in. This mixture was selected for the chamber and throat area, and nickel-coated alumina with a K value of 3.19 with a pure alumina topcoat K = 1.6 was selected for the divergent section from 5.0 in. downstream of the throat to the exit. The thickness was tailored to result in gradual increase in t/K from 100 to 600 in.^{2}-sec-°F/Btu. See Figure 12.

Planned test conditions were as follows:

Water Flow Rate	170 lb/sec
Tank Pressure	1100 psia
Inlet Pressure	850 psia
Outlet Pressure	450 psia

Test instrumentation used was the same as for SN 01.

4. Static Test SN 02

The second test firing (Nozzle SN 02) was accomplished at AFRPL on 20 September 1968. The firing was of full duration with no observed abnormality. Visual inspection of the nozzle after firing showed no tube rupture or leakage. A layer of Al_2O_3 had plated out over the entire nozzle. This layer was approximately 1/16 in. thick over the tube crowns in the throat area and 3/8 in. thick in the exit area. The alumina had shrunk away from the nozzle at cooldown and had a network of cracks. Figure 18 shows the coated nozzle. Figure 19 shows the condition of the nozzle immediately after firing.

5. Post-Test Analysis SN 02

a. Laboratory Investigation

The fired nozzle was leak checked with air at 100 psig. There appeared to be a leak in the forward section in the area just below the remaining ablative insert. This area had approximately 0.080 in. of Al_2O_3 in addition to the original plasma-arc-sprayed coating. A section about 2.0 in. square was removed and examined. No evidence of cracks or burnthrough could be found. It was concluded that the leak may have been in an adjacent area and a leak path was formed under the Al_2O_3 permitting the air to escape through a crack in the Al_2O_3 several inches away. No other leaks were indicated. Since the Al_2O_3 from the propellant was in general adhering tightly, it was felt that the cost of finding the leak was not warranted.

Sections were cut from the fired nozzle in the forward section, at the throat and the aft section. These were mounted, polished, and examined metallographically. Measurements were made of the plasma-arc-sprayed

thermal barrier and of the tube thickness at the throat. Photomicrographs of the forward section, throat and aft section are shown in Figures 20 through 22. The measurements taken are shown below.

	Forward	Throat	Aft
Coating	0.0048 (min)	0.0040 (min)	0.0080 (min)
Tubes	0.020	0.013 min	0.020

Figure 12 illustrates the nominal coating thicknesses. The thermal barrier was constructed to give a thermal resistance of 100 in^2-sec-°F/Btu in the throat and forward section with an approximately constant increase to 600 in^2-sec-°F/Btu at the aft end.

The coating in the forward section and throat (Figures 20 and 21) appears to have a void between the nickel aluminide primer and the topcoat. This occurred either in the sectioning and polishing process or when the propellant Al_2O_3 cracked and fell off due to shrinking while cooling. Pieces of the Al_2O_3 have been examined by X-ray diffraction for the existence of either Mo or Ni on the underside. The results of the analysis are that only alpha Al_2O_3 was observed. The conclusion was made that the plasma-arc-sprayed coating was still in place and did not come off with the propellant deposited Al_2O_3 on cooldown.

In addition, pieces of the Al_2O_3 were sectioned, mounted, and polished for metallographic examination. Figure 23 is a section at the throat and is particularly interesting in that it shows three phases of growth. The propellant Al_2O_3 evidently plated out on the relatively cold tube walls and valleys ($<$ 3100°F) during the first few seconds of firing, then when the

thickness of the deposit was such that the hot side exceeded 3630°F, the Al_2O_3 became molten and sluffed off while remaining semi-molten underneath. Then as P_c dropped off and the heat flux decreased, the molten and semi-molten layer solidified and as further cooling occurred, this area was again covered with the same type of random grain deposit indicated in the layer near the tube. This is, of course, speculation; however, no other explanation for the three phases suggests itself. Figure 24 shows the large columnar grains in a well-defined band. These grains are translucent and crystalline in appearance.

To summarize the results of the metallographic part of post-test analysis:

1. The wall thickness in the throat area was successfully reduced from 20 to 13 mils by controlled grit blasting.

2. The plasma-arc-sprayed thermal barrier survived the start-up and stayed on even after the propellant deposited Al_2O_3 cracked and fell off on cooling.

3. The aluminum from the propellant oxidized and plated out over the coating in a uniform manner exhibiting what appeared to be three phases.

b. Heat Transfer Analysis

(1) Local Coolant Bulk Temperatures

In addition to the regular coolant inlet and outlet temperature data, two sets of four thermocouples were installed to measure local coolant bulk temperatures. The first set was located in line with the solid propellant grain pattern peaks and the other in the grain valleys.

The four thermocouples were located in the following axial positions: (1) 3.9 in. upstream of throat, (2) 0.6 in. upstream of throat, (3) 4.0 in. downstream of throat, and (4) 2.3 in. from the aft end. The data from these thermocouples for the first 8 sec are shown in Figures 25 and 26. The temperatures in Figure 25 are those in line with the propellant peaks with T1 upstream of throat and T4 near the aft end. Figure 26 represents temperatures in the propellant valleys with T8 located near the aft end. All eight thermocouples were installed in downtubes.

(a) Local Heat Flux

It is immediately apparent that the local coolant temperatures decrease instead of increasing as one would expect in a downtube. This decrease is attributed to the hot-side fluid mixing with the cooler backside fluid. It is not possible, therefore, to determine local heat fluxes directly from these data.

(b) Propellant Grain Pattern Effects

These coolant temperatures indicate that the propellant peak region (Figure 25) is hotter than the propellant valley region (Figure 26). This is most noticeable in comparing T1 and T5 both located 3.9 in. upstream of the throat. Thermocouple T1 peaked at 101°F in 1.5 sec while T5 peaked at 99°F in 2.5 sec. This information verified the burnout pattern notices in chamber SN 01 after the first test where the burnouts were apparently in line with the peaks.

Calculations were made to determine the difference in heat load between the propellant peaks and valleys. First, it was assumed that T4 and T8 represented the average coolant bulk temperatures near the aft end. Using these temperatures and knowing the heat transfer surface areas, an average heat flux was calculated for each region. The results indicated that at 8 sec the average heat flux in the peak region was approximately 22.5 percent higher than that in the valleys.

(2) Coolant Inlet and Outlet Temperatures

Chamber coolant inlet and outlet temperatures were taken, and for this test the average inlet temperature was 67°F. The chamber coolant bulk temperature rise vs time is shown in Figure 27. This figure represents an average temperature rise of the chamber coolant, and, therefore, and average heat transfer rate, but these averages do not necessarily represent the local circumferential variation as shown by the local data. However, these data were used to compare test results to the predicted.

(a) Test Data Bulk Temperature Rise

The overall bulk temperature rise (Figure 27) peaked out at 32°F in 8 sec, held approximately constant to 15 sec, then decreased continually to 21°F at 60 sec. This decrease can be attributed to both the chamber pressure profile and the plating out effects of the alumina on the coated tubes. Calculations were made at 8 sec, the maximum coolant outlet temperature indicated, to determine the temperature rise at the propellant grain peak region.

In the previous calculation it was determined that the peaks were 22.5 percent higher than the valleys. Also, if it were conservatively assumed that the 8 sec $\triangle T$ of 32°F represented the valley data, then the peak $\triangle T$ would calculate to be approximately 39°F. This value is then compared to the predicted value of 44°F temperature rise.

(b) Comparison of Test to Prediction

The predicted coolant bulk temperature rise of 44°F was made based on a thermal model modified in the divergent section of the chamber to account for the two-dimensional axisymmetric flow field (Ref. 5). This modification was based on recent temperature data obtained from the identically contoured Titan IIIM Stage II chamber program and was similar to that currently used in all Titan IIIM Stage I chambers.

The test data maximum temperature rise of 39°F compares to 44°F of the new predicted value. Considering other uncertainties such as the effect of additional alumina plating out on the tubes, it is felt that no correction in the analytical model is necessary, i.e., the test data substantiated the use of the current analytical model, as it is without modification.

(3) Conclusions

(a) Local heat flux data cannot be obtained from the local coolant bulk temperature data.

(b) The average heat flux in the propellant grain peak regions is approximately 22.5 percent greater than the valley region.

(c) The overall coolant bulk temperature rise maximum was 32°F at 8 sec and decreased to 21°F at 60 sec.

(d) The current analytical model is satisfactory for future analysis.

c. Selection of Design, Coating System and Test Conditions for Third Static Test

(1) Revised Test Requirements

Post-test analysis of the first test nozzle indicated that the high local heat fluxes due to the propellant grain pattern would have to be accounted for in the next test. The successful test of the second nozzle

was evidence that this could be done by employment of a properly designed and applied thermal barrier and increased water flow. Based on the apparent behavior of the propellant plated Al_2O_3 and the reduction in predicted bulk temperature rise, it was theorized that after 8 seconds, the water flow could be reduced to coincide approximately with the reduction in heat flux to the coolant as evidenced by the curve in Figure 27. Negotiations with NASA resulted in agreement to change the program scope to include an analysis of the effects of the plated out alumina and to prepare a test program to include gradual reduction in coolant flow after 8 or more seconds.

An additional change in scope added a requirement to include several high melting point ceramics over the original thermal barrier coating of the third nozzle with the objective of determining the reaction, if any, of these materials with Al_2O_3 and the gas species.

(2) Heat Transfer Analysis

To determine minimum water flow requirements under safe conditions while accounting for the thermal resistance of the propellant plated alumina, two heat transfer analyses were made for the coated chamber. The first assumed no alumina plating and the severe thermal conditions experienced during the start transients with coating temperatures of 3200°F. The second analysis assumed alumina plating at 3700°F and realistic coolant bulk temperatures experienced in the second test. In both, the water tank pressure was assumed to be 1100 psia and the water flow rate was reduced from 170 to 50 lb/sec, or approximately 1225 to 360 gpm.

The maximum burnout heat flux ratios and wall temperatures are shown in Figures 28 and 29. For the severe start conditions at full flow (170 lb/sec) and R_{Bo} is 0.53 and the minimum flow for R_{Bo} of 1.0 is 70 lb/sec or approximately 510 gpm. Assuming that alumina plating does occur the R_{Bo} at full flow (170 lb/sec) is 0.39 and to achieve an R_{Bo} of 1.0 the water could be reduced to 50 lb/sec. These predictions are valid only if the original coating remains intact. The recommendations based on the above analysis was to reduce the water flow rate after 10 seconds in stepdown to a minimum of 80 lb/sec holding each step for a minimum of 5 seconds.

(3) Selection of Experimental Coatings

The basic criteria for selection of high temperature coating materials for evaluation by test firing was that the melting points should be above 4700°F and that they should be compatible with Al_2O_3 and the exhaust gas species.

A literature search was made covering recent data on high-temperature oxides. Table XIII lists these materials and their thermal and chemical properties. Data was not available for several of the oxides and mixed oxides. The thermal conductivity and thermal expansion values are for 100% dense materials except where noted.

Table XIV indicates candidate coating materials compatibility with the gas species based on the free energies of the materials and the gas species. A plus number indicates a condition unfavorable to a reaction while minus number indicates conditions for reaction as favorable.

ZrO_2, HfO_2 and $SrO{\cdot}ZrO_2$ were selected for testing in the nozzle exit section. These materials have melting points of 4700°F or above and are easily plasma-arc-sprayed. Zirconia and hafnia have very low

thermal conductivity and are known to have good thermal shock resistance when used as thin coatings. Aerojet has had little experience with Strontium Zirconate and there is little published data other than that its thermal shock resistance is somewhat inferior to zirconia and other zirconates and its porosity is somewhat higher. When magnesium oxide was eliminated because it proved impossible to plasma-arc-spray, $SrO \cdot ZrO_2$ was substituted due to its availability and ease of spraying.

MgO, ZrO_2, HfO_2 and ThO_2 are attractive due to their low thermal conductivity. There is no experience recorded concerning plasma-arc-spraying of thoria. This is probably due to its reported radioactivity and poor thermal shock properties. A special facility would be required for spraying thoria. MgO is reported to be difficult or impossible to plasma spray due to its vaporization. This was confirmed by a laboratory test where 10 passes of the plasma torch over a substrate failed to result in a measurable increase in specimen thickness. The melting point of BeO at 4660°F is near the target of 4700°F, however, its thermal conductivity is high, it reacts with H_2O above 3000°F and its reported toxicity creates unknown handling problems. The other candidate materials listed have melting points considerably lower than 4700°F and were eliminated from further consideration for that reason.

6. Static Test SN 03

The third test firing (Nozzle SN 03) was accomplished on 19 January 1969. The firing was of full duration. The LN_2 tank to H_2O tank was regulator valve malfunctioned at approximately 27.621 and was below tank pressure at 36.054 seconds causing a loss of flow and inlet pressure. Visual

inspection after firing showed no evidence of leakage or loss of coating. The appearance of the tested nozzle was nearly identical to SN 02. The experimental coating materials that had been sprayed in the exit end appeared as multicolored bands.

Planned test conditions were as follows:

	Initial	T + 12 1st Reduction	T + 22 2nd Reduction
Water Flow Rate, lb/sec	170	125	80
Inlet Pressure, psia	900		
Outlet Pressure, psia	450		

7. Post-Test Analysis SN 03

a. Laboratory Investigation

The tested nozzle was removed from the stand and returned to Aerojet. Visual inspection indicated no damage or abnormalities. The condition of the ablative inserts and the coating was nearly identical to that of the previous test nozzle SN 02.

The nozzle was sectioned to obtain specimens of the experimental coatings in the aft section. These were mounted and polished for microprobe analysis. A specimen was made for each condition shown in Table XV.

The purpose of the microprobe analysis was to determine the extent of reaction, if any, between the plasma-arc-sprayed layers and between the top layer and the Al_2O_3 of the propellant. On specimens B, D, F, the 2nd and 3rd layer interface and the 3rd layer surface were examined. On specimens C, E, G, containing the tungsten topcoat, the 3-4th layer interface and the 4th layer surface were examined. Results tabulated by specimen and material layer are delineated below:

Specimen	Element	Layer	Results
B	Al	2-3	No diffusion
B	Hf	3	Found, no diffusion
B	Al	Surface	Residue $\sim$ 2 to 10 μ thick
C	Al	3-4	No diffusion
C	Hf	3	Found, no diffusion
C	W	4	$<$ 4% Al all through
C	Al	Surface	Residue $\sim$ 2 to 3 μ thick
D	Al	2-3	No diffusion
D	Zr	3	Found, no diffusion
D	Al	Surface	Small residue
E	Al	3-4	No diffusion
E	Zr	3	Found, no diffusion
E	W	4	$<$ 4% Al content
E	Al	Surface	2 to 3 μ residue
F	Al	2-3	No diffusion
F	Zr	3	Found, no diffusion
F	Al	Surface	Residue $<$ 2 μ thick
G	Al	3-4	No diffusion
G	Zr	3	Found, no diffusion
G	W	4	$<$ 5% Al content throughout
G	Al	Surface	Residue $<$ 2 μ thick

b. Data Analysis

Review of the digital data indicated that initial flow rates were somewhat higher than planned and higher than indicated by the visual and quick look data. Table XVI summarizes the significant data and sequence of events. At 27.621 seconds regulator pressure dropped below tank pressure and continued to reduce to zero at 36.054 seconds. At approximately 45 seconds the remove control downstream valve was opened permitting an increased flow while pressure in the pressure out continued to fall off. Flow did not fall below the planned 600 gpm maximum. Because of the valve malfunction the actual test conditions were out of the range of conditions studied; therefore, it was necessary to perform a heat transfer analysis using the actual test conditions. Calculations indicated a maximum burnout heat flux ratio of 0.74 which is approximately 18% higher than would have been experienced if the regulator had not malfunctioned. The corresponding tube wall temperature on the coating side was calculated to be 1425°F. These maximum conditions occurred at 44 seconds when the minimum flow (610 gpm) and maximum local coolant bulk temperature (85°F) were experienced. Table XVII compares predicted burnout heat flux ratios (R_{Bo}) at representative points during the test. The fact that the water temperature was 47.5°F rather than 70°F provided a small margin in R_{Bo}. This, coupled with quick action by NASA and AFRPL personnel in opening the downstream valve when H_2 pressure regulator valve closed, contributed to obtaining a successful test under potentially hazardous conditions.

The 610 gpm water flow rate represents a reduction of 58% under the actual starting flow rate and 52% under the planned starting flow rate.

V. CONCLUSIONS AND RECOMMENDATIONS

Several candidate Al_2O_3 base plasma-arc-sprayed thermal barrier materials were analyzed for compatibility with the exhaust gas species of the 260-in. solid propellant rocket motor. The promising coatings were further evaluated by laboratory testing for resistance to thermal shock and corrosion.

Three coating systems were superior to all others. These were 80 Al_2O_3/ 20 Ni, Ni-coated Al_2O_3, both with a pure Al_2O_3 topcoat, and Ni/Al_2O_3 in various weight percents.

Two subscale tests were made using coated water-cooled nozzles and Wing I Minuteman solid propellant motors. The thermal barrier materials used in both tests were a 70 Mo/30 Al_2O_3 mixture in the chamber and throat area and a Ni-coated Al_2O_3 plus Al_2O_3 topcoat in the exit area. The coating survived the tests with no evidence of erosion or cracking and remained intact when the Al_2O_3 in the propellant plated out over the nozzle and cracked and fell off on cooldown.

To test the theory that the propellant alumina which plates out over the nozzle is itself an effective thermal barrier during the coated nozzle test, the water flow rate was reduced by 52% under that predicted safe during start transient conditions. Post-test inspection revealed appearance to be nearly identical to the previous test with no evidence of loss to coating.

On the basis of testing and analysis performed during the program the conclusions are:

1. The alumina-based thermal barriers developed are capable of surviving the environment of the Minuteman exhaust gases and functioning as a thermal barrier to provide a substantial reduction in heat flux to the coolant.

2. The alumina in the propellant plates out over the nozzle in a uniform manner, reaches a surface temperature ~3700°F at which time it melts and sluffs off. At tailoff it increases in thickness; then on cooldown it shrinks and cracks.

3. By employing a plasma-arc-sprayed thermal barrier and taking advantage of the effect of propellant plated alumina in reducing the heat flux, water flow rates can be reduced at least by 52% after 10 seconds.

The alumina in the propellant plates out on the nozzle walls up to 3/8 in. thick. Its weight and its effect on performance are not known. The employment of thermal barrier materials capable of operating at a surface temperature >4500°F would prevent the alumina from plating out. In addition, a thermal barrier operating at >4500°F would provide a greater thermal resistance and thereby reduce coolant requirements. For these reasons, it is recommended that higher temperature thermal barriers be developed for use on water-cooled nozzles. To further reduce coolant requirements, it is recommended that studies be initiated for developing other methods of obtaining more efficient utilization of the coolant.

4. The total bulk temperature rise of the coolant was low (∿40°F) in all cases in relation to the temperature rise to the point of boiling (∿400°F). This was because of the high flow rates required by this chamber design to prevent burnout.

REFERENCES

1. Parker, W.J., et al, "Flash Method of Determining Thermal Diffusivity, Heat Capacity, and Thermal Conductivity", Journal of Applied Physics, 32, 1679 (1961).

2. Grisaffe, S.J., "Analysis of Shear Bond Strength of Plasma Sprayed Alumina Coatings on Stainless Steel," NASA TND-3113, November 1965.

3. Harrington, D.G., and Adair, S.E., "Development of Thermal Barrier Coatings for Regeneratively Cooled Rocket Engine Thrust Chambers (U)", BSD-TDR-119, Contract AF 04(647)-652 SA4, 20 June 1963 (C).

4. Zorich, D.R. and Bassoni, A.A., "Description of a Gas-Pressurized Water-Flow System for the NASA Water-Cooled Nozzle Program", Technical Report AFRPL-TR-68-163, September 1968.

5. Beck, L.H., Massier, P.F., and Gies, H.L., "Convective Heat Transfer in a Convergent-Divergent Nozzle", Technical Report 32-415, 15 November 1963, Jet Propulsion Laboratory, Pasadena, California.

6. JANEF Thermochemical Data, Dow Chemical Co., Midland, Michigan.

7. Ignition of Metals in Oxygen, E.S. White, J. J. Ward, Battelle Institute, DMIC Report 224, 1 Feb., 1966.

8. Oxide Ceramics, E. Ryshkewitch, Academic Press, 1960.

9. Engineering Properties of Ceramics, Lynch, Ruderu, Duckworth, Battelle Memorial Institute, AFML TR-66-52, June 1966.

10. High Temperature Inorganic Coatings, John Huminick, Jr., Reinhold Publishing Co., New York, 1963.

11. Properties of Refractory Materials: Collected Data and References LMSD-2466, Lockheed Aircraft Corporation, Sunnyvale, Calif.

12. Unpublished Data, Aerojet-General Corporation, Sacramento, Calif.

13. Summary of 13th Refractory Composites Working Group Meeting, AFML TR-68-84, Captain Blvin Beardslee.

14. Engineering Properties of Ceramics, Lynch, Ruderu, Duckworth, Batelle Memorial Institute, AFML TR-66-52, June 1966.

15. High Temperature Inorganic Coatings, John Huminick, Jr., Reinhold Publishing Co., New York, 1963.

16. Oxide Ceramics, E. Ryshkewitch, Academic Press, 1960.

17. Unpublished Data, Aerojet-General Corporation, Sacramento, Calif.

18. Summary of 13th Refractory Composites Working Group Meeting, AFML-TR-68-84, Captain Elvin Beardslee.

19. Properties of Refractory Materials: Collected Data and References LMSD-2466, Lockheed Aircraft Corporation, Sunnyvale,Calif.

BIBLIOGRAPHY

1. Plasma Arc Materials Testing for Re-Entry, Aerospace Corp., Report TDR-269(4240-10)-11, June 1964.

2. JANAF Thermochemical Tables

3. Ignition of Metals in Oxygen, Battelle Memorial Institute - DMIC Report 224, Feb. 1966.

4. Aluminide and Beryllide Protective Coatings for Tantalum - Paper presented at AIME Conference on High Temp Materials, April 1961, by D. D. Lawthers and L. Sama.

5. Gas-Metal Reactions in Rocket Nozzles, Air Force Materials Lab Report ASD-TDR 62-327, May 1963.

6. Chemical Corrosion of Rocket Liner Materials and Propellant Performance Studies, Vol. I and II, Philco Aeronautronics Lab., Pub. No. V-2384, Dec. 1963.

7. Thermal Barrier Liners in High Performance Rocket Engines - D.G. Harrington - Paper Presented to AIAA Propulsion Conference, Colo. Springs, June 1965.

8. Alumina - Metal Cermets, T.S. Serlin, 1960.

9. Chromium-Alumina Base Cermets, C. L. Marshall, 8 & 9 Edited by J. R. Tinklepaugh, 1960.

10. Analysis of Bonding Mechanism Between Plasma Sprayed Tungsten and Stainless Steel Substrate, S. J. Grisaffe, NASA TND 2461 - Sept. 1964.

11. Analysis of Shear Bond Strength of Plasma Sprayed Alumina Coatings on Stainless Steel, S. J. Grisaffe, NASA TND-3113, Nov. 1965.

12. Investigation of Mechanisms for Oxidation Protection and Failure of Intermetallic Coatings for Refractory Metals, Aeronutronic Res. Lab, AST-TDR-63-753, Sept. 1965.

13. Properties of Refractory Materials: Collected Data and References - Lockheed Aircraft Corp., LMSD 2466, dtd 24 June 1958.

14. Tungsten and Rocket Motors, Stanford Research Institute - Report to Special Projects Office, Dept. of the Navy, Contract No. NORD-18619(FBM) SRI Project SW-2785, dtd 23 March 1961.

TABLE I. THERMOCHEMICAL DATA FOR CERTAIN METAL OXIDES

	Melting Point, °C	Boiling Point, °C	Density, gm/cc	Heat of Fusion K cal/mol
Cr_2O_3	2435	4000	5.21	-
WO_3	1473	-	7.16	15.0
Al_2O_3	2045	2980	3.96	26.0
MoO_3	795	1155	4.69	-
ZrO_2	2715	-	5.6	20.8
NiO	1990	-	6.65	12.1

	F, K cal/mol		
	1227°C (2240°F)	1727°C (3140°F)	2227°C (4040°F)
ZrO_2	-193.8	-172.3	-150.07
WO_3	-111.4	-83.6	-56.5
Cr_2O_3	-178.6	-147.9	-115.6
MoO_3	-159.7	-95.9	-88.1
Al_2O_3	-286.08	-247.6	-209.8
NiO	-25.8	-15.1	-3.7

TABLE II. COMPATIBILITY OF CANDIDATE MATERIALS WITH THE EXHAUST GAS SPECIES

Reaction		Free Energy of Reactions, F, Kcal-mole^{-1} to 500 psi		
		2000°F	3000°F	4000°F
$3H_{2(g)} + Al_2O_3$	$3H_2O_{(g)} + 2Al$	+172	-153	+136
$6H_{(g)} + Al_2O_3$	$2Al + 3H_2O_{(g)}$	- 63	- 42	- 36
$6HCl_{(g)} + Al_2O_3$	$3H_2O_{(g)} + 2AlCl_{3(g)}$	+ 54	+ 60	+ 71
$2HCl_{(g)} + W$	$WCl_{2(g)} + H_{2(g)}$	+ 74	+ 69	+ 65
$H_2O_{(g)} + Al_2O_3$	$2Al\ O_2H_{(g)}$	+257	+230	+207
$2CO + Al_2O_3$	$Al_2O_{(g)} + 2CO_{2(g)}$	+171	+148	+123
$2W + 2CO$	$W_2C + CO_2$		+ 12	+ 31
W + H	No Reaction			
$3W + 9H_2O$	$W_3O_{9(g)} + 9H_2$			+ 42
$Mo + 2CO$	$MoC + CO_2$	- 0.5	- 11	+ 8
Mo + H	No Reaction			
$Mo + 3H_2O$	$MoO_3 + 3H_2$	+ 27	+ 12	- 5
$W + 3CO_2$	$WO_3 + 3CO$	+ 9.7	+10.4	+ 2.7
$Mo + 3CO_2$	$MoO_3 + 3CO$	+ 31	+ 9.5	-13.5
$2\ Ni + 2\ CO_2$	$2NiO + 2CO$	- 7	+ 25	
$Ni + H_2O$	$NiO + H_2$	- 16	+ 18	
$2Ni + O_2$	$2NiO$	- 50	- 30	
$4\ Cr + 6\ CO_2$	$2CrO_2 + 6CO$	-128	-132	
$CR + 3H_2O$	$CrO_2 + 3H_2$	- 61	- 51	
$4CR + 3O_2$	$2CrO_2$	-393	-329	

TABLE III. PROPERTIES OF THERMAL BARRIER COATINGS - 1st SERIES DISC SPECIMENS

Spec. No.	Al_2O_3 Wt %	Mo Wt %	W Wt %	Cr Wt %	Coating Thickness, in.	Primer Composition	Primer Thickness in.	Surface Temp, °F	Regression Rate, mil/sec	Thermal Resistance t/K in^2-sec-°F/Btu	K x 10^5 (Thermal Cond.) Btu/sec/in^2/°F/in.
1 (1)	65		35		.013	$NiAl_3$	.005	3780	.073	432.4	3.01
2 (1)	48		52		.013	$NiAl_3$	.005	3480	.064	382.4	3.40
3 (1)	20		70		.019	$NiAl_3$	.005	3700	.100	419.1	4.53
4	20		80		.025	$NiAl_3$	.005	3830	.173	440.8	5.67
5	15		85		.032	$NiAl_3$	.005	4080	.250	482.4	6.63
6	84	16			.011	$NiAl_3$	.005	3650	.064	510.8	2.17
7	70	30			.012	$NiAl_3$	.005	3650	.055	510.8	2.35
8	50	50			.016	$NiAl_3$	.005	3620	.091	405.8	3.95
9	30	70			.025	$NiAl_3$	.005	3780	.145	432.4	5.78
10(2)	20	80			.033	$NiAl_3$	.005				
11(2)	9	91			.050	$NiAl_3$	.005				
12	71			29	.014	$NiAl_3$	.005	3650	.105	510.8	2.74
13	50			50	.020	$NiAl_3$	.005	3290	.200	350.8	5.70
14	30			70	.030	$NiAl_3$	.005	3150	.240	327.4	9.16
15	15			85	.042	$NiAl_3$	.005	3230	.410	340.8	12.30
16	70	30			.014	None		3615	.036	428.1	3.27
17	70	30			.014	Nichrome	.009	3660	.073	419.1	3.34
18	70	30			.014	$NiAl_3$	.005	3700	.064	419.1	3.34

(1) Specimens 1, 2 and 3 were run in a nitrogen-hydrogen plasma. All others were run in a nitrogen plasma.
(2) Coatings cracked and parted from steel backing plates on Specs 10 and 11 prior to thermal testing.
(3) Heat flux 6 Btu/$in.^2$-sec-°F.

TABLE IV. PROPERTIES OF THERMAL BARRIER COATINGS - 2nd SERIES DISC SPECIMENS

Spec. No.	$NiAl_3$ Primer Thickness, in.	Coating Thickness, in.	Coating Composition Wt %	Surface Temperature,(4) °F	Regression Rate, mil/sec	Thermal Resistance t/k in^2-sec-°F/Btu	K x 10^5 (Therm. Cond.) Btu-in/sec in^2 °F
19	.005	.009	$65Al_2O_3/35W$	3240	.033	296	3.04
20	.005	.009	$48Al_2O_3/52W$	3220	.025	280	3.21
21	.005	.012	$30\ Al_2O_3/70W$	3480	.050	317	3.79
22	.005	.017	$15Al_2O_3/85W$	3485	.083	3.8	5.34
23	.005	.005	$84Al_2O_3/16Mo$	3345	.0125	298	1.68
24	.005	.0065	$70Al_2O_3/30Mo$	3355	.0125	299	2.17
25	.005	.0095	$50Al_2O_3/50Mo$	3545	.050	327	2.90
26	.005	.0155	$30Al_2O_3/70Mo$	3485	.092	318	4.87
27	.005	.007	$71Al_2O_3/29Cr$	3330	.021	296	2.36
28	.005	.027	$30Al_2O_3/70Cr$	3280	.158	288	9.37
29	.005	.003 .0025	Ni Coated Al_2O_3(1) Al_2O_3(2)	3395	.0058	305(3)	1.97(3)
30	.005	.003 .004	Ni Coated Al_2O_3(1)(2) $70Al_2O_3/30Mo$	3365	.0085	301(3)	2.16(3)
31	.005	.003	$85W/12Al_2O_3/3Si$	3250	.087	284	5.98
32	.005	.017	$(85W/12Al_2O_3/3Si)$-97% Cu - 3%	2995	.100	248	6.45
33	.005	.017	(85W/12Al 0 /3Si)-95% Cu - 5%	2930	.107	239	7.23

(1) First of two layers.
(2) Second layer
(3) Values are for two-layer composite coatings.
(4) Plasma arc heat flux at specimen surface was 7 Btu/$in.^2$-sec-°F.

TABLE V. THERMAL CONDUCTIVITY OF PLASMA SPRAYED MATERIALS AS DETERMINED BY THERMAL DIFFUSIVITY MEASUREMENTS

Material	Temperature, °F		
	RT	750	1400
Al_2O_3			1.61
Ni Coated Al_2O_3			3.19
80 Al_2O_3/20 Ni			1.42
Nickel Aluminite (Metco 404)			11.2
84 Al_2O_3/16 Mo	2.43	1.53	1.82
50 Al_2O_3/50 Mo	2.79	2.10	2.71
			4.92
30 Al_2O_3/70 Mo	4.28	3.16	4.55
Al_2O_3/Mo wires			1.74

K = Btu-in./sec.in.^{2} F x 10^{-5}

TABLE VI. THERMAL BARRIER ADHERENCE EVALUATION

Specimen No.	Surface Finish, Microinches RMS	Primer	Coating (Weight %)	Ultimate Shear Strength, psi
1	25	None	70 Al_2O_3/30 Mo	664
2	25	Ni Cr	70Al_2O_3/30 Mo	1245
3	25	None	70Mv/30Al_2O_3	1250
4	25	Ni Cr	70Mo/30Al_2O_3	1110
5	250	None	70Al_2O_3/30 Mv	744
6	240	Ni Cr	70Al_2O_3/30 Mo	1542
7	250	Mo	70Al_2O_3/30Mo	1010
8	240	$NiAl_3$(wire)	70Al_2O_3/MO Mo	2044
9	250	$NiAl_3$(powder)	70Al_2O_3/30 Mo	1670
10	250	None	70Mo/30Al_2O3	1998
11	250	Ni Cr	70M /30Al_2O_3	1750
12	250	No	70Mo/30Al_2O_3	1198
13	250	$NiAl_3$(wire)	70 M./30Al_2O_3	3320
14	250	$NiAl_3$(Powder)	70 Mv/30Al_2O_3	2480

TABLE VII. THERMAL SHOCK TEST RESULTS - 1st SERIES - 5 TUBE SPECIMENS

Disc No. Ref.	Spec. No.	$NiAl_3$ Primer Thickness, in.	Coating Thickness, in.	Coating Composition, Wt %	Plasma Arc Gas Mixture(3)			Coating Regression		Condition of Coatings Following 10 Cycle Thermal Shock Tests. Observations under 40X Microscope
					Carrier N_2, scf^2/hr	Introduced O_2, scf/hr	Gases C_2H_2, scf/hr	60 sec Continuous Exposure, mil/sec	10 Cycles - 10 sec in Plasma Arc/10 sec out, mil/sec	
19	W1	.005	.009	$65Al_2O_3/35W$	100	130	50	.05	.07	No cracks. Molten ceramic, Al_2O_3, and WO_3 (yellow) were observed.
22	W2	.005	.008	$15Al_2O_3/85W$	100	130	50	.017	.06	No cracking. Some molten Al_2O_3 observed but less than Spec. W1.
24	W3	.005	.005	$70Al_2O_3/30$ Mo	100	130	50	.017	.01	No apparent cracking or melting of Al_2O_3 Copper colored area observed.
25	W4	.005	.008	$50Al_2O_3/50$ Mo	100	130	50	Nil	.12(4)	No cracking in coating. Molten areas of Al_2O_3 which were cracked and flaking off were seen.
26	W5	.005	.012	$30Al_2O_3/70$ Mo	100	96.5	37.5	.017	.05	No apparent cracking. Molten areas of Al_2O_3 were observed.
29	W6	.005	.003 .003	Ni Coated Al_2O_3(1) Al_2O_3(2)		100	37.5	Nil	Nil	No visible cracks.

(1) First of two layers.
(2) Second layer.
(3) Produced a heat flux of 6 Btu/$in.^2$-sec-°F at specimen surface.
(4) Test stopped during fifth cycle because of tube leak.

TABLE VIII. THERMAL SHOCK TEST RESULTS - 2nd SERIES - 5-TUBE SPECIMENS

Spec. No.	NiAl Primer Thickness, in.	Coating Thickness, in.	Coating Composition, Wt %	Plasma Arc Gas Mixture[1]			Coating Regression	
				Carrier	Introduced Gases		150 sec Continuous Exposure, mil/sec	25 Cycles Plasma Arc 10 sec - In/5 sec - Cut, mil/sec
				N_2, scf/hr	O_2, scf/hr	CH_4, scf/hr		
X7	.002	.003 .003	Ni Coated Al_2O_3 Al_2O_3	100	100	50	(2)	.004
X8	.002	.003	Ni Coated Al_2O_3 Al_2O_3	100	100	50	.0033	.0008
X9	.002	.003 .0025	Ni Coated Al_2O_3 Al_2O_3	100	100	50	.0033	.0012
X10	.002	.006	70 Al_2O_3/30 Mo	100	100	50	.0066	.0200
X11	.002	.006	70 Al_2O_3/30 Mo	100	100	50	.0066	.0160
X12	.002	.006	70 Al_2O_3/30 Mo	100	100	50	.0066	.0180
X13	.002	.003 .003	70 Al_2O_3/30 Mo Al_2O_3	100	100	50	.0033	.0260
X14	.002	.003 .002	70 Al_2O_3/30 Mo Al_2O_3	100	100	50	.0035	.0140
X15	.003	.003 .004	70 Al_2O_3/30 Mo Al_2O_3	100	100	50	.0013	.0040
X16	.003	.003 .003	80 Al_2O_3/20 Ni Al_2O_3	100	100[3]	50[3]	.0033	.0080
X17	.003	.003 .003	80 Al_2O_3/20 Ni Al_2O_3	100	100	50	.0133	.0020
X18	.003	.003 .003	80 Al_2O_3/20 Ni Al_2O_3	100	100	50	Nil	Nil
X19	.003	.005	Al_2O_3	100	100	50	.0066	.0020

(1) Heat flux adjusted to 6 Btu/in^2-sec at specimen surface before introduction of O_2 and CH_4. Nominal surface temperature 3000°F. t/k = 250 in^2-sec-°F/Btu.
(2) No regression. Al_2O_3 powder fed into plasma arc for first 30 sec of test caused buildup on specimen.
(3) CH_4 introduced through powder feed hole in nozzle; O_2 introduced in nozzle ring. Gas introduction points were reversed on all other specimens.

TABLE IX. COMPARISON OF REGRESSION RATES OF Ni-COATED Al_2O_3 AND $80Al_2O_3/20Ni$ COATINGS

Type of Specimen	Spec. No.	Coating Layer Composition	Coating Layer Thickness, In.	Plasma Arc Exposure: Heat Flux, Btu/in^2-sec	Plasma Arc Exposure: No. of Cycles	Plasma Arc Exposure: Total, Sec	Regression Rate Cycle Test, mil/sec	Regression Rate 150 Sec Test, mil/sec
5-Tube	W6	NiAl Ni-Coated Al_2O_3 Al_2O_3	0.005 0.003 0.003	6.0	10 cyc. - 10 sec ea.	100	Nil	Nil(3)
5-Tube	X8	NiAl Ni-Coated Al_2O_3 Al_2O_3	0.002 0.003 0.003	6.0	25 cyc. - 10 sec ea.	250	0.0008	0.0033
5-Tube	X9	NiAl Ni-Coated Al_2O_3 Al_2O_3	0.002 0.003 0.0025	6.0	25 cyc. - 10 sec ea.	250	0.0012	0.0033
Disc	29	NiAl Ni-Coated Al_2O_3 Al_2O_3	0.005 0.003 0.0025	7.0	10 cyc. - 10 sec ea.	100	0.0058 0.0019(1)	0.0022(1)
5-Tube	X16	NiAl $80Al_2O_3/20$ Ni Al_2O_3	0.003 0.003	6.0	25 cyc. - 10 sec ea.	250	0.0080	0.0033
5-Tube	X17	NiAl $80Al_2O_3/20$ Ni Al_2O_3	0.003 0.003 0.003	6.0	25 cyc. - 10 sec ea.	250	0.0020	0.0133
5-Tube	X18	NiAl $80Al_2O_3/20$ Ni Al_2O_3	0.003 0.003	6.0	25 cyc. - 10 sec ea.	250	Nil	Nil
Disc	34	NiAl 80 $Al_2O_3/20$ Ni Al_2O_3	0.005 0.003 0.0025	7.0	1 cyc. - 30 sec 7 cyc. - 10 sec ea.	100	0.030	
Disc	35	NiAl $80Al_2O_3/20Ni$ Al_2O_3	0.005 0.003 0.0025	7.6	1 cyc. - 30 sec 7 cyc. - 10 sec ea.	100	0.020 0.012(2)	0.0055(2)

(1) Average for Ni-Coated Al_2O_3
(2) Average for $80Al_2O_3/20Ni$
(3) 60 sec exposure.

TABLE X. WIRE-REINFORCED COATING TESTS - DISC SPECIMENS

Disc Spec. No.	Coating Composition: Primer NiAl	Mo Wires Al_2O_3	Top Coat Al_2O_3	Wire Feed: Vibrator Setting	Wire Feed: Ft^3/hr Argon	Surface[1] Temperature °F: Max.	Surface[1] Temperature °F: Ave.	No. of Cycles[2]	Regression Rate, Mil/sec	Observations: During Test	Observations: After Test Inspect at 40X
A	.002	.003	.002	10	20	3300	3280	25	.002		Small cracks
B	.002	.003	.002	10	10	3340	3290	25	0		One small crack
C	.002	.005		10	10	3240	3240	25	.004		No cracks
D	.002	.005		10	10	3240	3230	25	0		No cracks
E	.002	.003	.002	7	6	3320	3315	25	0	Slight melting at 3300°F maximum	
F	.002	.003	.002	7	6	3340	3310	25	0		Slight melt, small crack
G	.002	.005		7	6	3320	3280	25	0		Melting, small cracks
H	.002	.005		7	6	3340	3320	21	.0009	Plasma nozzles shorted out; specimen discolored	

(1) Heat Flux 6.9 Btu/in^2-sec-°F
(2) 10-sec exposure, 5-sec cooldown.

TABLE XI. OXIDATION AND THERMAL SHOCK TESTS WIRE-REINFORCED COATINGS - 5 TUBE SPECIMENS

5-Tube Specimen No.	Primer Ni Al	Mo Wires Al_2O_3	Ni Coated Al_2O_3	20 Ni 80 Al_2O_3	50 Mo 50 Al_2O_3	Top Coat Al_2O_3	Surface Temperature, °F Max	Surface Temperature, °F Ave.	No. Cycles	Regression Rate, Mils/sec	Observations During Test	Observations After Test Inspect at 10X
I	.002		.020			.010	3525		23	.000002		Melting - cracks in topcoat.
J	.002		.020			.010	3400	3120	23	.000002		Several deep cracks.
K	.002		.020			.010	3310	2190	21	.000004		Microcracks
L	.002			.010		.010	3350	3090	24	.000002		Slight melt, microcracks.
M	.002			.010		.010	3290	3120	24	.0000008		Microcracks
N	.002			.010		.010	3200	3080	25	-		Slight melt, microcracks.
O	.002				.035		3780	3620	25	.000064	Too hot - melting, spalling, oxidation.	Melt, oxidation, cracks.
P	.002				.035		3680	3600	26	.000038	Too hot - melting, spalling, oxidation.	Melt, oxidation, cracks.
Q	.002	.031					3250	3110	25	0		Copper & Copper oxide, small cracks.
R	.002	.031					3710	3350	25	.000004	Too hot, slight spalling.	Cracks, appears dirty, voids.
S	.002	.031					3590	3400	25	.0000024	Too hot, slight spalling.	Cracks, appears dirty, voids.
T	.007	.005					3030	3000	25	0		No cracks; voids, foreign matter.
U	.002	.005					3030	3000	25	0		No cracks; voids, foreign matter.

TABLE XII. INSTRUMENTATION SPECIFICATION LIST

INSTRUMENTATION INSTRUCTION SHEET				TEST NUMBER	PROJECT TITLE NOZZLE, H_2O COOLED				DATE 7/3/68
ITEM NR.	PARAMETER	LOCATION	TRANSDUCER TYPE	TRANSDUCER RANGE	CALIBRATION RANGE	FREQUENCY RESPONSE	RECORDING SYSTEM	CHANNEL	REMARKS
26/F1A	Thrust	Fwd. Closure	Bridge-Resist. Type	0-50000 lb	0-50000 lb	50 cps	Dig OSC	20	Gain Setting -28.3
27/F1B	"	"	"	"	"	"	Dig	22	" " "
28/PC-1	Press. Ign.	"	"	0-1000 psig	0-1000 psig	"	meter Dig OSC	24	" " "
29/PC-2	"	"	"	"	"	"	Dig	26	" " "
30/PCI-3	Press.	Coolant In.	"	"	"	"	Dig OSC	28	" " "
31/PCO-4	"	Coolant Out	"	"	"	"	meter Dig OSC	30	" " "
32/PWT-5	"	Water Tank	"	"	"	"	meter Dig OSC	32	" " "
33/PCR-6	"	Reg. Press.	"	"	"	"	Dig meter	34	" " "
34/LP-1	Position	Coolant Out	Linear Pot	0-2.5 inch	0-2.5 inch	"	meter Dig OSC	0	
35/CW-1	Vol. Flow	Cool. Flow	Turbine Type	101.12-1266.21 gpm	25-315 cps	"	"	1	
1/TCN1	Temp	Noz. Tube	Cu/C	-300°F to 750°F	0° to 250°F	3 cps	Dig	21	Gain Setting -10.0
2/TCN2	"	"	"	"	"	"	"	23	" " "
3/TCN3	"	"	"	"	"	"	"	25	" " "
4/TCN4	"	"	"	"	"	"	"	27	" " "
5/TCN5	"	"	"	"	"	"	"	29	" " "
6/TCN6	"	"	"	"	"	"	"	31	" " "
7/TCN7	"	"	"	"	"	"	"	33	" " "
8/TCN8	"	"	"	"	"	"	"	35	" " "
9/TCCI	"	Coolant In	"	"	"	"	Dig OSC	37	" " "

Table XII
(Page 1 of 2)

TABLE XII. INSTRUMENTATION SPECIFICATION LIST (Cont.)

INSTRUMENTATION INSTRUCTION SHEET				TEST NUMBER		PROJECT TITLE NOZZLE, H_2O COOLED			DATE 7/3/68
ITEM NR.	PARAMETER	LOCATION	TRANSDUCER TYPE	TRANSDUCER RANGE	CALIBRATION RANGE	FREQUENCY RESPONSE	RECORDING SYSTEM	CHANNEL	REMARKS
10/TCCI-10	Temp	Coolant In	Cu/C	-300°F to 750°F	0° to 250°F	3 cps	Dig	39	Gain Setting -10.0
11/TCCI-11	"	"	"	"	"	"	"	40	" " "
12/TCCI-12	"	"	"	"	"	"	"	41	" " "
13/TCCI-13	"	"	"	"	"	"	"	42	" " "
14/TCCI-14	"	Coolant Out	"	"	"	"	meter Dig OSC	43	" " "
15/TCCI-15	"	"	"	"	"	"	Dig	44	" " "
16/TCCI-16	"	"	"	"	"	"	"	45	" " "
17/TCCI-17	"	"	"	"	"	"	"	46	" " "
18/TCCI-18	"	"	"	"	"	"	"	47	" " "
19/TCCI-19	"	H_2O Tank	"	"	-50°F to 150°F	"	"	48	" " "
X-1	Ign-Pulse		Critical Event				Dig OSC	C-1	
X-2	0.5 pps timing		Normal Event				Dig	N-30	
X-3	0.05 pps timing		"				"	N-31	
X-4	0.0125 pps timing		"				"	N-32	
X-5	2 pps timing		"				OSC		
X-6	10 pps timing		"				OSC		
	1. Flowmeter converter pulse output shall be recorded on oscillograph.								

Table XII
(Page 2 of 2)

TABLE XIII. HIGH-TEMPERATURE OXIDE COATINGS

Material	Melt Point, °F	Eutectic Al_2O_3 °F	Thermal Conductivity Btu/Hr/Ft/°F 2000°F	3000°F	4000°F	% Thermal Expansion RT to 2000°F	3000°F	4000°F	Remarks - Compatibility with Al_2O_3, W Gas Species
MgO	5160 (14)	3630 (16) 3470 (15)	2.2	2.3 (14)		1.4	2.4	3.4	72% dense. No reaction with Al_2O_3, W or gas species. Vaporization occurs by dissociation into elements (15).
Cr_2O_3	4170 (14)	3720 (16)	7.2 (15)	-		0.7	1.1	1.5(14)	No reaction with Al_2O_3, W, Co or H_2. Poor thermal shock (19).
Al_2O_3	3720 (15)	-	0.69	0.69	0.69 (17)	0.88	1.5	- (14)	80% dense.
ZrO_2	4700 (14)	3090 (15) 3460 (16)	0.47	0.61	0.35 (17)	1.2	1.6	2.0(14)	85% dense. Reacts with atomic hydrogen at high temp. (14) No reaction with Al_2O_3 or W.
$HfO_2/5\%$ Y_2O_3	5090 (15)	-	0.65	0.35	0.35 (17)	1.0	1.7	2.4(14)	85% dense. Probable reaction with H at high temp. Similar to ZrO_2 chemically
CeO_2	3180 (15)	-	-	0.5 (14)	-	1.3	2.2 (14)	-	Reacts with H_2O at high temp. (14).
$CaO \cdot ZrO_2$	4250 (14)	-	-	-	-	1.1 (14)	-	-	Reacts with CO above 3100°F (14). No reaction with Al_2O_3 W, H.
$CaO \cdot Cr_2O_3$	3940 (14)	-	-	-	-	-	-	-	No reaction with W, Al_2O_3, Co, H_2.
$CaO_2 \cdot Cr_2O_3$	4420 (14)	-	-	-	-	-	-	-	No thermodynamic free energy data available on CeO. Mixture with Cr_2O_3 may react with H_2O at high temp.
$MgO \cdot Zr_2O_3$	3900 (14)	-	-	-	-	-	-	-	No reaction with Al_2O_3, W or gas species.
$SrO_2 \cdot ZrO_2$	5070 (18) 4890 (14)	-	-	-	-	1.1 (14)	-	-	Reacts with Al_2O_3 at elevated temp. (14). No reaction with W, H or CO.
BeO	4660 (15)	3430 (15)	10.0 (14)	5.0 (14)	-	0.9	1.4	2.7 (14)	Toxic. Reacts with water above 3000°F.
ThO_2	5800 (15)	3180 (15)	1.8	1.2	1.1 (14)	0.9	1.5	2.3 (14)	Poor thermal shock, radiactive (15)
W	6170	-	36	30	30 (17)	.37	.65	.85(17)	90% dense.

TABLE XIV. COMPATIBILITY OF OXIDE COATINGS WITH SOME EXHAUST GAS SPECIES
PROPELLANT ANP 2746

	Δ F, K cal at 400 psia			
Temp.	2000°F	3000°F	4000°F	
$MgO + 2HCl \longrightarrow MgCl_2 + H_2O$	+9	+13	+10	Reference (6)
$MgO + 2H_2O \longrightarrow 2MgOH + H_2$	+136	+117	+97	"
$2MgO + H_2 \longrightarrow 2Mg\ OH$	+95	+74	+72	"
$MgO + CO \longrightarrow Mg + CO_2$	+62	+48	+35	"
$MgO + H \longrightarrow MgOH$	+13	+13	+9	"
$ZrO_2 + 2HCl \longrightarrow ZrO_2 + H_2O$	+111	+95	+54	"
$2ZrO_2 + H_2O \longrightarrow 2Zr\ OH + O_2$	No data	$\longrightarrow$		"
$2ZrO_2 + H_2 \longrightarrow 2Zr\ H + 2O_2$	+591	+540	+426	"
$ZrO_2 + 4H \longrightarrow 2H_2O + Zr$	-42	-14	-5	"
$ZrO_2 + 2CO \longrightarrow 2CO_2 + ZrC$	+115	+117	+117	"
$HfO_2 + 2HCl \longrightarrow HfCl + H_2O$	No data	$\longrightarrow$		(Reference 6 and 7)
$HfO_2 + 2H \longrightarrow Hf + 2H_2O$	+116	+111	-	"
$HfO_2 + 4H \longrightarrow Hf + 2H_2$	-38	-9	-	"
$2HfO_2 + 2CO \longrightarrow 2HfC + 3O_2$	+134	+184	+132	"
$CaO + H_2 \longrightarrow Ca + H_2O$	+73	+63	+48	"
$Cr_2O_3 + 3H \longrightarrow 2Cr + 3H_2O$	+55	+49	+40	"
$SrO + H_2 \longrightarrow Sr + H_2O$	+65	+55	-	"

TABLE XIV (cont.)

	Δ F, K cal at 400 psia			
	2000°F	3000°F	4000°F	
$CaO + Co \longrightarrow Ca + CO_2$	+74	+68	+57	Reference 6
$Cr_2O_3 + 3CO \longrightarrow 2Cr + 3CO_2$	+58	+64	+64	"
$SrO + CO \longrightarrow Sr + CO_2$	+66	+60	-	"
COMPATIBILITY OF OXIDE COATINGS WITH TUNGSTEN				
$Al_2O_3 + W \longrightarrow WO_3 + 2Al$	+175	+164	+153	Reference 6
$Cr_2O_3 + W \longrightarrow WO_3 + 2Cr$	+67	+65	+59	"
$3ZrO_2 + 2W \longrightarrow 2WO_3 + 3Zr$	+360	+350	+338	"
$3HfO_2 + 2W \longrightarrow 2WO_3 + 3Hf$	+372	+365	-	"
$3MgO + W \longrightarrow WO_3 + 3Mg$	+81	+65	+53	"
$3CaO + W \longrightarrow WO_3 + 3Ca$	+231	+205	+165	"
$3SrO + W \longrightarrow WO_3 + 3Sr$	+210	+180	-	"

No Free energy data available on CeO_2, chlorides or hydroxides of Ca, Hf, Cr, or Sr.

TABLE XV. MICROPROBE ANALYSIS - EXPERIMENTAL COATINGS

A	BARE GRIT BLASTED					
	Primer	1st	2nd	3rd	4th	Propellant
B	$NiAl_3$	Ni-Coated Al_2O_3	Al_2O_3	HfO_2	-	Al_2O_3
C	"	"	"	"	W	"
D	"	"	"	$SrO \cdot ZrO_2$	-	"
E	"	"	"	"	W	"
F	"	"	"	ZrO_2	-	"
G	"	"	"	"	W	"

TABLE XVI. WATER FLOW DATA FOR TEST NO. 3

Approx. Time, sec	$P_{chamber}$, psia	P_{tank}, psig	P_{in}, psig	P_{out}, psig	W, gpm	W, lb/sec	
Start	345	1085	823	357	1430	198	
16.1	375		819	355	1420	197	(1)
19.6	382		950	708	1025	142	
25.0	392		960	712	1020	142	(2)
26.6	392	1100	1022	893	730	101	(3)
32.0	393	956	915	800	625	87	
35.0	389	900	850	745	655	91	
40.0	383	825	780	680	640	89	
45.0	373	765	695	585	700	97	(4)
47.0	368	747	659	500	805	112	
52.0	371	680	603	459	770	107	
57.0	369	630	560	422	757	105	
62.0	368	590	520	394	728	101	
63.0	Web Time						
66.0	0						

(1) First flow reduction maneuver

(2) Second Flow reduction maneuver

(3) Reg. pressure goes to zero

(4) Downstream valve opened to raise flow rate.

TABLE XVII. BURNOUT HEAT FLUX RATIO AT SEVERAL POINTS - TEST NO. 3

Time, sec	W, gpm	W, lb/sec	R_{Bo} Test 47.5°F	R_{Bo} Test 70°F	R_{Bo} Predicted 70°F
.8 - 1.2	1423.2	197.5	.34	.35	0.37
15.0 - 15.4	1420.6	197.2	.35	.37	0.37
21.0 - 21.5	1017.9	141.3	.44	.46	0.44
31.5 - 32.0	681.2	94.6	.63	.66	0.60
41.5 - 42.0	626.3	86.9	.71	.74	0.64
44.1 - 44.25	610.9	84.8	.74	.78	0.66
61.5 - 62.0	728.9	101.1	.66	.69	0.97

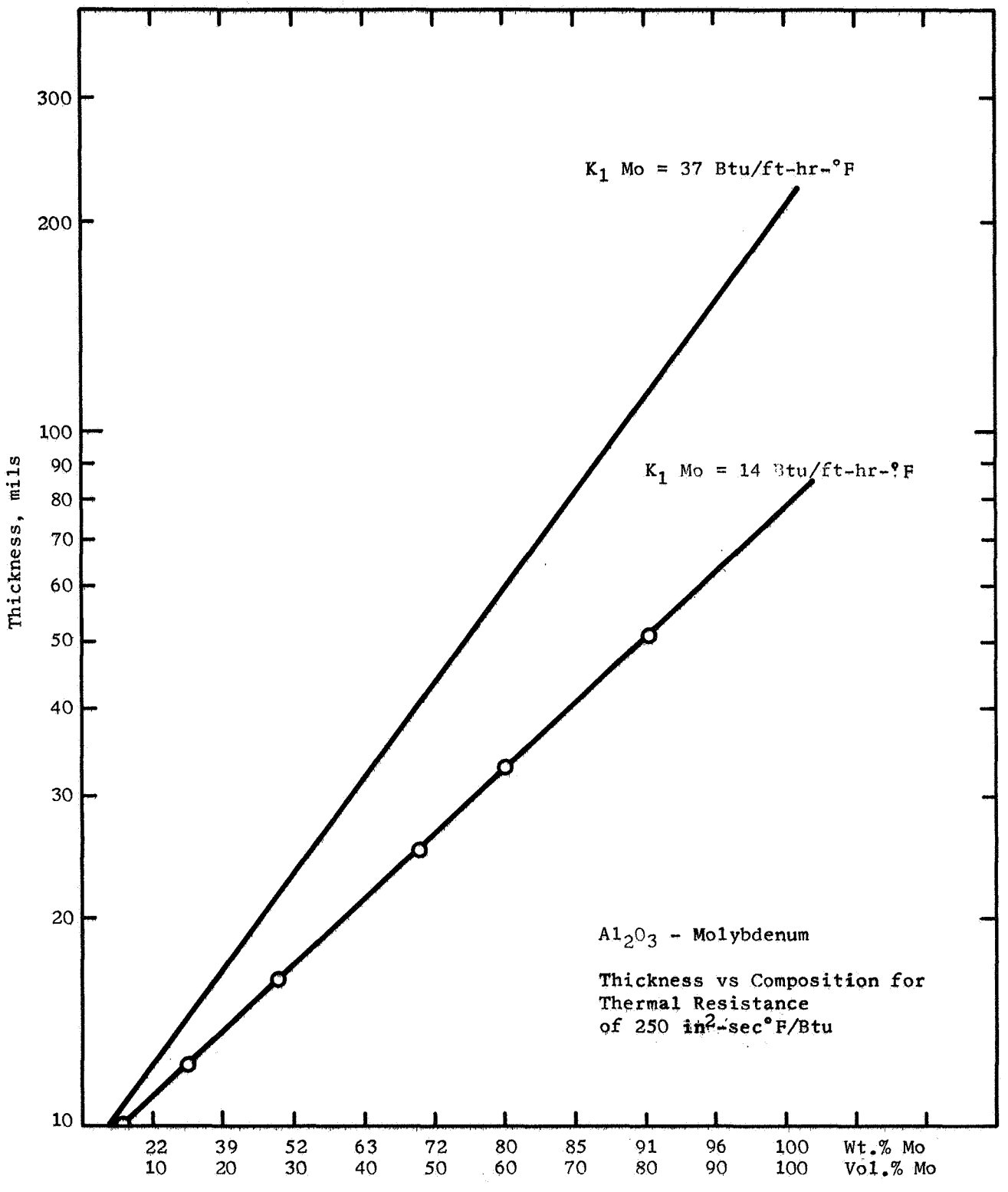

Thermal Resistance of Al_2O_3-Mo Mixtures as a Function of Coating Thicknesses and Composition

Figure 1

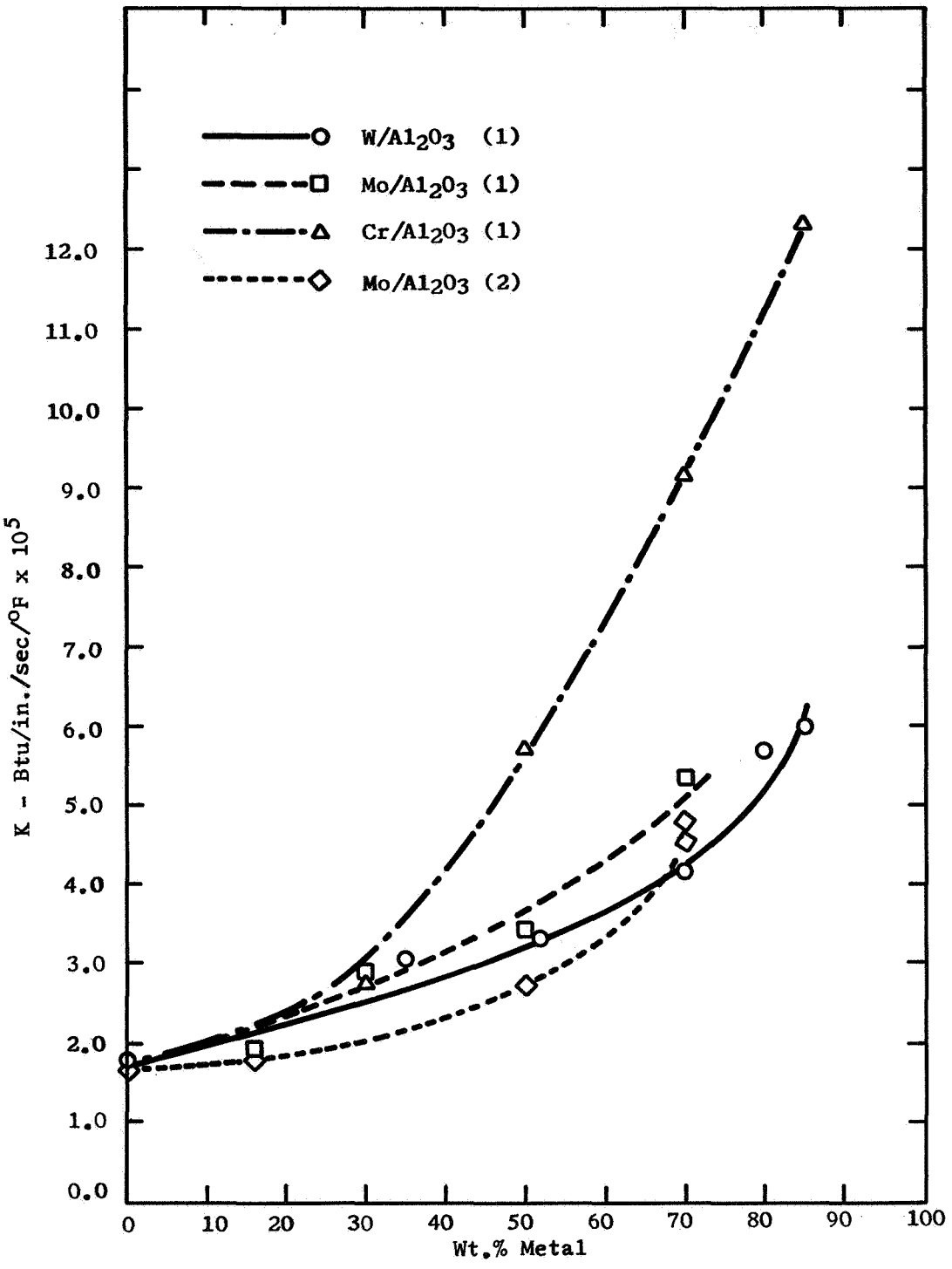

(1) K calculate from Q/A = $\Delta T/t/K$
(2) K calculated from K = $\alpha \rho Cp$ at 1400°F

Thermal Conductivity of Metal/Al_2O_3 Coatings at 2000°F

Figure 2

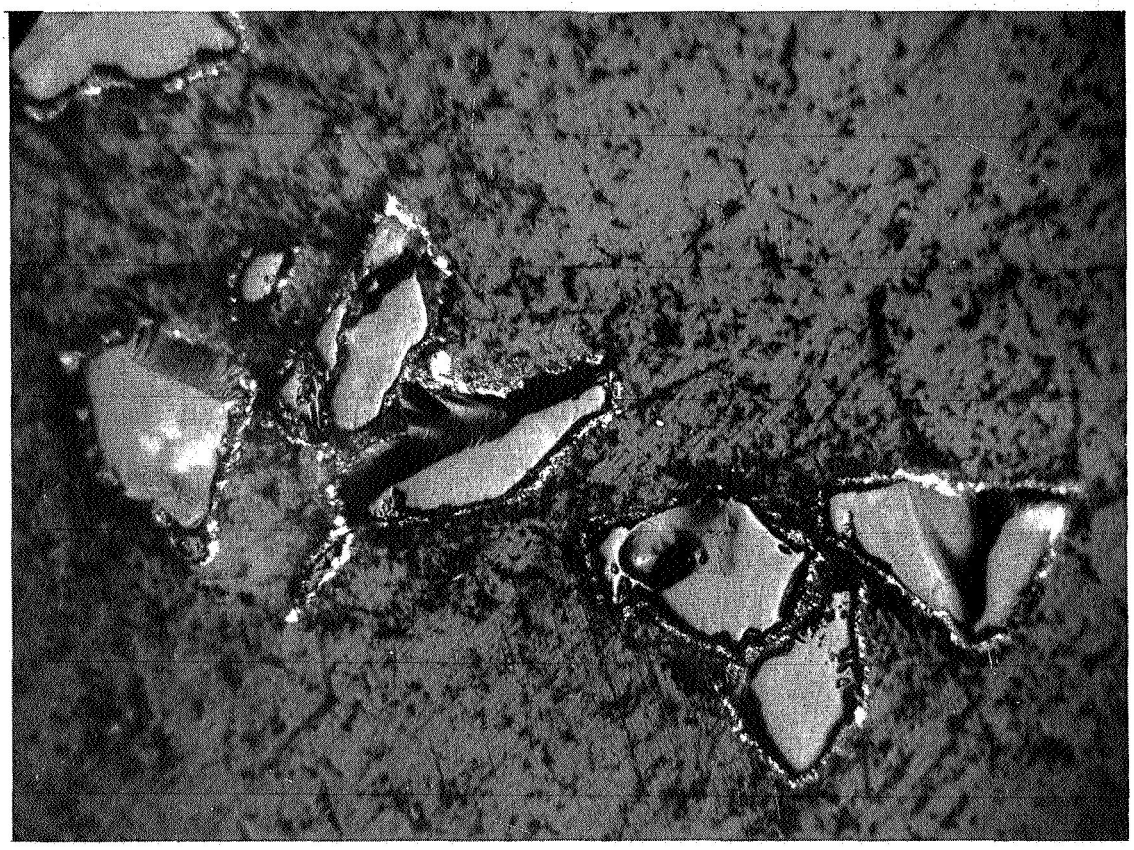

250X

Nickel-Coated Alumina Powder

Figure 3

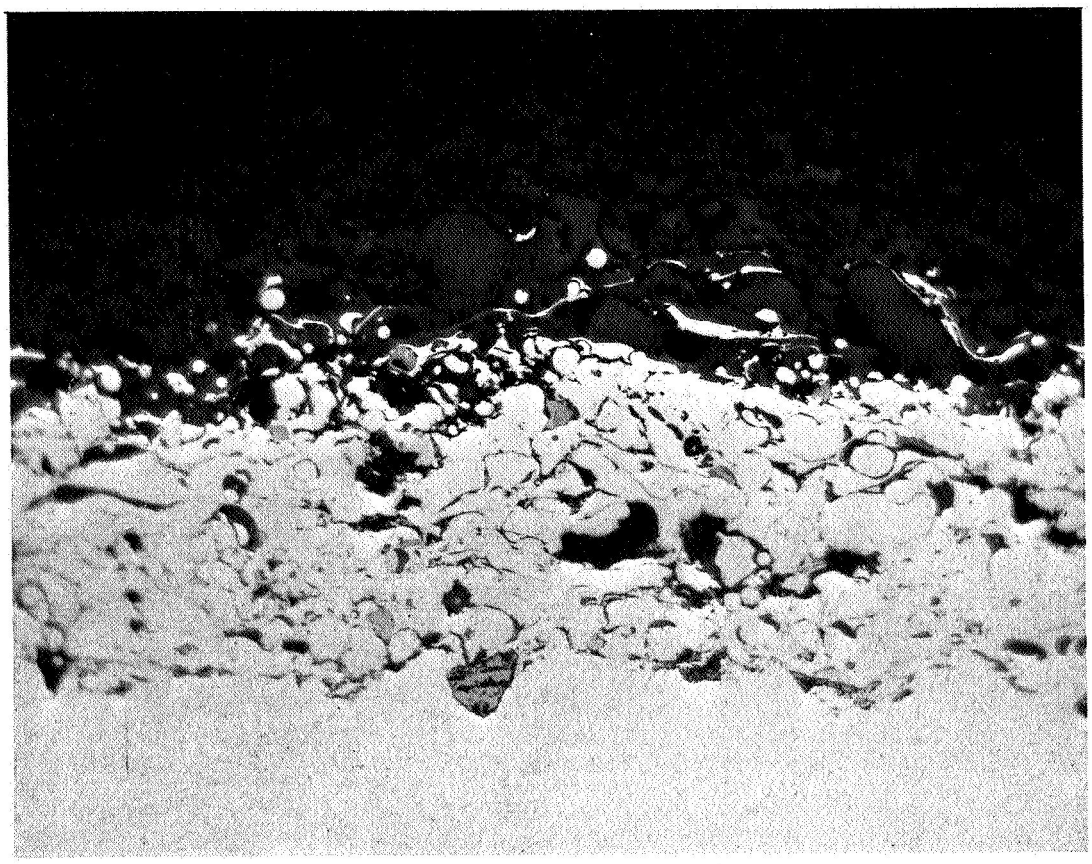

350X

Specimen W6 Ni-Coated Al_2O_3 Intermediate Coating

Figure 4

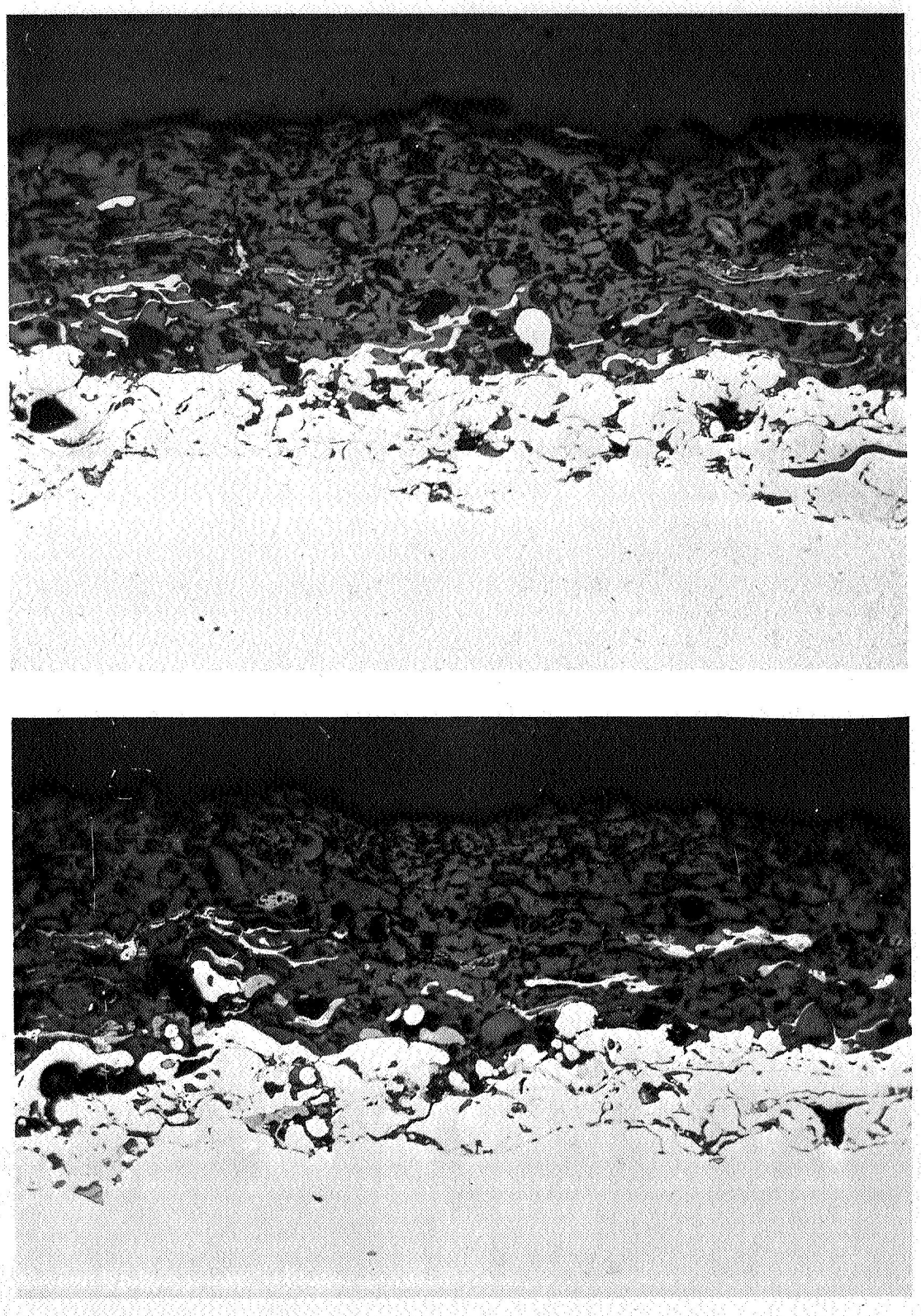

250X

Specimen X18 Before (upper) and After Testing (lower)

Figure 5

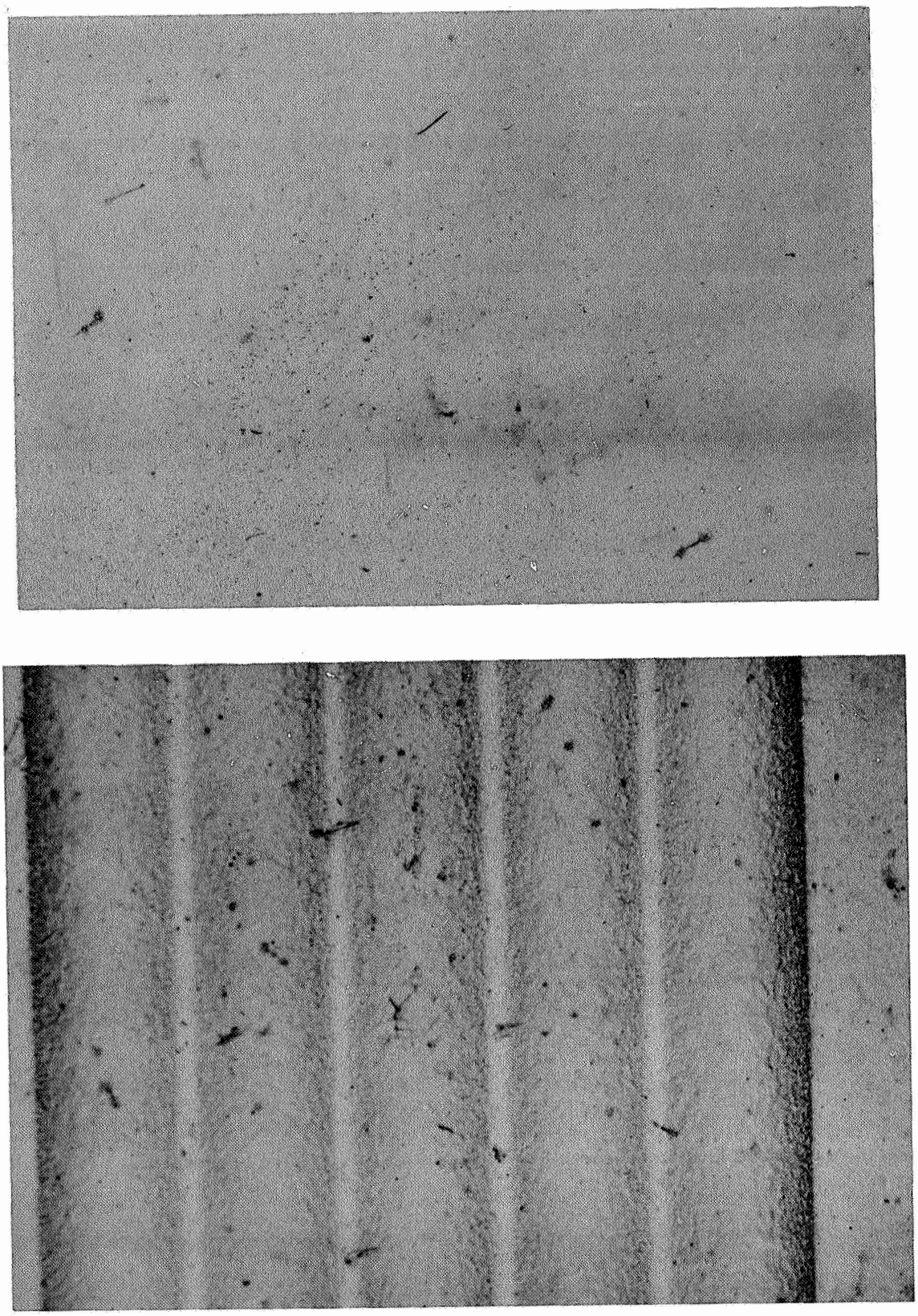

6X

Specimens, Mo Wires/Al_2O_3

Figure 6

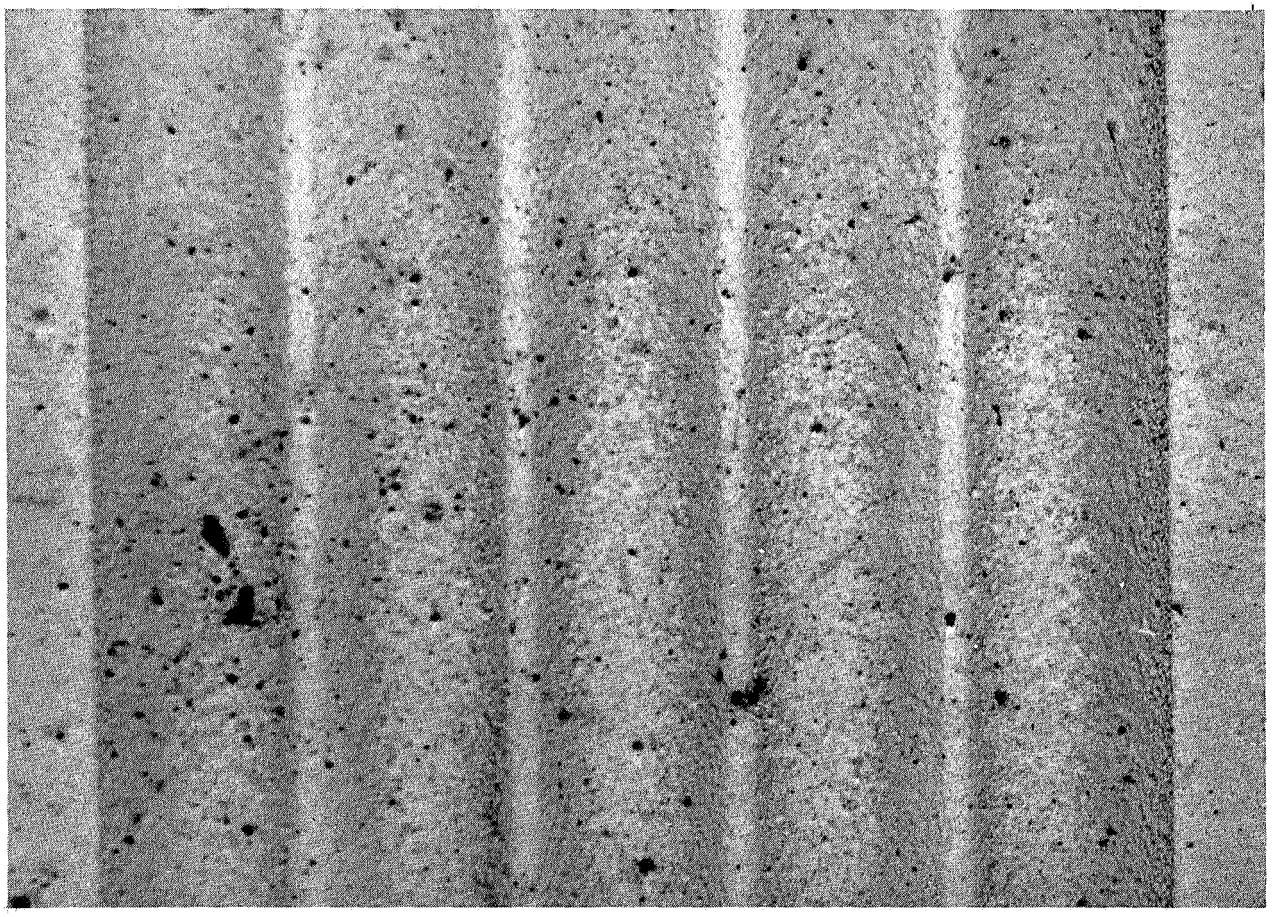

Top View 6X

5-Tube Specimen, Mo Wire/Al_2O_3 After Testing

Figure 7

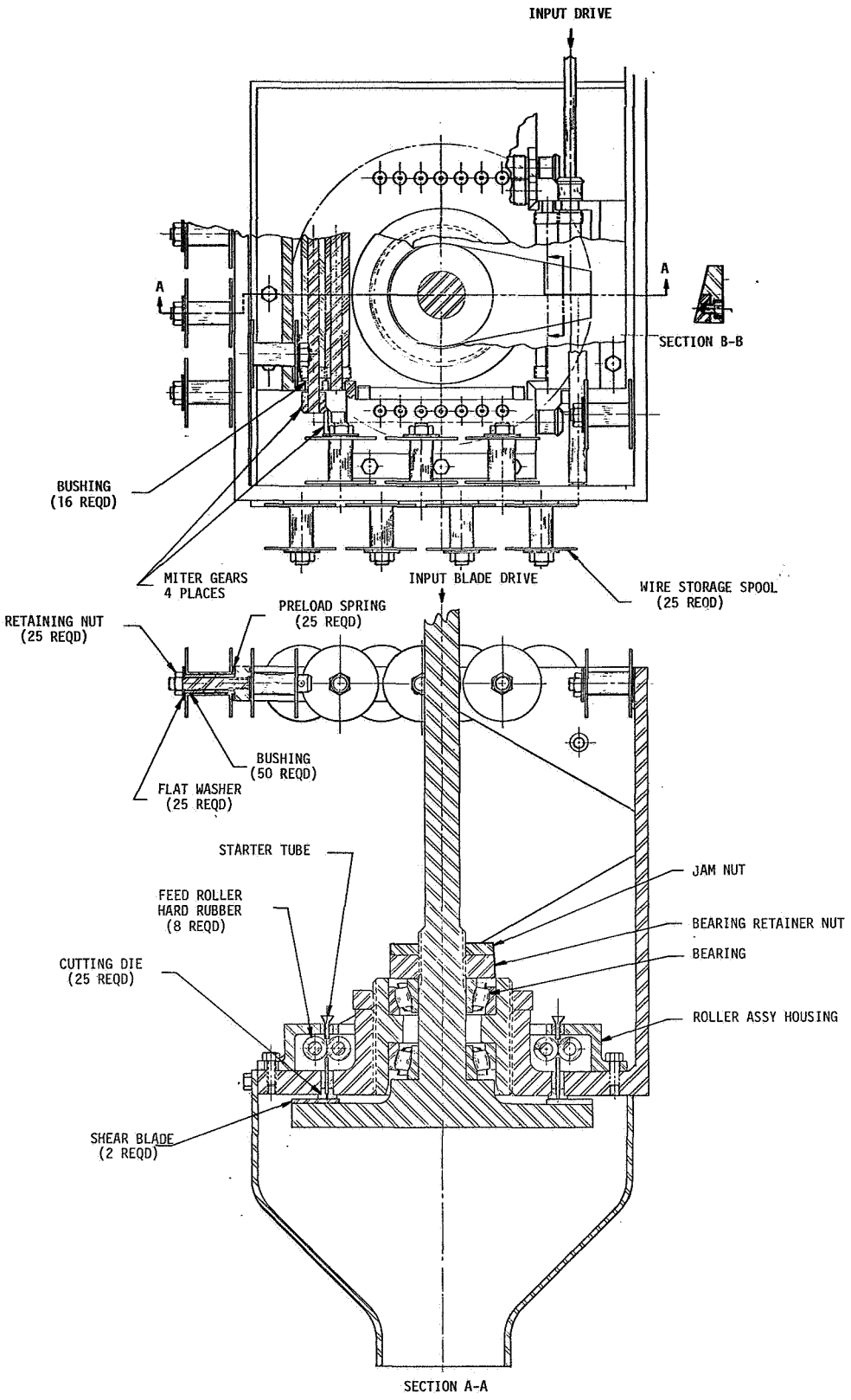

Wire Cutting Machine

Figure 8

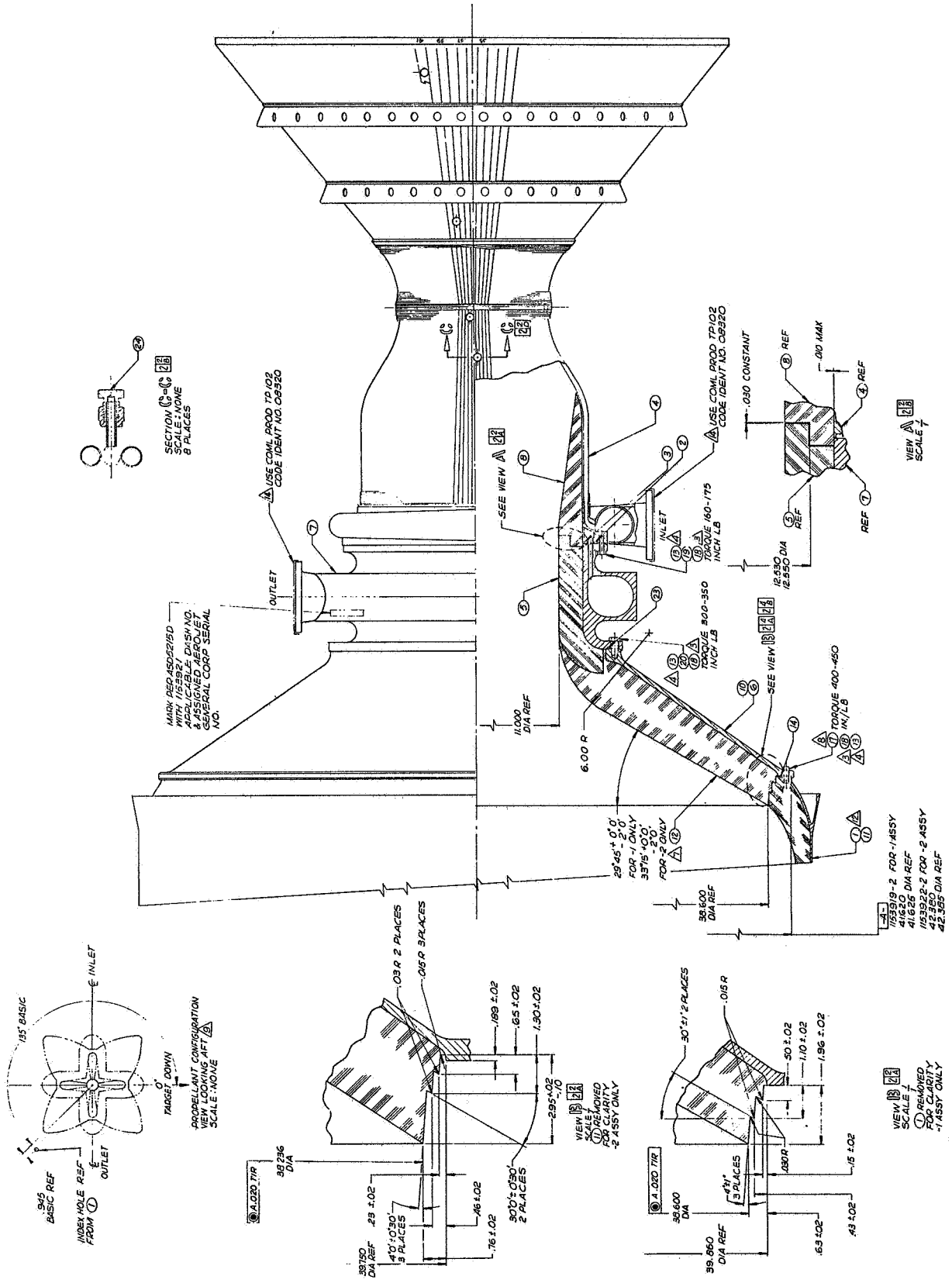

Figure 9

Nozzle Design

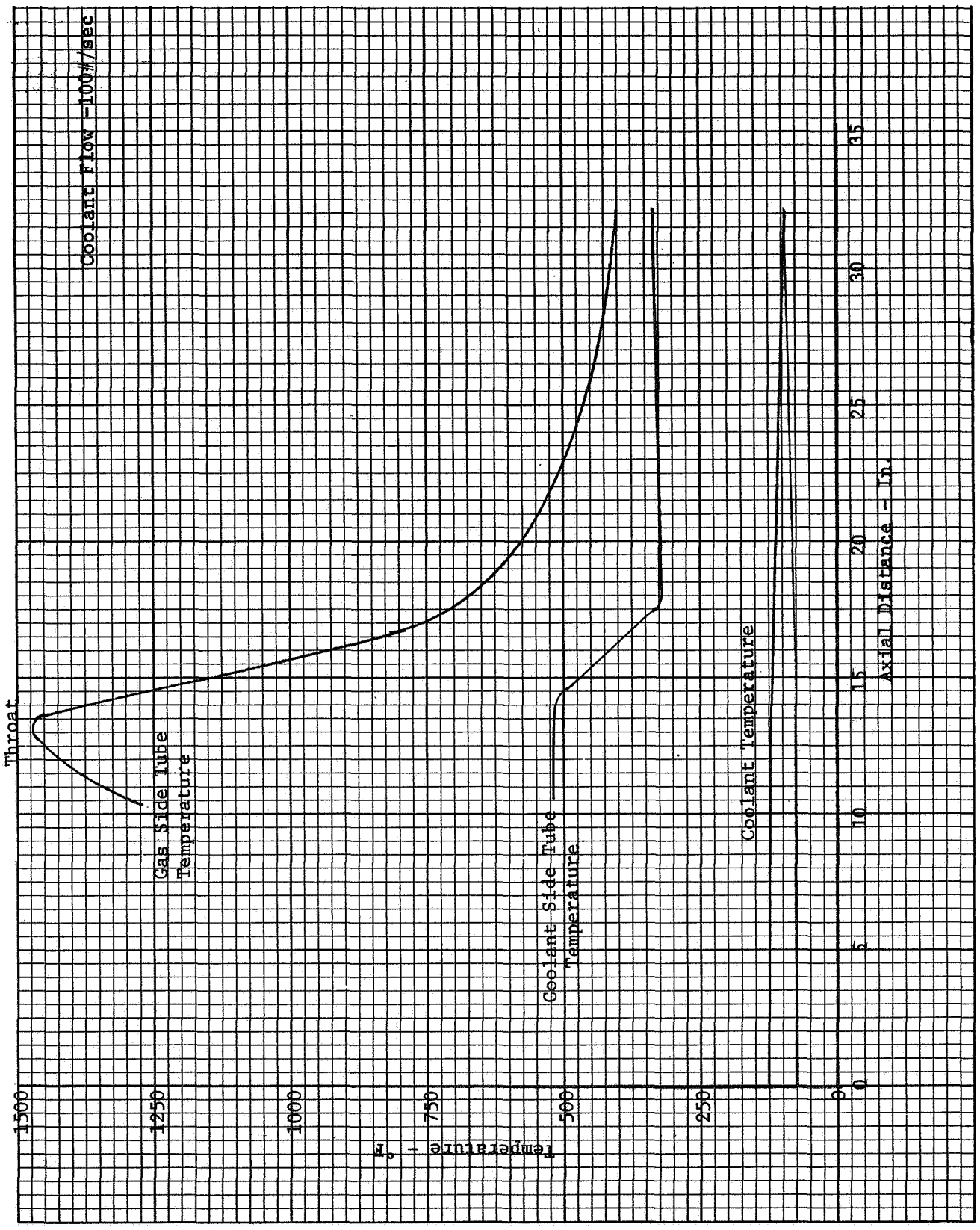

Uncoated Nozzle Temperatures

Figure 10

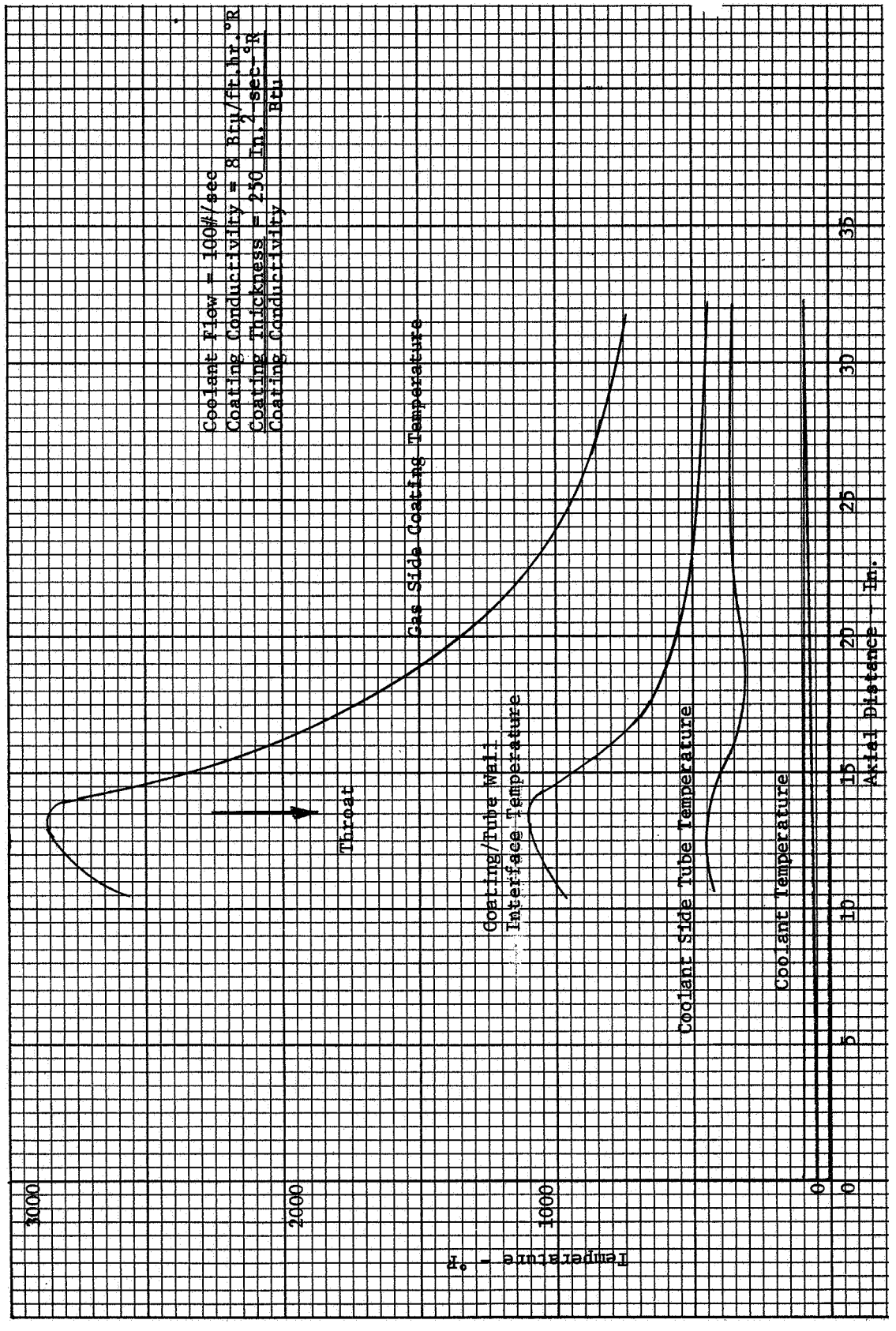

Coated Nozzle Temperatures

Figure 11

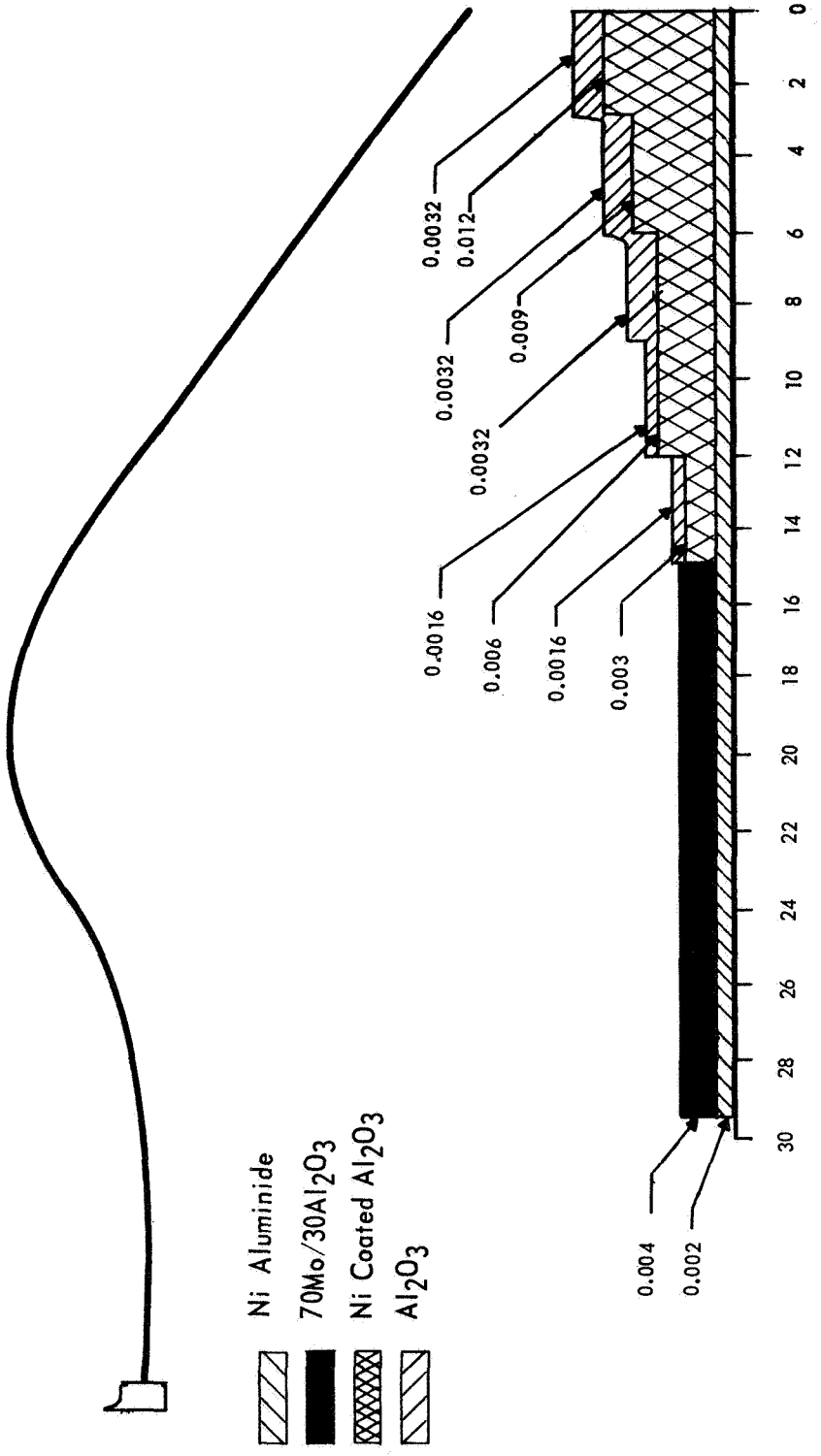

Thermal Barrier Configuration for Nozzle S/N 02

Figure 12

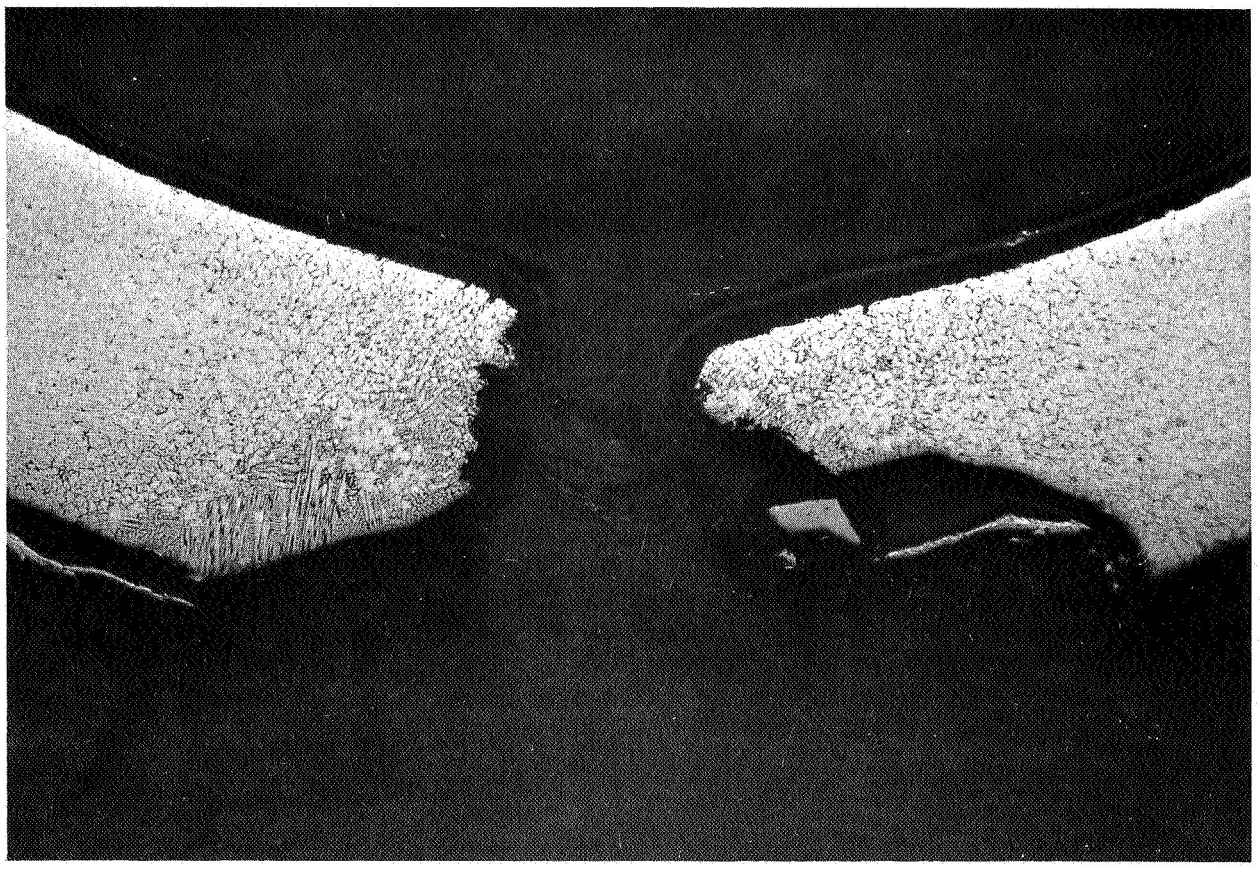

100X

Burned Tube at Throat

Figure 13

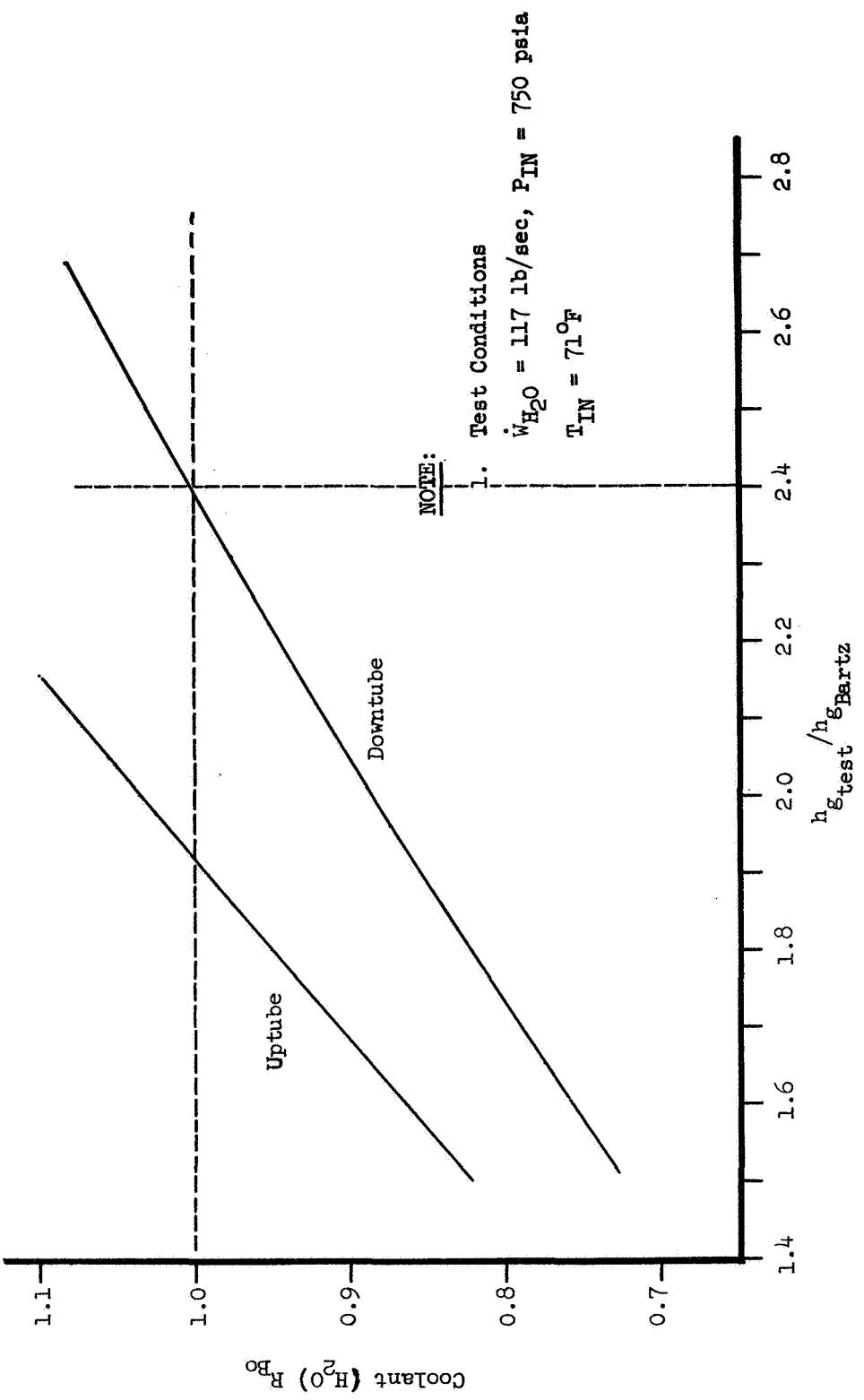
COATING DEVELOPMENT PROGRAM
UNCOATED TUBE TEST ANALYSIS
Coolant (H_2O) R_{Bo}
1.1
1.0
0.9
0.8
0.7
1.4
1.6
1.8
2.0
2.2
2.4
2.6
2.8
$h_{g_{test}}/h_{g_{Bartz}}$
Uptube
Downtube
NOTE:
1. Test Conditions
$\dot{W}_{H_2O}$ = 117 lb/sec, P_{IN} = 750 psia
T_{IN} = 71°F
Heat Flux at Test Conditions R_{Bo} = 1.0

Figure 14

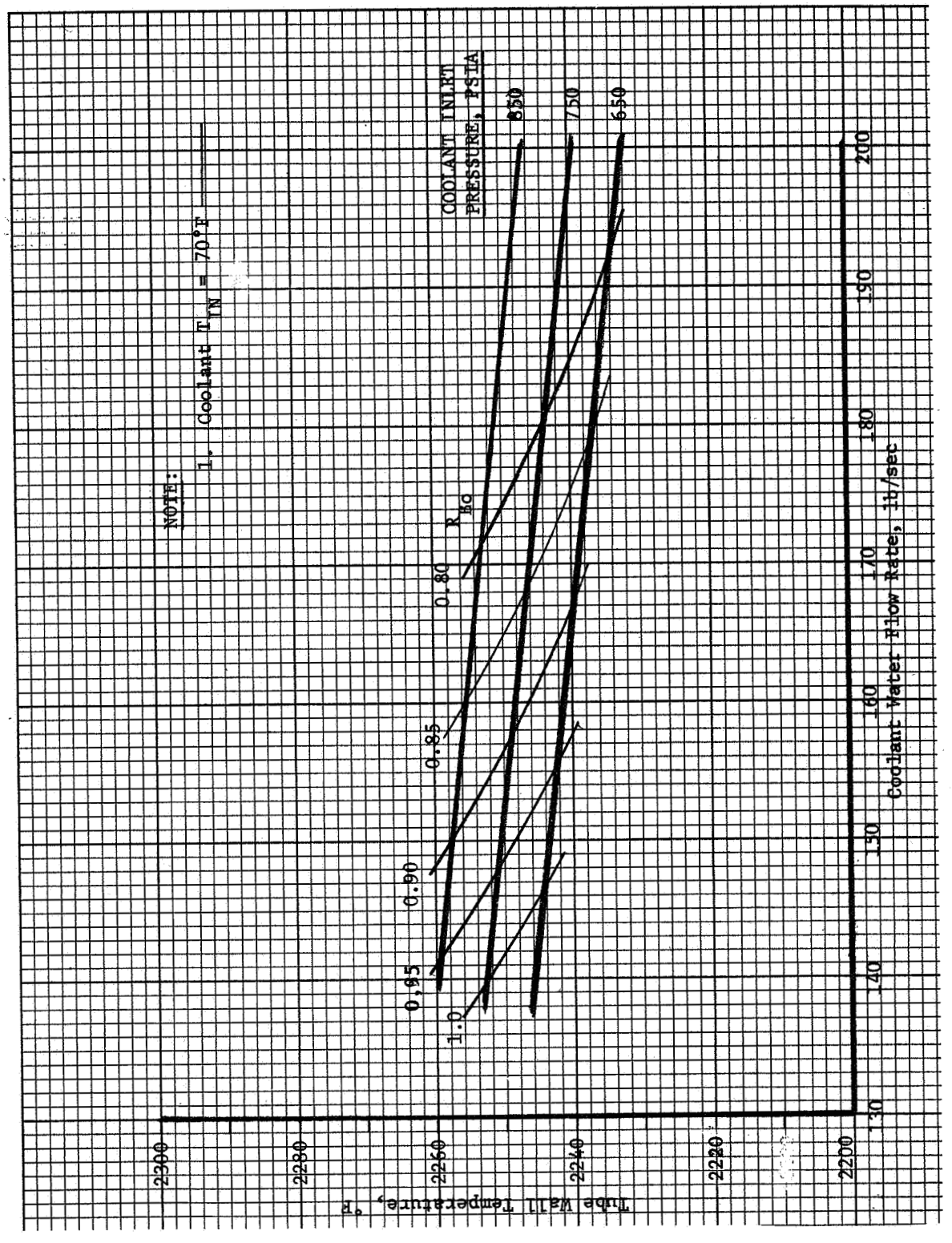

Tube Wall Temperatures - Uncoated Nozzle

Figure 15

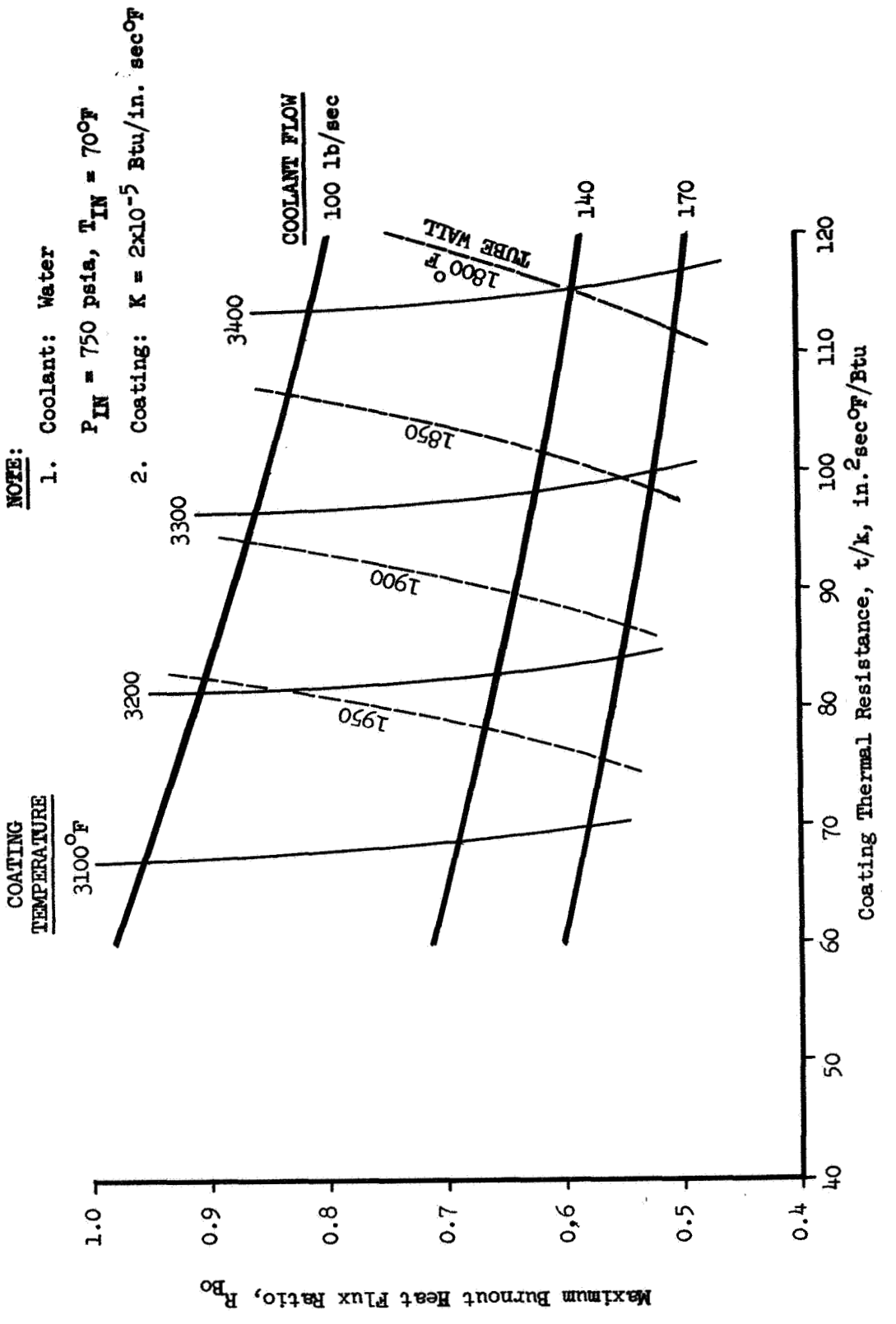

Parametric Study - Cooled Nozzle

Figure 16

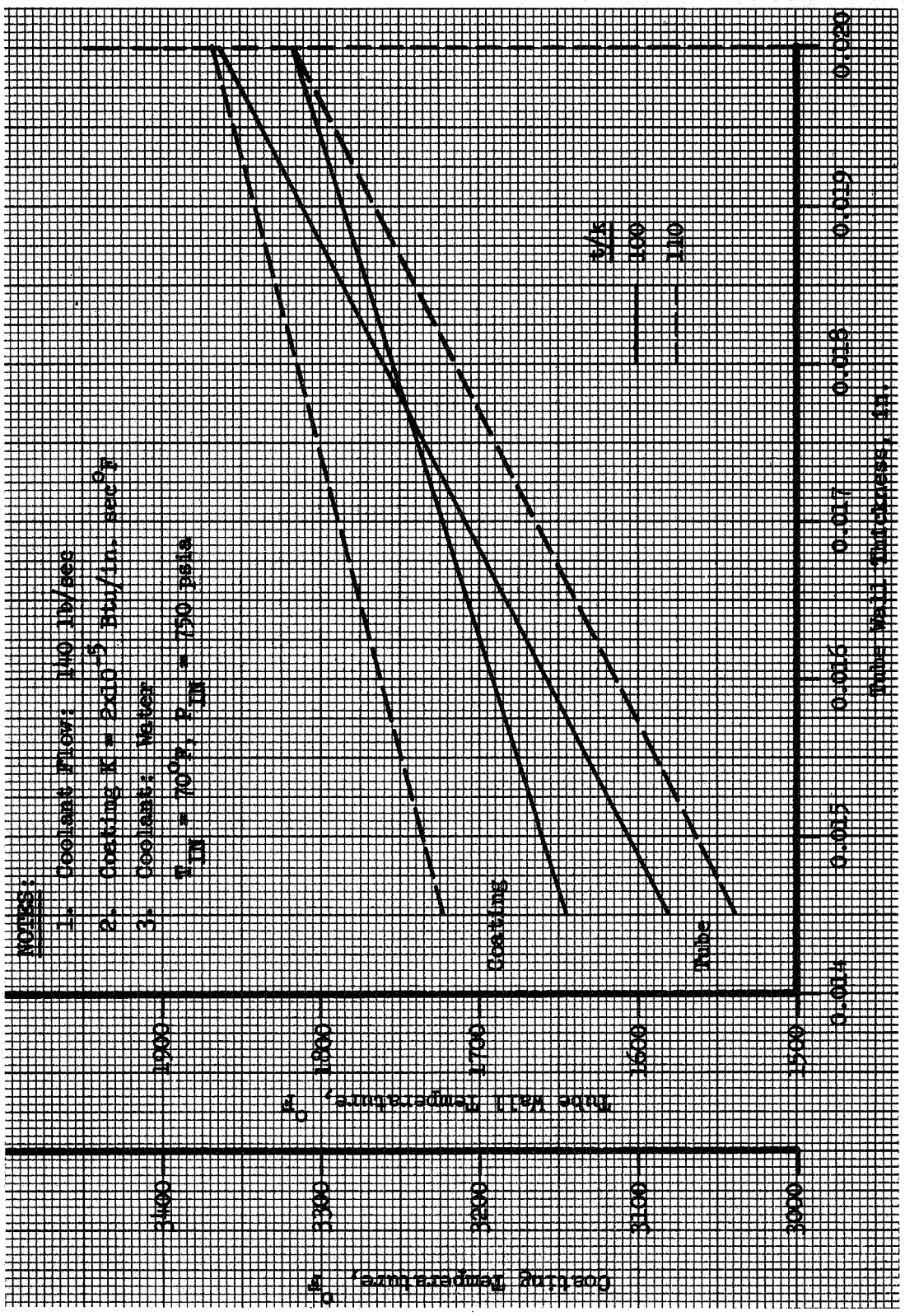

Effect of Tube Wall Thickness on Maximum Wall Temperatures - Coated Nozzle

Figure 17

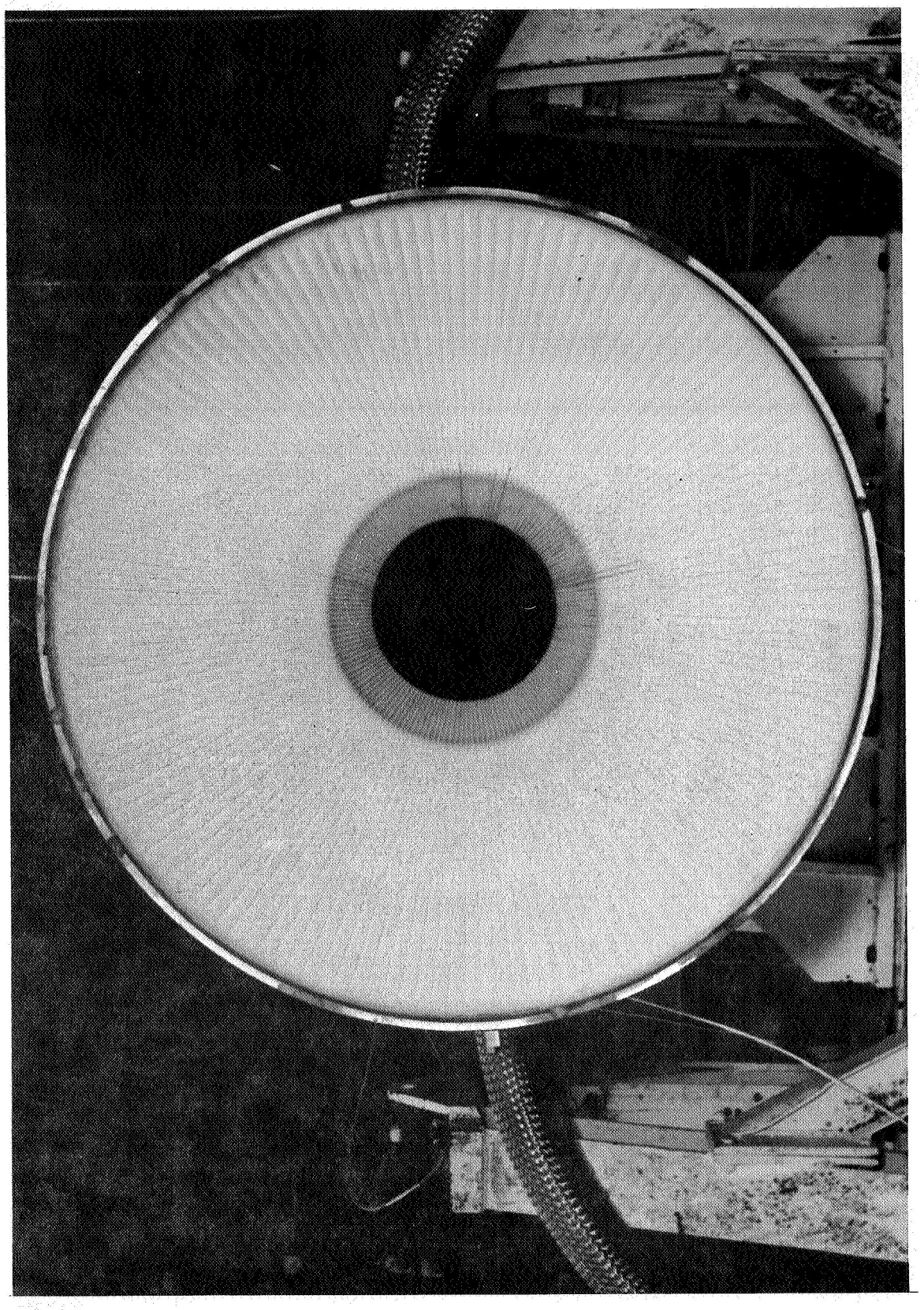

Coated Nozzle

Figure 18

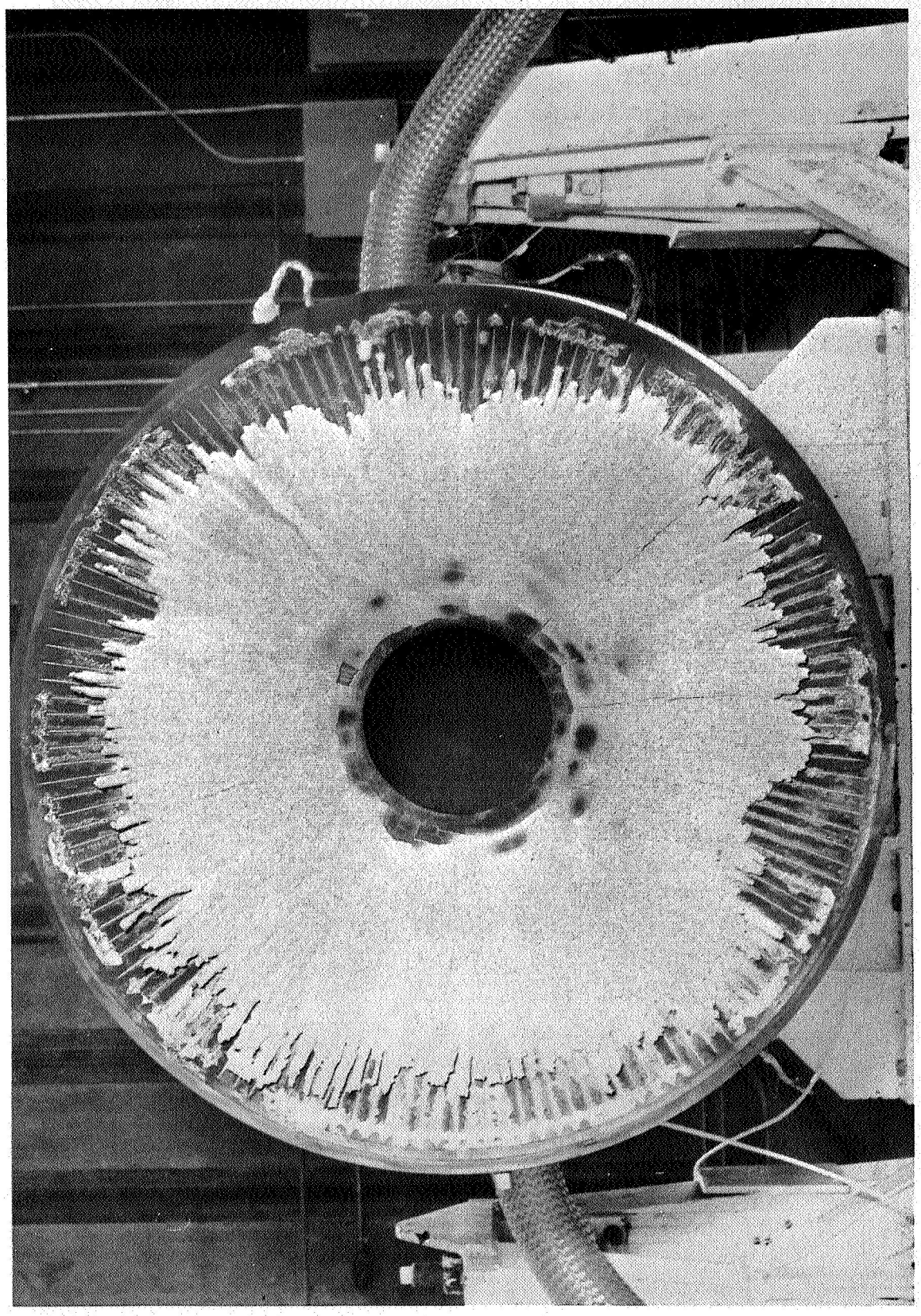

Nozzle SN 02 After Test

Figure 19

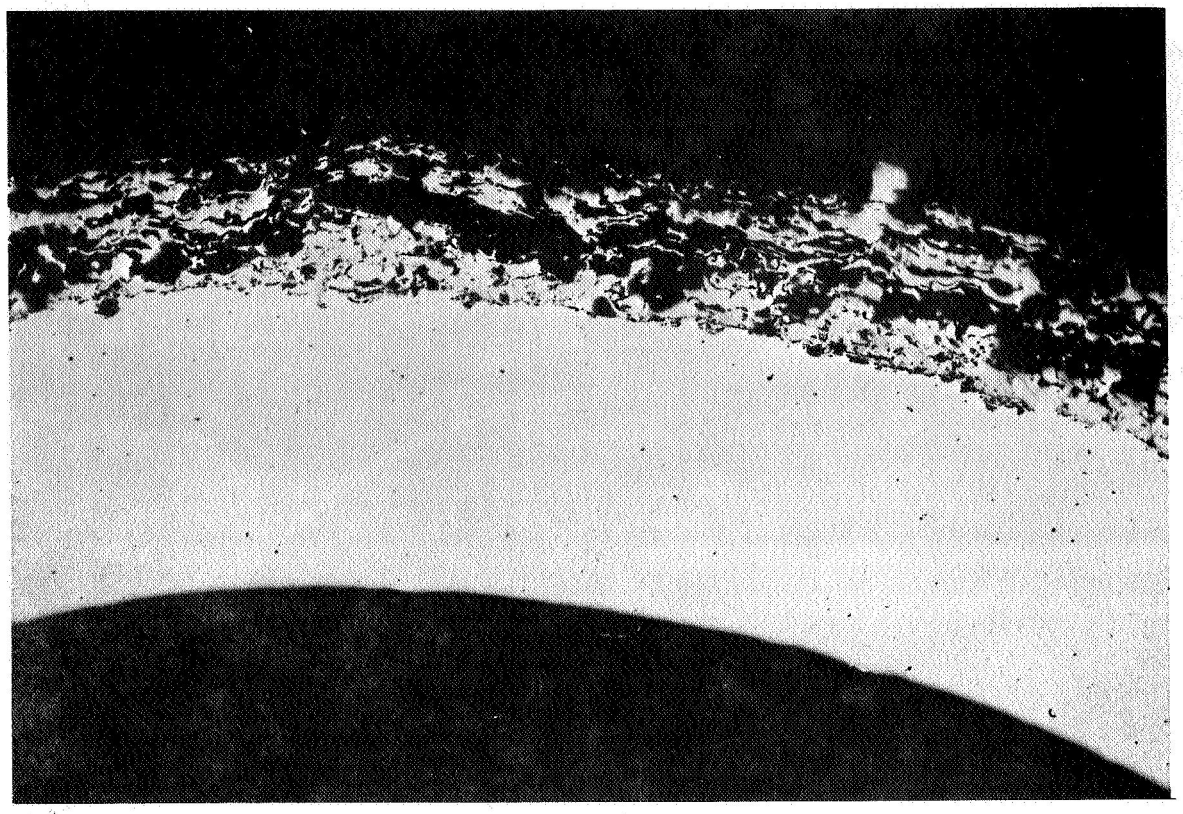

100X

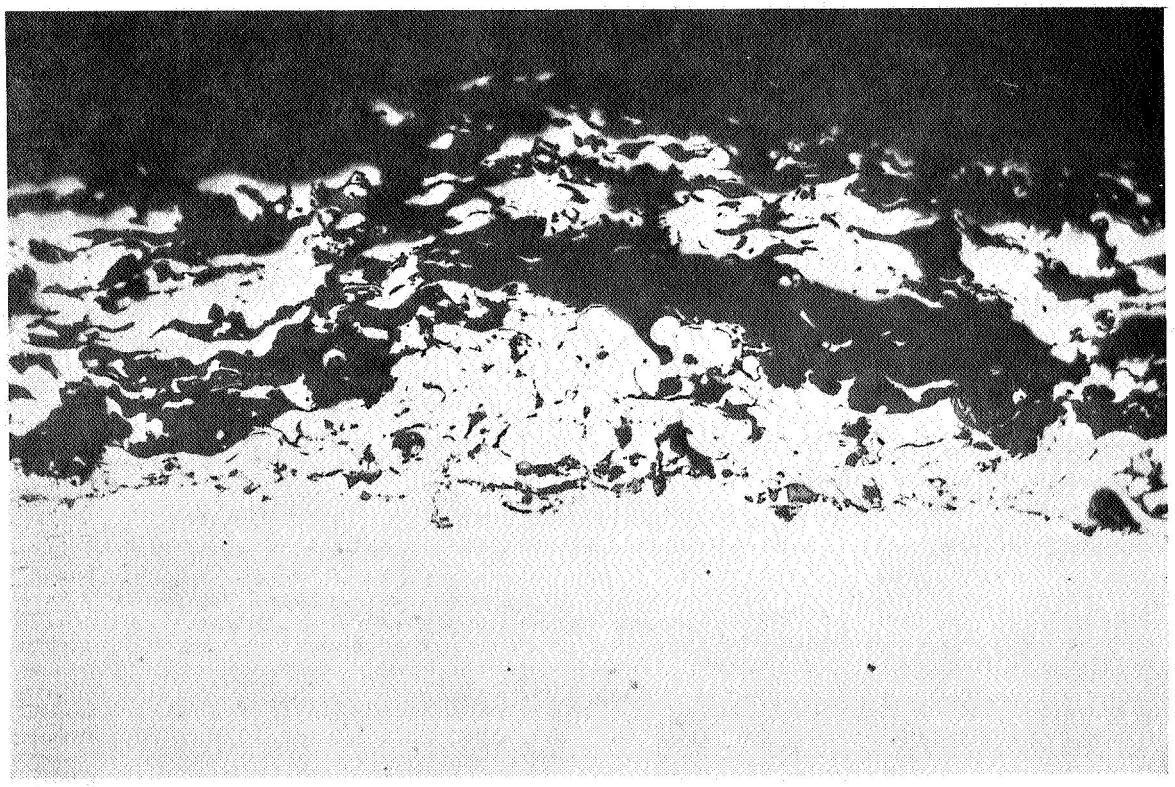

Forward Section - 250X

Figure 20

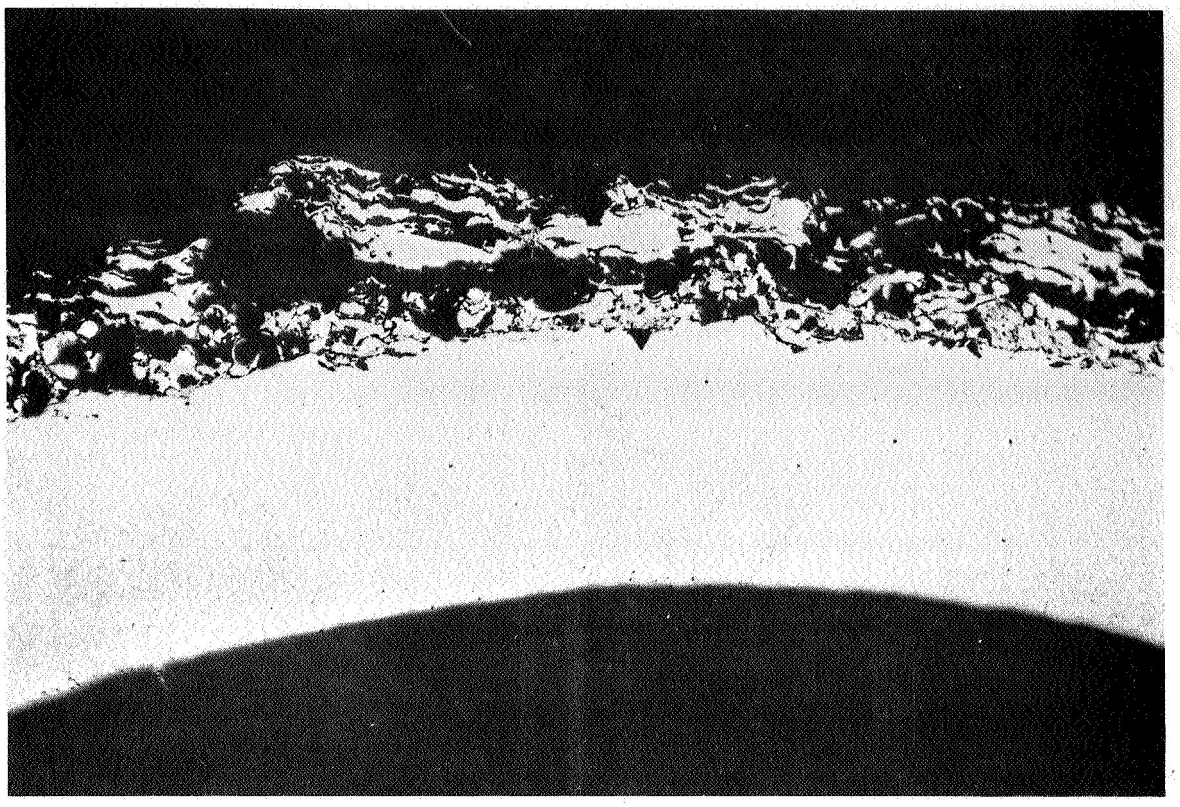

100X

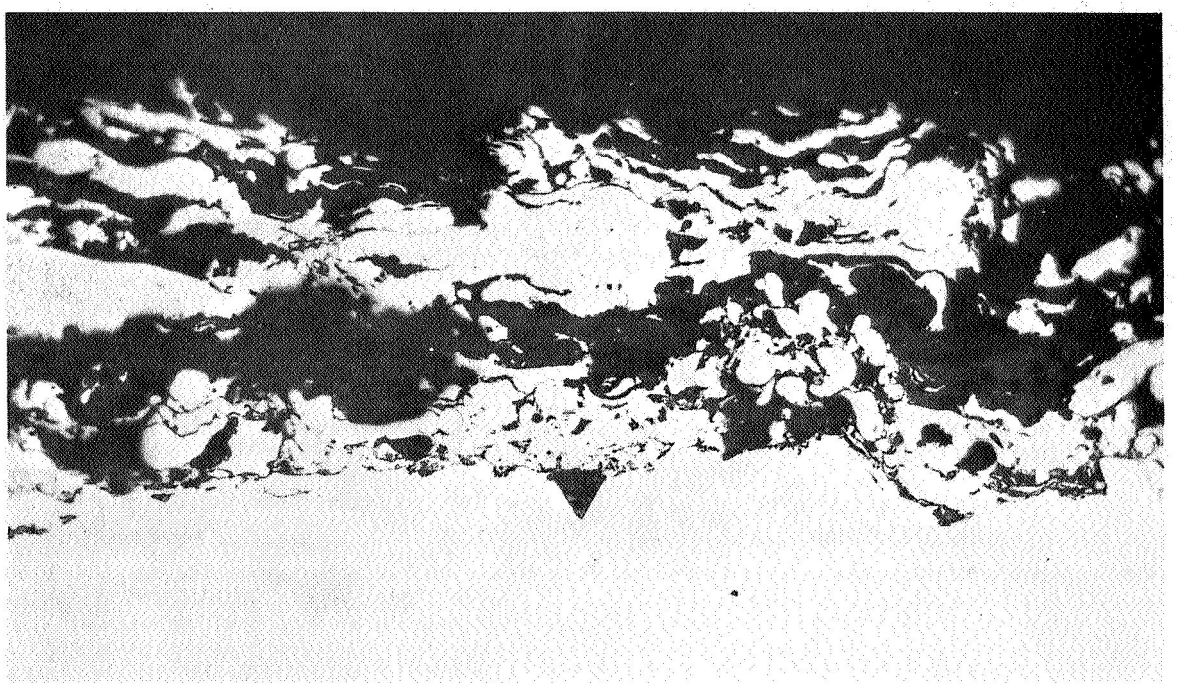

Throat - 250X

Figure 21

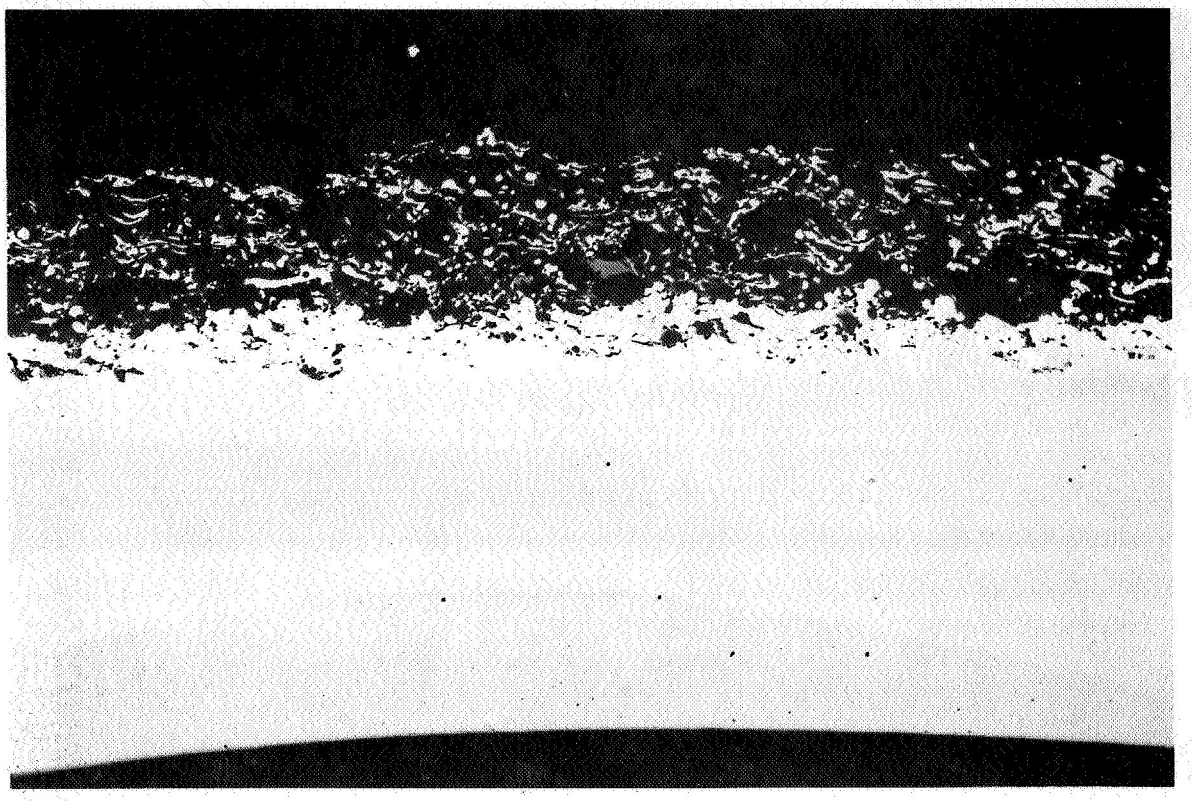

100X

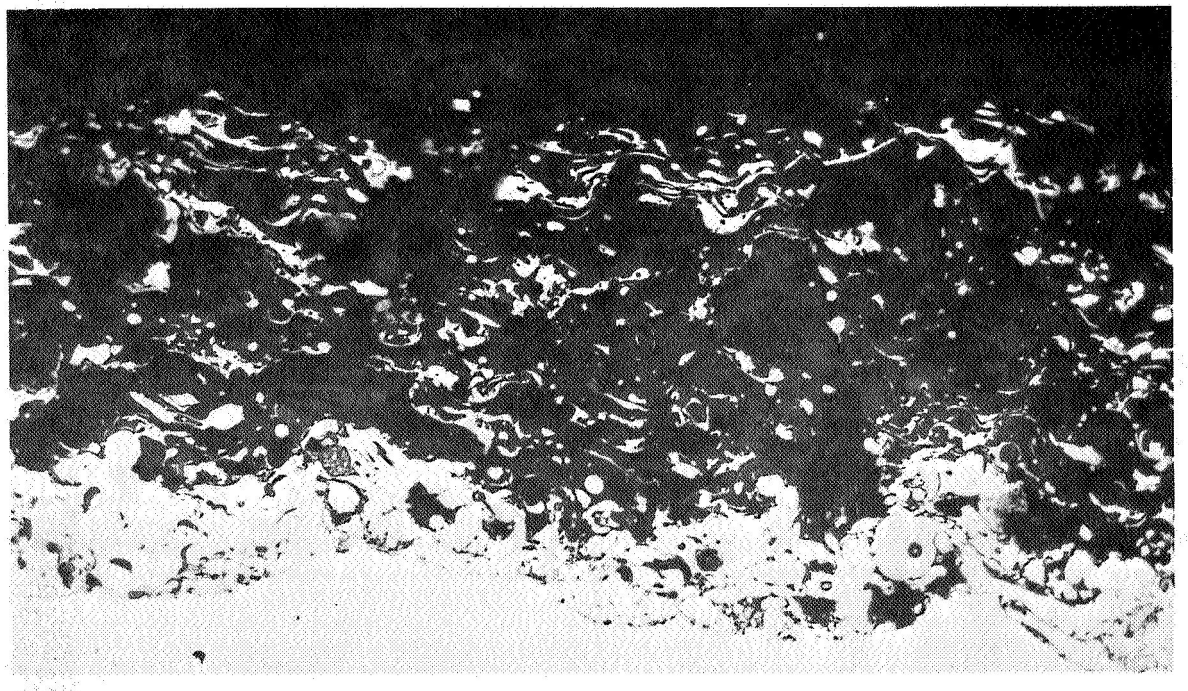

Aft End - 250X

Figure 22

Section of Propellant Deposited Al_2O_3 Throat Area - 16X

Figure 23

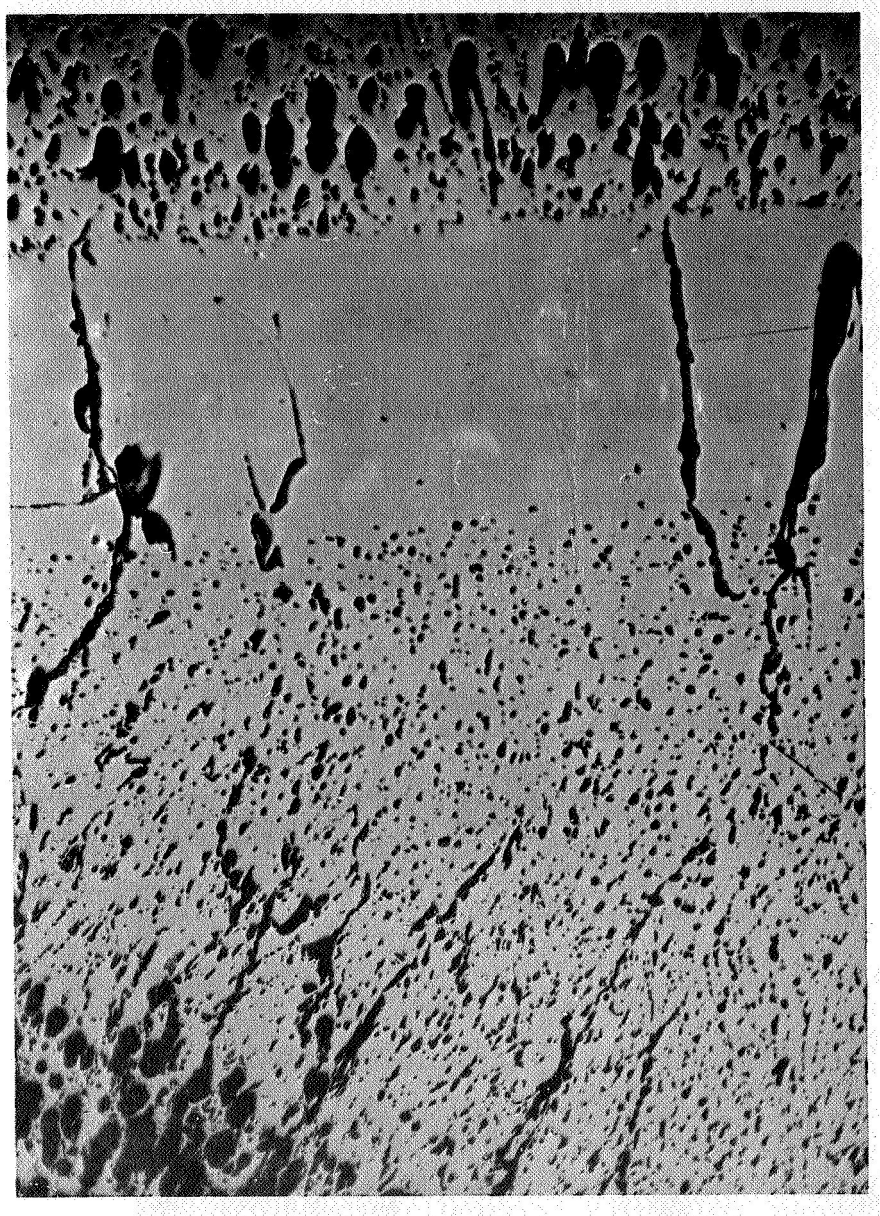

Section of Propellant Deposited Al_2O_3 Throat Area
Showing Band of Large Columnar Grains - 100X

Figure 24

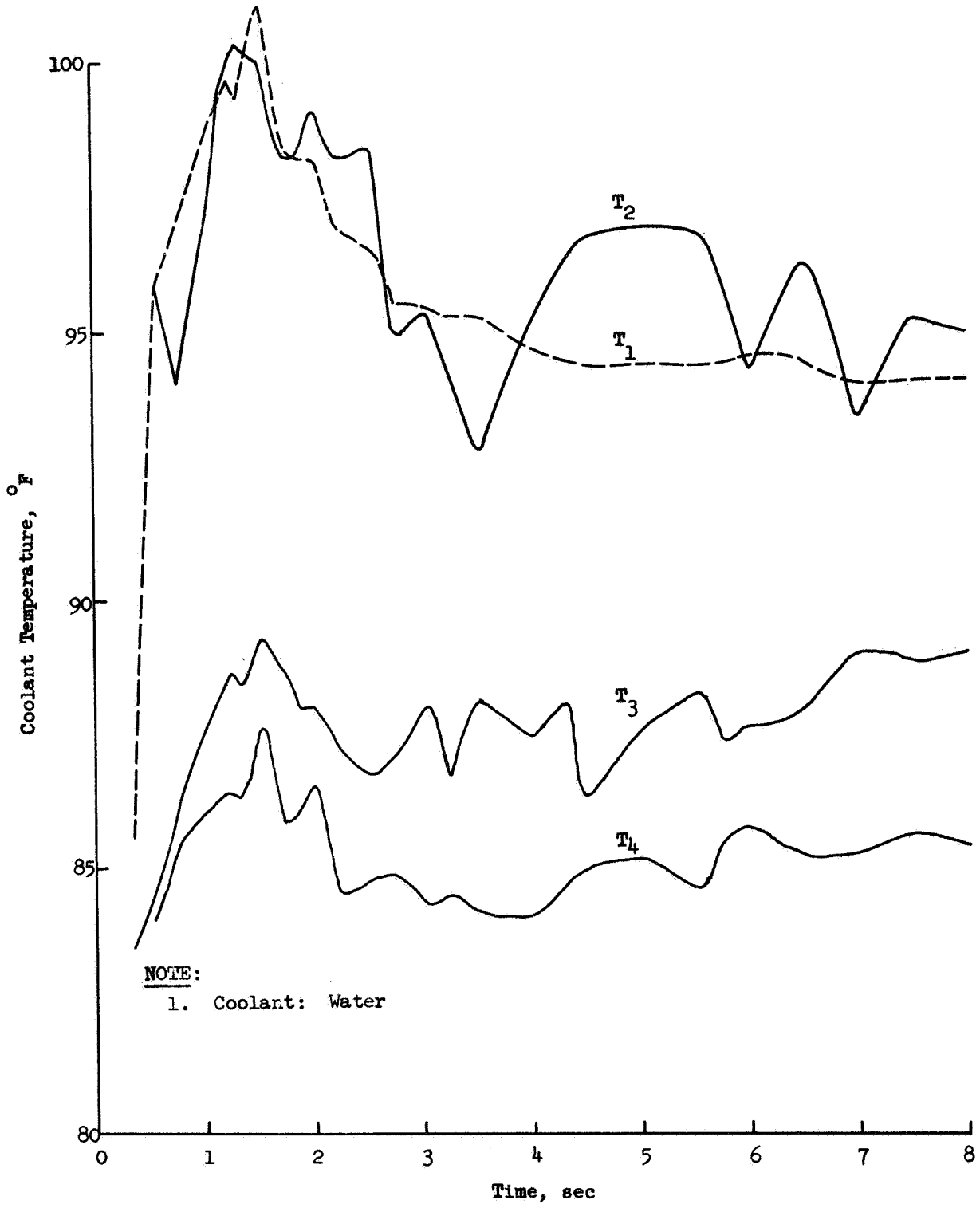

Coolant Bulk Temperature Thermocouple Data SN 02

Figure 25

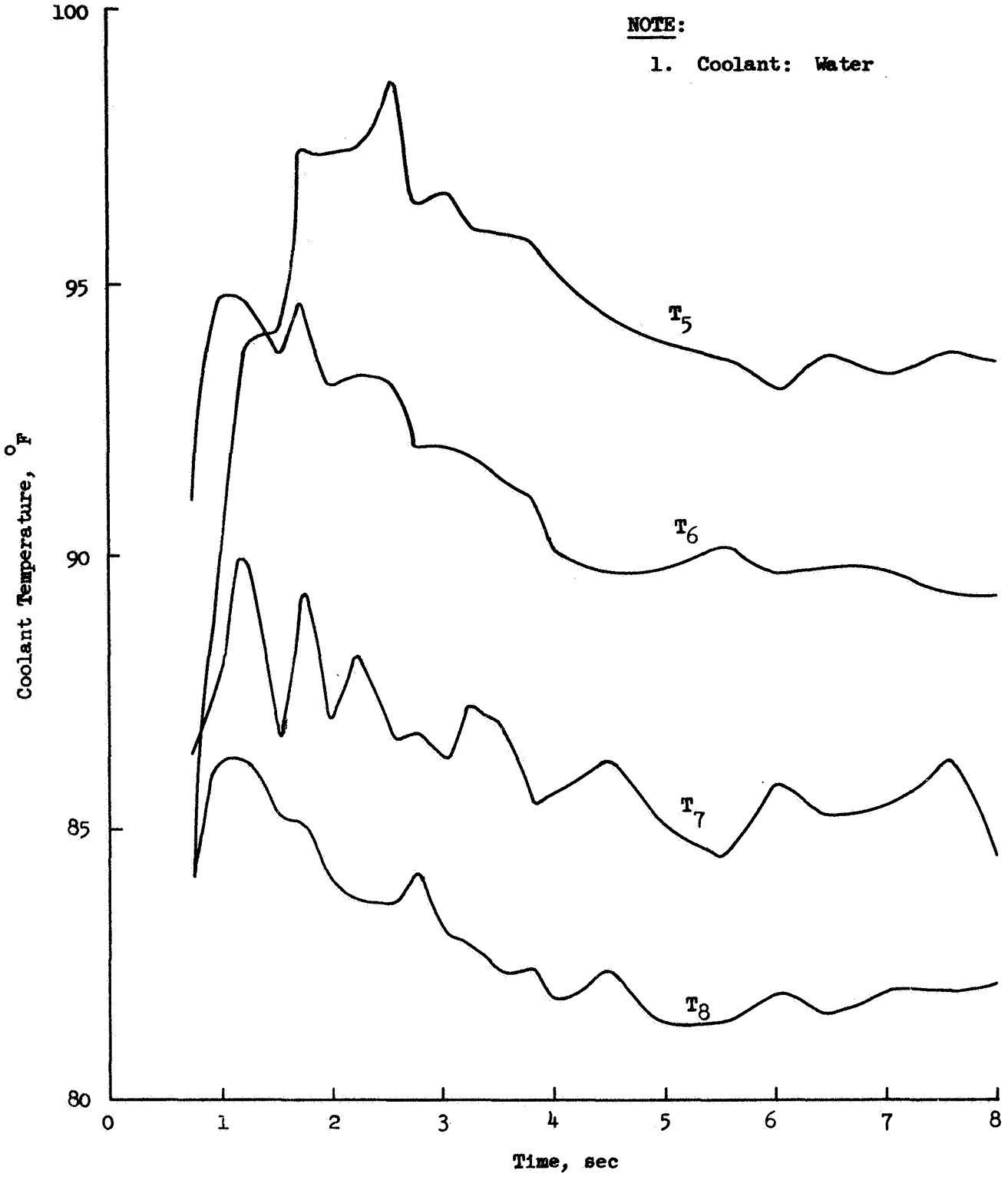

Coolant Bulk Temperature Thermocouple Data SN 02

Figure 26

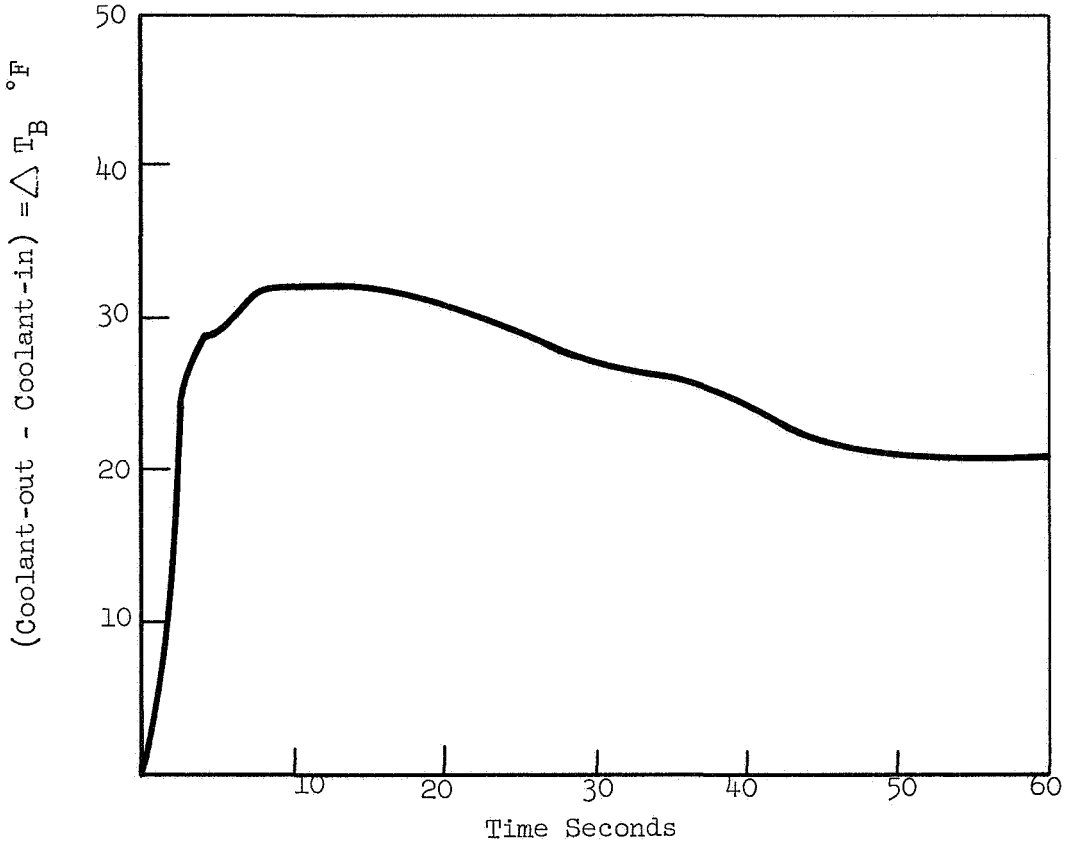

Coolant Bulk Temperature Rise

Figure 27

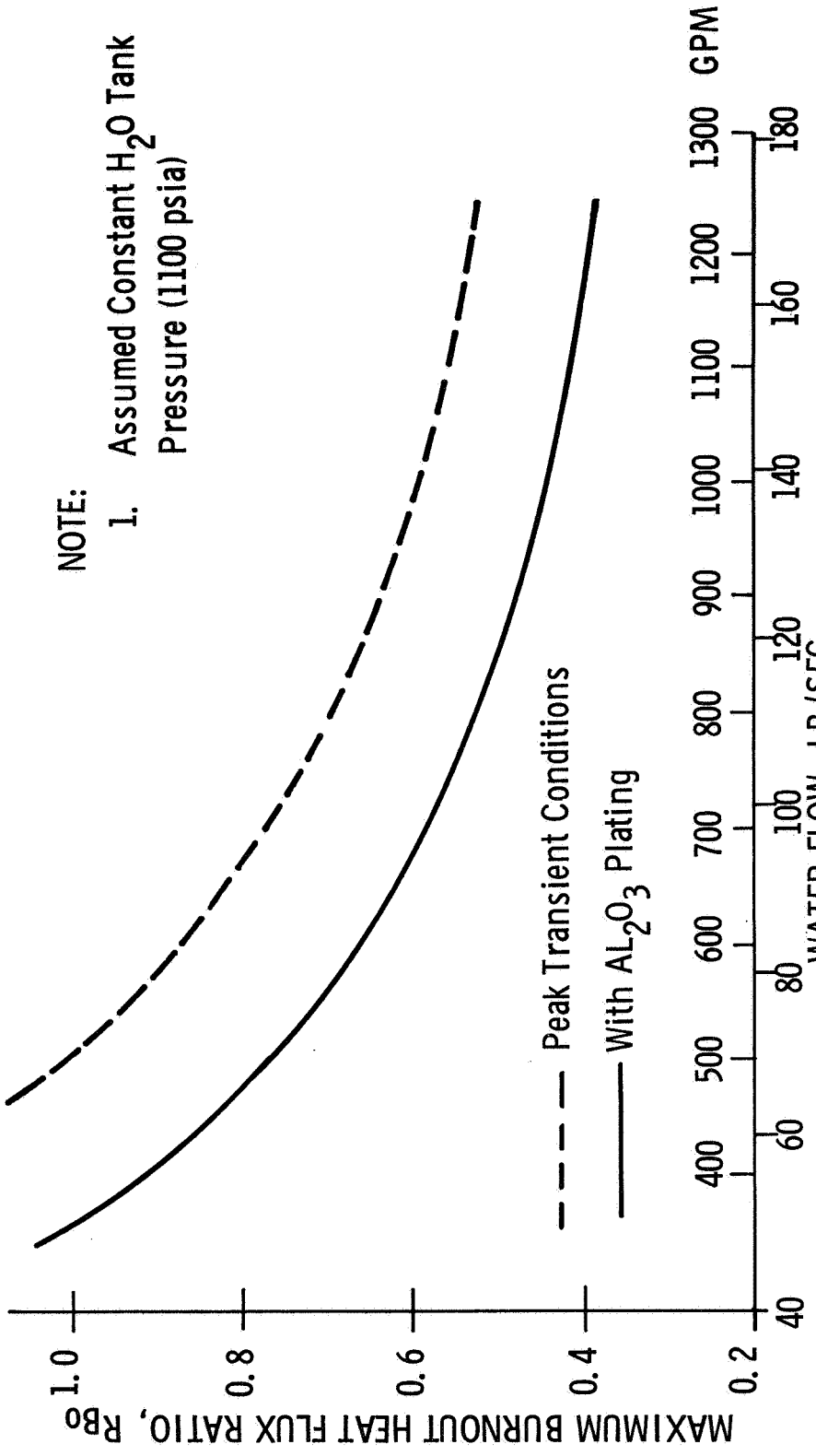

Effect of Coolant Flow Reduction with Al_2O_3 Plating

Figure 28

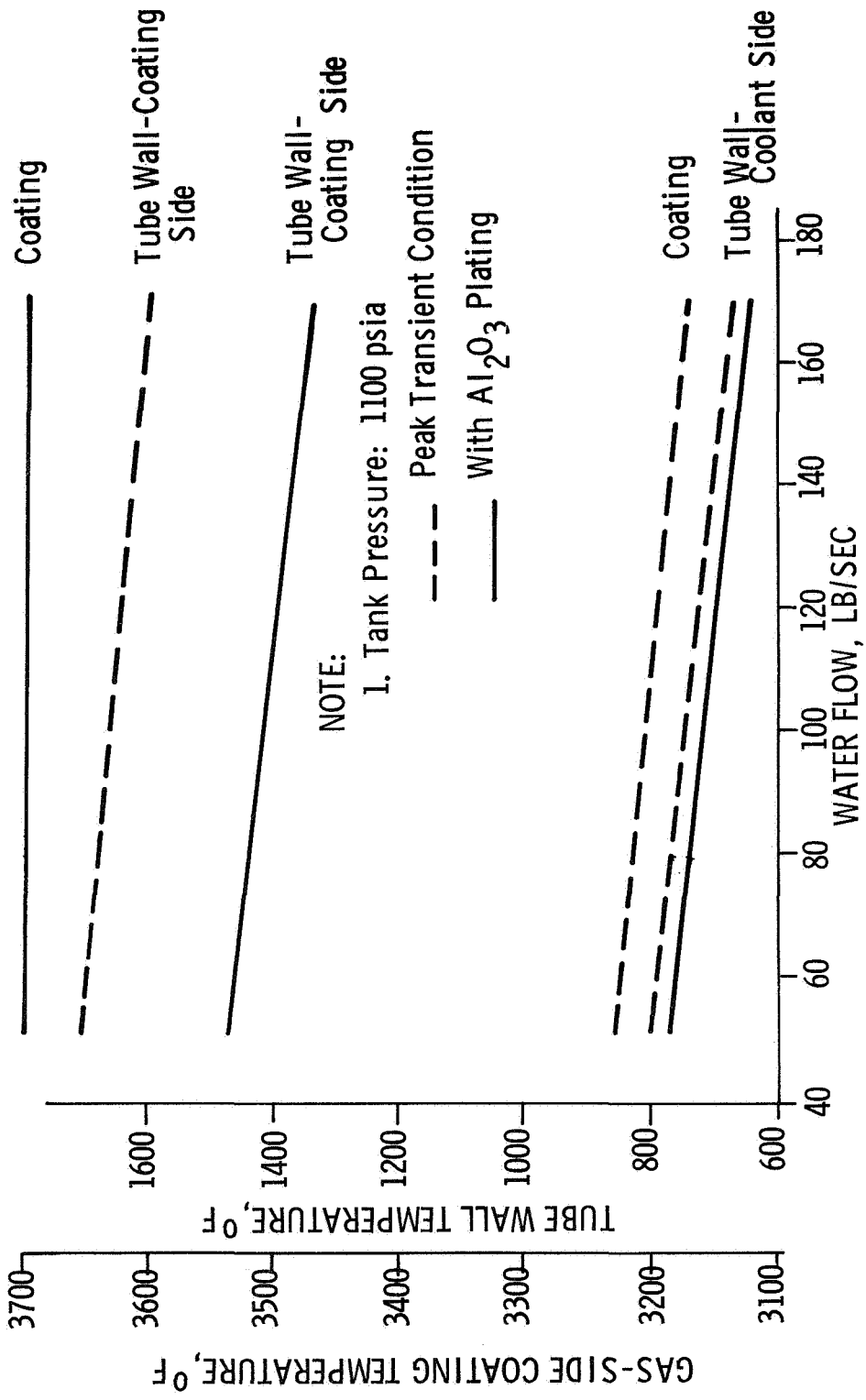

Nozzle Wall Temperatures with Al_2O_3 Plating

Figure 29

FINAL REPORT DISTRIBUTION LIST

SOLID ROCKET TECHNOLOGY

NASA Lewis Research Center
21000 Brookpark Road
Cleveland, Ohio 44135
Attn: Contracting Officer
Mail Stop 500-313 (1)
Solid Rocket Technology Branch
Mail Stop 500-205 (8)
Technical Library
Mail Stop 60-3 (2)
Tech. Report Control Office
Mail Stop 5-5 (1)
J. Kennard
Mail Stop 3-17 (1)
Tech. Unitization Office
Mail Stop 3-19 (1)
Patent Counsel
Mail Stop 500-311 (1)

National Aeronautics and
Space Administration
Washington, D.C. 20546
Attn: RPM/William Cohen (3)
RPS/Robert W. Ziem (1)
ATSS-AL/Technical Library (2)

NASA Ames Research Center
Moffett Field, California 94035
Attn: Technical Library (1)

NASA Langley Research Center
Langley Station
Hampton, Virginia 23365
Attn: Robert L. Swain (1)
Technical Library (1)

NASA Goddard Space Flight Center
Greenbelt, Maryland 20771
Attn: Technical Library (1)

NASA Manned Spacecraft Center
2101 Webster Seabrook Road
Houston, Texas 77058
Attn: Technical Library (1)

NASA George C. Marshall Space
Flight Center
Redstone Arsenal
Huntsville, Alabama 35812
Attn: Technical Library (1)
R-P&VE-PA/K.,Chandler (1)

Jet Propulsion Laboratory
Calif. Institute of Technology
4800 Oak Grove Drive
Pasadena, California 91103
Attn: Richard Bailey (1)
Technical Library (1)

Scientific & Technical Information
Facility
NASA Representative
P. O. Box 33
College Park, Maryland 20740
Attn: CRT (6)

GOVERNMENT INSTALLATIONS

AF Space Systems Division
Air Force Unit Post Office
Los Angeles, California 90045
Attn: Col. E. Fink (1)

AF Research and Technology Division
Bolling AFB, D. C. 20332
Attn: Dr. Leon Green, Jr. (1)

AF Rocket Propulsion Laboratory
Edwards AFB, California 93523
Attn: RPM/Mr. C. Cook (2)
RPMCH/Mr. W. Payne (1)
RPMCH/Lt. D. Zorich (1)
RPMCH/Mr. A. Bissoni (1)

AF Materials Laboratory
Wright-Patterson AFB, Ohio 45433
Attn: MANC/D, Schmidt (1)
MAAE (1)

AF Ballistic Missile Division
P. O. Box 262
San Bernardino, California
Attn: WDSOT (1)

Structures Division
Wright-Patterson AFB, Ohio 45433
Attn: FDT/R. F. Hoener (1)

Army Missile Command
Redstone Scientific Information Center
Redstone Arsenal, Alabama 34809
Attn: Chief, Document Section (1)

Ballistic Research Laboratory
Aberdeen Proving Ground,
Maryland 21005
Attn: Technical Library (1)

Picatinny Arsenal
Dover, New Jersey 07801
Attn: Technical Library (1)

Navy Special Projects Office
Washington, D.C. 20360
Attn: H. Bernstein (1)

Naval Air Systems Command
Washington, D.C. 20360
Attn: AIR-330/Dr. O. H. Johnson (1)

Naval Propellant Plant
Indian Head, Maryland 20640
Attn: Technical Library (1)

Naval Ordnance Laboratory
White Oak
Silver Spring, Maryland 20910
Attn: Technical Library (1)

Naval Ordnance Test Station
China Lake, California 93557
Attn: Technical Library (1)
C. J. Thelen (1)

Naval Research Laboratory
Washington, D.C. 20390
Attn: Technical Library (1)

Chemical Propulsion Information
Agency
Applied Physics Laboratory
8621 Georgia Avenue
Silver Spring, Maryland 20910 (1)

Defense Documentation Center
Cameron Station
5010 Duke Street
Alexandria, Virginia 22314 (1)

Defense Materials Information Ctr
Battelle Memorial Institute
505 King Avenue
Columbus, Ohio 43201 (1)

Materials Advisory Board
National Academy of Science
2101 Constitution Ave., N.W.
Washington, D.C. 20418
Attn: Capt. A. M. Blamphin (1)

Institute for Defense Analyses
1666 Connecticut Ave., N.W.
Washington, D.C.
Attn: Technical Library (1)

Advanced Research Projects Agency
Pentagon, Room 3D154
Washington, D. C. 20301
Attn: Tech. Information Office (1)

INDUSTRY CONTRACTORS

Aerojet-General Corporation
P. O. Box 1168
Solid Rocket Plant
Sacramento, California 94086
Attn: Dr. B. Simmons (1)
Tech. Information Ctr. (1)
Research & Tech. Dept. (8)

Aerojet-General Corporation
P. O. Box 296
Azusa, California 91702
Attn: Technical Library (1)

Aerospace Corporation
2400 East El Segundo Boulevard
El Segundo, California 90245
Attn: Technical Library (1)
Solid Motor Dev. Office (1)

Aerospace Corporation
P. O. Box 95085
Los Angeles, California 90045
Attn: Technical Library (1)

Atlantic Research Corporation
Shirley Highway at Edsall Road
Alexandria, Virginia 22314
Attn: Technical Library (1)

Battelle Memorial Library
505 King Avenue
Columbus, Ohio 43201
Attn: Edward Unger (1)

Boeing Company
P. O. Box 3999
Seattle, Washington 98124
Attn: Technical Library (1)

Chrysler Corporation
Space Division
Michoud Operations
New Orleans, Louisiana
Attn: Technical Library (1)

Douglas Missiles & Space Systems
Huntington Beach, California
Attn: T. J. Gordon (1)

Hercules Company
Allegany Ballistics Laboratory
P. O. Box 210
Cumberland, Maryland 21502
Attn: Technical Library (1)

Hercules Company
Bacchus Works
P. O. Box 98
Magna, Utah 84044
Attn: Technical Library (1)

Lockheed Missiles & Space Company
P. O. Box 504
Sunnyvale, California
Attn: Technical Library (1)

Lockheed Propulsion Company
P. O. Box 111
Redlands, California 93273
Attn: Bud White (1)

Martin Marietta Corporation
Baltimore Division
Baltimore, Maryland 21203
Attn: Technical Library (1)

Mathematical Sciences Corporation
278 Renook Way
Arcadia, California 91107
Attn: M. Fourney (1)

Philco Corporation
Aeronutronics Division
Ford Road
Newport Beach, California 92660
Attn: F. C. Price (1)

Rocketdyne
Solid Propulsion Operations
P. O. Box 548
McGregor, Texas
Attn: Technical Library (1)

Rocketdyne
6633 Canoga Avenue
Canoga Park, California 91304
Attn: Technical Library (1)

Rohm and Haas
Redstone Arsenal Research Division
Huntsville, Alabama 35807
Attn: Technical Library (1)

Rohr Corporation
Space Products Division
8200 Arlington Boulevard
Riverside, California
Attn: H. Clements (1)

Thiokol Chemical Corporation
Wasatch Division
Brigham City, Utah 94302
Attn: Dan Hess (1)
Technical Library (1)

Thiokol Chemical Corporation
Elkton, Division
Elkton, Maryland 21921
Attn: Technical Library (1)

Thiokol Chemical Corporation
Huntsville Division
Huntsville, Alabama 35807
Attn: Technical Library (1)

Thompson, Ramo, Wooldridge, Inc.
Structures Division
23444 Euclid Avenue
Cleveland, Ohio 44117
Attn: L. Russell (1)

United Technology Center
P. O. Box 358
Sunnyvale, California 94088
Attn: Technical Library (1)

Sun Ship & Dry Dock Company
Aero/Hydro Space Division
Foot of Morton Street
Chester, Pennsylvania
Attn: C. Garland (1)

IIT Research Institute Technology Ctr
Chicago, Illinois 60616
Attn: M. A. Schwartz (1)

Norton Company
Worcester, Massachusetts 01606
Attn: Product Development Dept. (1)